NONLINEAR, TRANSONIC FLUTTER PREDICTION FOR F-16 STORES CONFIGURATION CLEARANCE

THESIS

Raymond G. Toth, Major, USAF

AFIT/GAE/ENY/03-8

DEPARTMENT OF THE AIR FORCE

AIR UNIVERSITY

AIR FORCE INSTITUTE OF TECHNOLOGY

Wright-Patterson Air Force Base, Ohio

The views expressed in this thesis are those of the author and do not reflect the official policy or position of the United States Air Force, Department of Defense, or the United States Government.

AFIT/GAE/ENY/03-8

Nonlinear, Transonic Flutter Prediction for F-16 Stores Configuration Clearance

THESIS

Presented to the Faculty of the Graduate School of Engineering and Management
of the Air Force Institute of Technology
Air University
In Partial Fulfillment of the
Requirements for the Degree of
Master of Science in Aeronautical Engineering

Raymond G. Toth, B.S.
Major, USAF

March, 2003

AFIT/GAE/ENY/03-8

Nonlinear, Transonic Flutter Prediction for F-16 Stores Configuration Clearance

Raymond G. Toth, B.S.

Major, USAF

Approved:

/signed/	
Lt Col Robert Canfield Ph.D. Thesis Advisor	Date
/signed/	
Bradley Liebst Ph.D. Committee Member	Date
/signed/	
Lt Col John Michael Phillips Ph.D. Committee Member	Date

Preface

This thesis would have been immensely more difficult if it were not for the help of many people. I would like to thank Lt Col Bob Canfield for his endless patience in attempting to teach a fighter pilot to understand the fundamentals of aircraft aeroelastic response (much like teaching a dog to read a wristwatch). I would also like to thank Dr. Reid Melville for lending his expertise in the field of Computational Fluid Dynamics and for providing much of the data required for this research, Dr. Chuck Denegri at the Air Force Seek Eagle Office for providing invaluable expertise in flight flutter testing, and finally Drs. Darius Sarhaddi and P. C. Chen at ZONA Technologies for their exhaustive help in developing and debugging the aerodynamic models used in my research.

I'd especially like to thank my wife for her unwavering support throughout this whole process, and indeed, my career. Without her devotion, love, understanding, and tireless commitment to our children I would not be where I am today.

Raymond G. Toth

Table of Contents

Page

List of Figures

List of Tables

List of Abbreviations

AFIT/GAE/ENY/03-8

Abstract

Wing flutter, or more accurately limit cycle oscillation (LCO), has been an issue for the F-16 since its operational deployment. Different store configurations and the permutations of those configurations after weapons are released will cause LCO to either disappear or appear. Unfortunately, the current method used by engineers for predicting LCO onset is based on linear, subsonic aerodynamic theory with no corrections for transonic effects. Predictions using this method are often good in frequency, but can be far off in predicting onset speed, forcing flutter engineers to rely more on experience and interpolation from similar configurations to design flight test parameters. During flight tests, very specific and stringent guidelines are adopted to ensure the aircraft does not encounter classical flutter or excessive LCO; consequently, these tests require a large investment in resources and time to validate any particular store configuration. A new approach, incorporating inherent nonlinearities that drive LCO is investigated in the following research. This approach (called ZTAIC - ZONA's Transonic Aerodynamic Influence Coefficient method) uses steady C_p data in conjunction with the Transonic Equivalent Strip (TES) method to generate a transonic modal aerodynamic influence coefficient (AIC) matrix which accounts for wing thickness effects and shock structure. This AIC is then used in the g-method flutter solution methodology (incorporating a damping perturbation technique) to extend the classical linear p-k flutter solution methodology to include first-order aerodynamic damping effects. Two F-16 store configurations are examined using the g-method to correlate predicted flutter onset speeds, frequencies and character (classical flutter, typical LCO, or non-typical LCO) with those found in flight test. Additionally, an investigation of the aerodynamic effects of modeling underwing stores on the flutter solution is accomplished.

Results show that predicting the flutter boundary is particularly dependent upon a highly accurate structural model. Small changes in the tuning of the structural model resulted in large changes in the flutter boundary. Flutter frequency, however, was predicted quite well. Also, the aerodynamic model could not be neglected, as the aerodynamic influence of underwing stores proved significant, particularly for the two most outboard wing stations. Most importantly, the character of the instability was predicted by the new method. This new method gives the flutter engineer valuable insight and allows for more focused, quicker, cheaper and safer flight-testing.

Nonlinear, Transonic Flutter Prediction for F-16 Stores Configuration Clearance

I. Introduction

The aeroelastic response of aircraft with either thin wings or large aspect ratios has long been a topic of discussion and research, and the F-16, with its relatively thin wing, has often been the focus of such studies. Originally designed as a lightweight, day only fighter, the F-16 evolved into a robust multi-role aircraft. This evolution was driven primarily by the retirement of aircraft such as the A-7, F-4E, and F-4G, and the need for a currently available fighter to assume their roles. As the F-16's versatility grew, so too did the types of stores that it needed to carry. Since the beginning of its operational life, however, the F-16 was known to exhibit flutter of the wing; the severity of which depended on the type and number of underwing stores carried. Necessarily, all store configurations had to be flight-tested to determine if any instability would occur, and, if so, how severe it would be. Flight-testing, however, is expensive, and a method was needed to enable engineers to predict flutter onset speeds so the tests could be narrowed to a specific flight regime. Initially, prediction methods were based on linearizing this inherently nonlinear phenomenon, and ignoring the aerodynamics of the underwing stores to reduce the complexity of the problem and facilitate numerical solutions. These methods, however, while often quite good at predicting flutter frequencies, were typically not very accurate at predicting flutter onset velocities [13]. Rapid advances in computing power over the last 10 years are now beginning to allow flutter solutions that include the aerodynamic effects of underwing stores and structural/aerodynamic nonlinearities.

The Air Force Seek Eagle Office (AFSEO) is responsible for certification of new store configurations for the F-16. Many times the requested configuration is

very similar to an existing cleared configuration, and, in these cases, AFSEO usually relies on previous experience to clear the new configuration across the same envelope. As the F-16's roles continue to expand however, more configuration requests are unique and require simulation and flight-testing before the flight envelope can be cleared. This process involves conducting exhaustive simulations of every possible "download"[1] of the requested configuration to determine which combinations are flutter sensitive, followed by flight-tests of the flutter sensitive combinations to validate the simulations across the flight envelope. The current methodology used by AFSEO to accomplish the simulations is called the Universal Flutter Analysis Program (UFAP). UFAP is a linear, subsonic aerodynamic solution routine tied to a linear structural solver. With this method only the wing is modeled aerodynamically; UFAP has no capability to aerodynamically model the underwing stores. The stores are accounted for by adjusting the mass and flexibility properties of the structure. Due to the inaccuracies involved with UFAP, AFSEO advertises a 12 to 24-month period from initial submission of a new configuration to final clearance.

1.1 Problem

The research problem described in this thesis is to determine whether nonlinear aerodynamic methods can more accurately predict flutter onset speeds and frequencies, the sensitivity of the solution to aerodynamic modelling of underwing stores, and the sensitivity of the solution to various levels of structural damping. This thesis presents a technique for more accurately predicting flutter onset speeds and frequencies for F-16 stores configurations. This method will be more computationally expensive than the current UFAP code, but greater accuracy in the predictions should shrink the flight test envelope, resulting in cost and time savings for flight-test validation, as well as enhanced flight test safety.

[1] A download is a permutation of the original configuration. For example, if the requested configuration is 2 AMRAAMs by 2 JDAMs, then every possible combination of these stores must be examined; i.e 1 AMRAAM x 2 JDAM, 0 AMRAAM x 2 JDAM, 2 AMRAAM x 1 JDAM, etc.

1.2 Scope

The research presented in this thesis is an investigation of an analysis technique which produces less error in predicting flutter than UFAP. A parametric complex eigenvalue (PCE) method combining a nonlinear capable aerodynamic solver, ZAERO 5.2, splined to a linear finite element structural solver, MSC/NASTRAN, is used to generate aeroelastic solutions for two F-16 standard combat loads (SCL) over a range of airspeeds and altitudes. Sensitivity analyses to transonic nonlinearities, aerodynamic modeling of underwing stores, and structural damping are included. Finally, predicted flutter onset speeds and frequencies are compared to flight-test results.

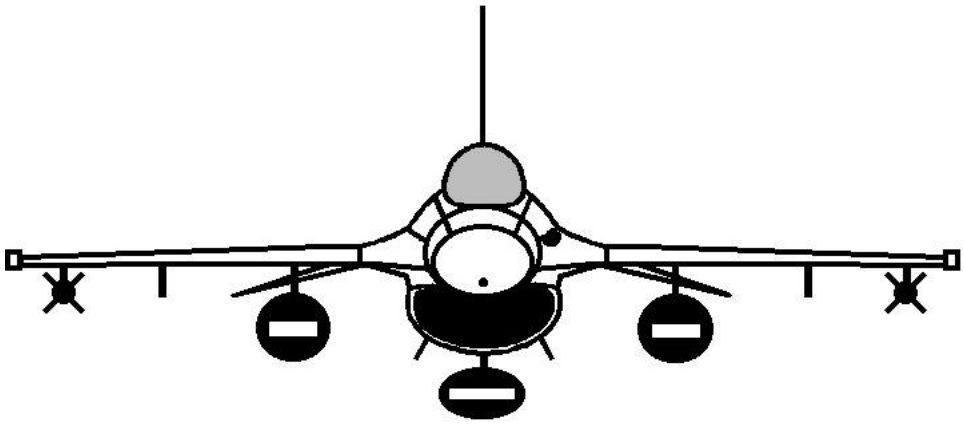

Figure 1.1 F-16 Standard Combat Load (SCL) 007

1.3 Approach/Methodology

The initial phase focuses on validating a new F-16 structural model, for the standard combat load shown in Figure 1.1, with previous research, using linear techniques without the effect of store aerodynamics or structural damping. Once the model is validated, a convergence study of the aerodynamic panel model of the aircraft wing is conducted. Next, nonlinear aerodynamic effects are investigated by supplying, to the transonic module of the aerodynamic solver, steady ΔC_p data generated from CFD modeling, where ΔC_p is the difference in pressure coefficients

between the upper and lower surfaces of the wing. This will test the sensitivity of the flutter onset speed to nonlinear shock effects in the transonic regime. Structural damping at various levels is then included in the aerodynamic module to gauge its effect on flutter onset speed and whether it can be considered an additive effect to the aerodynamic damping of the system, and then sensitivity to underwing stores is investigated to determine if the aerodynamic influence of these stores warrant their inclusion in the panel model. Finally, the results of the simulations are matched to flight test results of the SCL007 flown at Eglin AFB in 1991 [5].

II. Literature Review

2.1 Introduction

The following review supports research into quick and accurate prediction of the flutter onset speed of an F-16 Block 40/50 configured with external stores in the transonic flight regime. The terms, "flutter" and "limit cycle oscillation" (LCO), while often used interchangeably, mean something quite different. Classically, flutter is defined as oscillations that grow unbounded, after being excited by an initial disturbance, until the structure fails. The mechanism behind flutter is a coupling between aerodynamic, elastic, and inertial forces. LCO differs from classical flutter primarily in that highly nonlinear coupling between the aerodynamic and structural forces causes the oscillations to grow from an initial disturbance up to limited amplitude [4]. Unfortunately, current analytical methods do not allow us to tell whether an aircraft will experience classical flutter or LCO at any given airspeed and configuration; therefore, flight tests are used to try to determine flutter onset speeds. During flight tests, very specific and stringent guidelines are adopted to ensure the aircraft does not encounter classical flutter or excessive LCO; consequently, these tests require a large investment in resources and time to validate any particular store configuration.

The following sections of this review investigate current research into:

1. The mechanisms that drive LCO.
2. Methods for predicting, rather than simply correlating, the onset speeds and frequencies.
3. The methodology used by the Air Force Seek Eagle Office (AFSEO) to predict LCO for the F-16 under various store configurations.

This review was undertaken to determine whether an integrated software package for predicting LCO onset speeds and frequencies exists. The software should require

only modest computing effort and cost and allow AFSEO to run multiple test cases in a reasonable time period.

2.2 Mechanisms for LCO

Understanding the mechanisms that drive LCO is particularly important in the design and certification of the flight envelope of any military aircraft. The effects of LCO on a pilot's ability to work effectively within the cockpit, as well as fatigue effects on the aircraft structure, and vibration effects on aircraft stores while under an LCO condition drive this need [4]. Considerable research in the last 10 to 15 years into the mechanisms that drive flutter and LCO has led to great strides in understanding the phenomenon, but no consensus as to the predominant driving factor that causes LCO has yet been achieved. Flight-test results and some computational fluid dynamics/computational structural dynamics (CFD/CSD) research agree, however, that, in the case of the F-16 at least, flutter/LCO appears primarily as an antisymmetric phenomenon [4, 28]. Denegri notes that inboard and outboard wing motion contribute to both symmetric and antisymmetric LCO; however, rolling moments caused by wing motion in the antisymmetric case are lightly damped by structural and aerodynamic mechanisms, allowing more energy to transfer through the fuselage to the opposite wing [13].

While there seems to be little debate about how LCO is exhibited on the F-16, there are still questions about whether the driving factor is aerodynamic, structural, or some combination of both. Meijer and Cunningham describe the leading case for an aerodynamic mechanism in the transonic regime as shock-induced trailing edge separation (SITES) [25]. During transonic flight, while under LCO conditions (LCO seems to occur most frequently during transonic flight), the aircraft experiences a mixture of both attached and separated flow [25]. SITES is presumed to be one of the causes of this mixed flow, as well as the disturbance that can lead to LCO. Meijer also reports in a later paper that local shock induced separation (LSIS) couples with

SITES to induce LCO, especially as the angle of attack of the wing is increased above approximately five degrees [24]. While the onset and growth of LCO appear to be driven aerodynamically by SITES and LSIS, airflow disturbances at the leading edge of the wing appear to limit that growth. On a CFD model of a cropped delta wing, leading edge vortices seemed to act as "aerodynamic springs" that limited the amplitude of the structural oscillations [15]. Aerodynamic lags also appear to play a role in determining the amplitude of LCO. In their investigation of SITES, Meijer and Cunningham showed the time lag associated with the transition to SITES led to increasing amplitudes [25]; while phase lags between the structural modes, that combine to form the flutter mode, determine the final amplitude [15].

It is readily apparent that nonlinear aerodynamics play a role in the development of LCO; however, most of the studies linking these nonlinearities to LCO were conducted at angles of attack of four or more degrees. At transonic speeds, this range of angle of attack is typical of increased G loadings during maneuvering, but LCO is also known to occur during straight and level flight where angle of attack is normally less than two degrees. Also, most of the studies investigating the aerodynamic effects of LCO use a linear structural model with an assumed structural damping of zero percent; or, if a wind tunnel model is used, it is usually a rigid model which has less damping (due to its unitized construction and lack of mechanical joints between the stores and the wing) than an actual wing [8]. Tang and Dowell attempted to account for structural nonlinearities using linear aerodynamic theory coupled with a nonlinear structural solver on a delta wing model, and verified LCO onset and amplitude sensitivity to angle of attack, suggesting the effect is not necessarily due to aerodynamic nonlinearities [34].

Three observations about LCO also point to causes other than aerodynamic:

1. LCO occurs over airspeed ranges from subsonic to supersonic and once LCO starts, it continues through the transonic regime.

2. During wind tunnel testing flutter is encountered; but, during flight test, LCO is encountered. This can be linked to the use of stiff models in the wind tunnel and the variation of Reynolds number between wind tunnel tests and flight test.

3. Different aircraft carrying the same store configuration show a variation in LCO onset speeds, or no LCO at all. [29]

According to Chen, et al. [8], the above observations can be explained by nonlinear structural damping (NSD), unlike the aerodynamic theories previously discussed. NSD describes the frictional interaction that occurs between the wing/pylon and pylon/store. When aerodynamic forces become strong enough to overcome the static friction in these interfaces, the resulting dynamic friction acts to provide damping to the system. This provides an explanation for observations two and three, since the way in which the pylon is mounted on the aircraft, or how tightly the sway braces secure a store can change the coefficients of friction for each of those interfaces [8, 29]. This "stick/slip" friction effect, known as "stiction," is independent of Mach number, verifying observation one for NSD [29].

The conclusion drawn from the research of Chen, et. al. [8] and Mignolet, et. al. [29] above is that both the aerodynamic and structural nonlinearities should be accounted for, if possible, to ensure the most accurate prediction of LCO onset speed, frequency, and amplitude. Sheta, et al., showed the efficacy of this method during a CFD study on a NACA-0015 airfoil incorporating both fluid and structural nonlinearities and concluded:

> The mechanism of the instability (LCO) could be due to flow nonlinearities such as flow-separation and the presence of separation bubbles, the presence of an oscillating shock, the state of the boundary-layer, and shock/boundary-layer interaction. Other sources of the instability are structure nonlinearities which may be associated with kinematics, structural stiffness and damping properties, and pathologies such as internal resonances arising from design. [33]

2.3 Computational Methods

The aerodynamic and structural nonlinearities discussed above are accounted for in simulation using one of three broad classes of computing approaches: fully implicit aerodynamic/structural methods, conventional serial staggered (CSS) methods, and parametric complex eigenvalue (PCE) methods.

Fully implicit methods are typically more complex since they attempt to combine both the structural and fluid equations into one package that can be marched forward in time to yield complete solutions. The staggered method uses two separate codes, one for the structure and one for the fluid, and each medium is solved independently. The solutions are then transferred across the boundary interface between the fluid and structure using a splining technique [22]. Parametric complex eigenvalue methods are similar to CSS methods; they are not, however, concerned with the motion of the system over time, and hence cannot predict amplitudes. Instead, a structural solver is used to generate the structural natural modes, which are then used by an aerodynamic routine to generate flutter modes. This approach iterates over a parameter, generally velocity, to determine when the system will cross from stability to instability.

While computational fluid dynamics (CFD) and computational structural dynamics (CSD) packages have been around for quite a while, combining the two into a single implicit method for solving complex aeroelastic problems is a relatively recent development. Rapid advances in computing power throughout the 1990's made the integration possible; now, high-end desktop systems can solve problems that previously required a supercomputer. Simplifications are still made, however, to reduce the overall complexity of the system being modeled. For instance, Gordnier and Melville [15, 16] and Melville's [27, 28] research throughout the late 90's always coupled the nonlinear Navier-Stokes/Euler equations with linear structural equations. Similarly, most of their work did not include the effects of underwing stores on the aeroelastic response of the system. Flight test data from the F-5 and F-17 shows,

however, that nearly 40% of all configurations tested showed a sensitivity to underwing stores, which modified the flutter onset speed through changes in modal coupling [35]. And only recently have high order CFD studies included the effect of structural damping on the system. Ground vibration testing (GVT) typically places structural damping in the 1-2% range [8], and when 1% damping was included in an F-16 model, Melville [28] found it made the system very stable and concluded that neglecting the effects of structural damping leads to uncertainty in the flutter prediction. The CFD/CSD approach has yielded many insights into the mechanisms that drive and sustain LCO; however, they still have not been able to capture the entire range of LCO phenomenon. Most of the analyses predicted the onset speed fairly well in the subsonic range, but overpredicted the supersonic cases [16, 28]. Other limitations of these methods are software integration and computational cost. Because the fully implicit methods couple the structural and fluid equations into one package, updating the software as new structural or fluid solvers become available is a time consuming process. And, even though computing power continues to increase rapidly, the time required to generate a solution for a single configuration using these methods is not conducive to evaluation of hundreds of permutations on a given configuration.

Staggered methods, on the other hand, overcome the limitation of having to integrate newer computational routines into a unitary solver. Instead, as new software packages for structures or fluids are created or updated, they are inserted into the computing environment that couples the two solvers. The environment commonly used now is the Multi-Disciplinary Computing Environment (MDICE). Kolonay, et al., demonstrated the "plug and play" nature of this architecture on a generic fighter wing, coupling a Navier-Stokes/Euler fluid solver with two separate structural solvers, MSC/NASTRAN and ANSYS [22]. Since the CSS method is similar to fully implicit methods (the same equations can be used in both methods), similar results are expected. Greco, et al. [17], combined the Transonic Small Disturbance

equations with linear structural equations, producing results for the AGARD I-Wing 445.6 that were similar to fully implicit results reported by Gordnier and Melville [16], i.e., predicted subsonic flutter speeds showed good agreement with experiment while supersonic results were overestimated. The primary drawback related to CSS methods is that exact time synchronization between fluid and structure cannot be accomplished, introducing errors in transient analyses and time stability problems [22]. Pipeno, et al., addressed these issues with a novel approach to time discretization based on equating the work done by the structure to that done by the fluid pressure at the interface [31]. Generally, the order of time accuracy in a staggered method is one order less than the time accuracy of the structural and fluid solvers being used; however, they were able to achieve higher order time accuracy with this energy approach without significantly adding computational cost [29, 31].

Although CSS methods have some advantages in terms of adaptability, their results have not consistently proven any more accurate than fully implicit methods, and the computational cost is still prohibitive for generating results for many permutations on a given store configuration.

Accurately predicting the onset speed, frequency and amplitude of LCO is important to the Air Force Seek Eagle Office (AFSEO); doing it quickly for multiple configurations is equally important however. This requirement led AFSEO to use the parametric complex eigenvalue method (PCE) for predicting LCO onset. Since uncertainties persist in computational methods, flight-testing is still required to verify prediction, making flutter onset speed and frequency more critical factors than amplitude. The PCE method is quite robust and, like the staggered methods described above, is easily adaptable to new software. Until recently, most PCE solution methods used linear theory for both structural and aerodynamic solutions, however, the method is easily adaptable to account for nonlinearities by introducing structural damping effects and modifying the Aerodynamic Influence Coefficient (AIC) matrices. Brink-Spalink and Bruns [3], and Jadic, et al. [20], describe methods for

including nonlinearities in the flow, and reducing the computing cost of generating corrections to the AIC matrices. Using the method outlined by Jadic, et al., for linear analysis, one Enhanced Correction Factor Technique (ECFT) matrix is generated for each Mach number; but, to include nonlinear effects, additional ECFT matrices for the same Mach number are generated to account for additional aerodynamic data [20]. The necessity to generate multiple ECFT matrices to account for nonlinearities makes this method somewhat cumbersome. A more automated approach to correcting the AIC matrices for transonic solutions, developed by ZONA Technology, is available that solves the unsteady Transonic Small Disturbance (TSD) equation [36]. To generate the corrected AIC matrices, steady pressure data is required for the Mach number and angle of attack of the aircraft (steady pressure data is required by all of the AIC correction techniques); this data can be obtained from CFD calculations or experiment/flight test. Using the steady pressure data allows the software to determine the location and strength of the shock waves attached to the wing, as well as the associated equivalent airfoil shape [36]. From this information, a modal-based Transonic Aerodynamic Influence Coefficient (TAIC) matrix is built, based on the nonlinear, unsteady TSD equation [36]. Implementing the ZTAIC module is transparent, and performing a transonic calculation simply requires the additional input of steady pressure data.

2.4 AFSEO Methodology

Currently, AFSEO uses an analysis tool called the Universal Flutter Analysis Program (UFAP) to calculate flutter onset for all the permutations of a given store configuration [11]. In order to do this, engineers at AFSEO input the mass, geometry, and flexibility properties of the both the aircraft and stores to UFAP which then solves an eigenvalue problem to determine the natural frequencies, mode shapes, generalized masses, and generalized stiffnesses of the system. This part of the UFAP code is not finite-element based, however. In order to make changes to the structure

or stores, the engineers must manipulate the actual mass and flexibility matrices of the system. The aerodynamic influence coefficient (AIC) matrices (discussed in detail in chapter 3) are created by an external program using the Doublet-Lattice method (DLM) [1], which is a purely linear, subsonic method. With the structural modes and the AIC's known, UFAP then interpolates the natural modes to the aerodynamic panels of the DLM via a spline matrix and solves the complex eigenvalue problem using a version of the k-method (see chapter 3). Velocity vs. damping (V-g) and velocity vs. frequency (V-ω) curves for each vibration mode are output and critical flutter modes are identified as those modes whose flutter speeds fall within 15% of the desired carriage airspeed limit [12]. These critical cases are then submitted for flight testing.

The obvious limitation of UFAP is that it is a purely linear, subsonic flutter prediction method, whereas the phenomenon itself is known to be nonlinear with onset speed typically in the transonic and supersonic flight regimes. Work done by Johnson [21] has extended AFSEO's capability to include supersonic analysis using MSC/NASTRAN to generate the structural and aerodynamic solutions, however, no transonic capability exists.

2.5 Software Selection

The software used in this thesis was chosen to both expand AFSEO's prediction capability (throughout the entire flight regime) and to merge multiple linear solution methods into one with both linear and nonlinear capabilities.

ZONA Technology's ZAERO Version 5.2 software [37] uses a higher order linear method (based on constant pressure across each aerodynamic box) than DLM for subsonic analysis and adds a supersonic capability, both of which account for the effects of external stores and wing-store interference. In addition, ZAERO integrates a transonic method using the same general input requirements as the sub/supersonic methods with the additional requirement of steady C_p data. ZAERO still requires

that the natural modes of the system be generated by an external finite-element routine; however, now all the aerodynamics throughout the flight regime are bundled into one software package.

Linear subsonic and supersonic analysis methods have been available for quite some time and generally produce acceptable results. When these methods are used in the transonic regime, however, their results break down due to the highly non-linear nature of the flow. Of course, this is the region where LCO appears to occur most frequently, so a method for predicting the onset of LCO was needed. Research conducted in the 80's and 90's (refs [9], [14], [23], [30]) revealed a method for linearizing and separating the Transonic Small Disturbance (TSD) equation into sectional and spanwise components which then made solutions possible. ZONA made use of the principles outlined in the above references to create a transonic method known as ZTAIC (ZONA's Transonic Aerodynamic Influence Coefficient method) for their ZAERO software. Chen, et. al. [9] compared results from the ZTAIC method, their linear subsonic (ZONA6) method, and a CFD method known as CAP/TSD [2] for six wing planforms with wind tunnel results. These results showed:

1. ZTAIC was able to more accurately reproduce steady and unsteady pressure distributions than ZONA6 or XTRAN3 (a transonic equivalent strip (TES) method) .
2. ZTAIC results compared favorably with those generated by CAP-TSD (a higher order CFD code) using steady C_p's generated by both Euler and Navier-Stokes calculations.
3. ZTAIC flutter results also compared favorably with CAP-TSD, predicting a transonic dip that ZONA6 fails to find.

While these results were encouraging and led to the use of ZAERO in this thesis, some important comparisons and sensitivities were left out or neglected. Specifically, the research from Chen, et. al. was conducted only on wing planforms without

external stores attached, the steady C_p data used was based on a rigid wing (i.e. the pressure distributions are based on an undeflected wing at the measured flight condition), and no flutter predictions were made for an F-16 model.

This thesis will extend the investigation of ZTAIC flutter analysis capability to include the effects of modeling the entire aircraft with and without external stores (the stores will always be modeled structurally), the effect of using rigid versus flexible C_p (the pressure distribution on the deflected wing) data, and the effect of adding structural damping to the system. This thesis also marks the first application of the ZTAIC method to an F-16 model for flutter prediction.

III. Theoretical Background

This chapter presents the theoretical underpinnings of the solution techniques required for the flutter analysis presented in this thesis. First, section 3.1 presents the method for computing a system's natural modes. These modes are required in the calculations of section 3.2 for finding the unsteady flow conditions and the aerodynamic influence coefficient matrix (AIC). The AIC is then included in the modal equations of motion to generate the flutter solution by any of the three methods described in section 3.3. Finally, section 3.4 describes how nonlinearities such as shock structure and wing thickness effects are incorporated into the linear solution through the use of the transonic linear strip method.

3.1 Natural Modes Analysis

In order to effectively calculate the flutter boundary for an aircraft, the natural modes of the system must first be identified. These modes are used as generalized degrees of freedom (DOF) for calculating the unsteady flow conditions and AIC matrix. The multiple degree-of-freedom system of equations of motion are first linearized about some equilibrium position, and the natural modes are the eigensolution for the free vibration of the linearized equations of motion:

$$[k - \omega_i^2 m]\phi_i = 0, i = 1, 2, \ldots, n \tag{3.1}$$

where k is the stiffness matrix and m is the mass matrix. The eigenvalues of Eq (3.1) represent the square of the natural frequencies of each mode, ω_i, and the corresponding eigenvectors, ϕ_i, are the mode shapes (displacements of each degree of freedom in the model for a specific mode). The natural modes are then used in a modal transformation to generalized coordinates, q, such that:

$$x(t) = \Phi q(t) \tag{3.2}$$

The free vibration solution is decoupled due to the orthogonality of the natural modes [26]. The complete system of equations describing an aeroelastic vehicle in flight are formed by including the aerodynamic forces being applied to the structure. Typically these forces are broken into external forces (gust, turbulence, store ejection, etc.) and aerodynamic forces due to structural deformation. Excluding external forces (flutter analysis is interested in finding the self-excited response of the structure), the system of equations becomes (in the Laplace domain)[26]:

$$[s^2\mathbf{M} + s\mathbf{C} + \mathbf{K}]\mathbf{q} = \mathbf{F}_a \tag{3.3}$$

where:

$\mathbf{M} = \Phi^T$ m Φ	is the generalized mass matrix
$\mathbf{K} = \Phi^T$ k Φ	is the generalized stiffness matrix
$\mathbf{C} = \Phi^T$ c Φ	is the generalized viscous damping matrix
$\mathbf{q}$	are the generalized coordinates
Φ	is the modal transformation matrix
$\mathbf{F}_a$	are the aerodynamic forces produced by structural deformation

3.2 ZAERO Theoretical Formulation

ZONA Technology's ZAERO aeroelastic analysis software [37] is used in this thesis to generate the flutter solution for two F-16 configurations under various conditions. ZAERO uses a panel method that solves a parametric complex eigenvalue problem to generate the flutter boundary. The aerodynamic panel model is built by creating body-type and flat-panel type elements. These elements are then divided into a grid of boxes, and a control point is located in each box where the solution is defined (Fig 3.1). A technique for ensuring a converged solution to a given grid, based on the minimum box width in the flow direction, is described in detail in ref [36]. In order to understand how the flutter solution is calculated, this section

will provide a brief overview of the theory, outlined in ref [36], used to generate the unsteady pressure coefficients (C_p) and modal AICs.

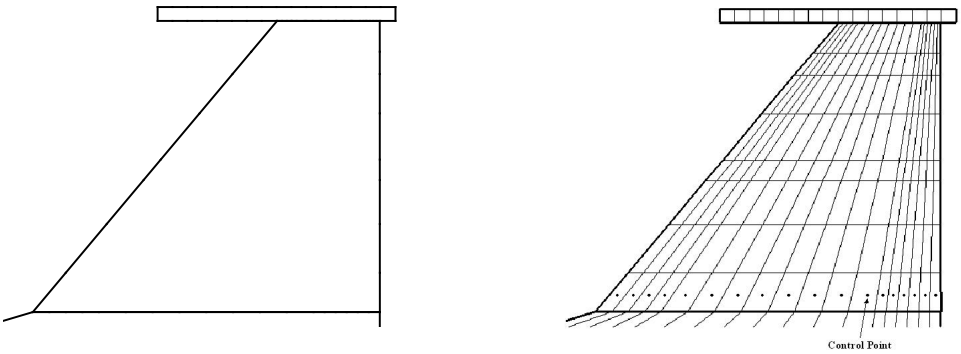

Figure 3.1 F-16 Wing Panel Discretization

3.2.1 ZONA6/7 Linear Formulation. The linear modules of ZAERO solve the linearized small disturbance equation for subsonic flow (ZONA6) and supersonic flow (ZONA7):

$$(1 - M_\infty^2)\Phi_{xx} + \Phi_{yy} + \Phi_{zz} - \frac{1}{a_\infty^2}\Phi_{tt} - \frac{2M_\infty}{a_\infty}\Phi_{xt} = 0 \tag{3.4}$$

by assuming a solution of the form:

$$\Phi = \phi_0 + \phi_1 \tag{3.5}$$

$$\phi_1 = \phi e^{i\omega t} \tag{3.6}$$

where:

$\phi_1 \ll \phi_0$

Φ	is the total velocity potential
ϕ_0	is the steady potential
ϕ_1	is the unsteady potential
ϕ	is the reduced-frequency domain potential
ω	is the oscillation frequency

First, the steady and unsteady components of Eq (3.4) are separated by substituting Eq (3.5) into Eq (3.4) and collecting like order terms, yielding:

$$(1 - M_\infty^2)\phi_{0xx} + \phi_{0yy} + \phi_{0zz} = 0 \tag{3.7}$$

$$(1 - M_\infty^2)\phi_{1xx} + \phi_{1yy} + \phi_{1zz} - \frac{1}{a_\infty^2}\phi_{1tt} - \frac{2M_\infty}{a_\infty}\phi_{1xt} = 0 \tag{3.8}$$

where Eq (3.7) is the steady linearized small disturbance equation and Eq (3.8) is the unsteady linearized small disturbance equation. By applying the linearized tangency condition to Eq (3.7), the steady velocity components, u_0, v_0, and w_0, are found, but are only required in the formulation of the AIC matrices to account for interference effects between the body elements and flat-plate elements. Solving Eq (3.8) for ϕ, the reduced-frequency domain potential, requires the structural mode shapes and the application of Green's Theorem and the linearized tangency condition for the source and doublet integrals. Green's Theorem is used to convert the partial differential equation, Eq (3.8), into elementary kernel integrals for the unsteady source and doublet singularity distributions at each aerodynamic box. These integrals are of the form:

$$\phi_B = -\frac{1}{E\pi}\int\int_{body} \sigma(x,y,z)e^{i\lambda M_\infty \xi} K dS \tag{3.9}$$

$$\phi_W = \frac{1}{E\pi}\int\int_{wing} \Delta\phi(x,y,z)e^{i\lambda M_\infty \xi}\frac{\partial}{\partial n} K dS \tag{3.10}$$

where:

σ	is the unsteady source singularity distribution
$\Delta\phi$	is the unsteady doublet singularity distribution
$\lambda = \frac{kM_\infty}{\beta}$	is the compressible reduced frequency
$\beta = \sqrt{\lvert 1 - M_\infty^2 \rvert}$	
ϕ_B	is the potential due to body-like components
ϕ_W	is the potential due to wing-like components
$\mathrm{E} = 4$	for $\mathrm{M}_\infty < 1$
$\mathrm{E} = 2$	for $\mathrm{M}_\infty > 1$
$\frac{\partial \overrightarrow{n}}{\partial n} = \overrightarrow{n} \cdot \overrightarrow{\nabla}$	gradient in the outward normal direction, where $\overrightarrow{n}$ is the out-normal vector
$\mathrm{K} = \frac{e^{-i\lambda R}}{R}$	for $\mathrm{M}_\infty < 1$
$\mathrm{K} = \frac{\cos(\lambda R)}{R}$	for $\mathrm{M}_\infty > 1$
$\mathrm{R} = \sqrt{\xi^2 + \mu\eta^2 + \mu\zeta^2}$	
$\xi = \left(\frac{x - x_0}{\beta L}\right)$	
$\zeta = \left(\frac{z - z_0}{L}\right)$	
$\eta = \left(\frac{y - y_0}{L}\right)$	

The boundary conditions are then applied to the control point in each aerodynamic box of the panel model to yield the solutions to each kernel equation. These solutions are then combined into the unsteady perturbation potential influence coefficient matrix (PIC) and the influence coefficient matrices (UIC, VIC, WIC) for the three components of velocity, u, v, and w. Combining the influence coefficient matrices and downwash functions yields the matrix equation:

$$[NIC] \left\{ \begin{array}{c} \sigma \\ \Delta C_p \end{array} \right\} = \left\{ \begin{array}{c} F_B \\ F_W \end{array} \right\} \tag{3.11}$$

where:

$$[NIC] = [n_x][UIC] + [n_y][VIC] + [n_z][WIC] \tag{3.12}$$

[UIC], [VIC], [WIC]	are the unsteady perturbation velocity influence coefficient matrices
$[n_x], [n_y], [n_z]$	are the wing section surface normal component matrices

(NIC) is the normal velocity influence coefficient matrix and F_B and F_W are body and wing downwash functions respectively. Eq (3.11) is solved for the source strength, σ, and the change in pressure coefficient over each box, ΔC_p, which are then used to find vectors of unsteady perturbation potential, ϕ, and unsteady perturbation velocity (u, v, w) values. Finally, the set of unsteady C_p's is generated using the steady mean flow conditions, unsteady perturbation quantities, reduced frequency, and the mode shapes and their derivatives. The unsteady C_p equation is the basis for the AIC matrix relating deformations to lift forces, described next.

3.2.2 Aerodynamic Influence Coefficient (AIC) Matrix Formulation. In order to generate the eigensolution for flutter, a modal AIC that relates the structural mode shapes to the unsteady aerodynamic forces must be calculated. By multiplying the area of each box of a wing-like component by the unsteady pressure on that box, the normal force may be computed. For body-like components, however, the normal forces are more complicated to calculate since they involve a coupling of the steady mean flow conditions, the perturbation potential and velocity influence matrices, and the structural mode shapes. These quantities are all available from the ZONA6/7 linear calculations. After expanding the normal force vector to include the force and moment components, a square matrix relating the structural mode shapes to the aerodynamic forces can be constructed:

$$\{\mathbf{L}_h\} = q_\infty [AIC]\{\mathbf{h}\} \tag{3.13}$$

where:

$$[AIC] = [[\overline{\mathbf{B}}][NIC]^{-1}[\overline{\mathbf{F}}] + [\overline{\mathbf{D}}]] \tag{3.14}$$

$$\{\mathbf{h}\} = [\mathbf{T}]\{x\} \tag{3.15}$$

$$\{\mathbf{L}_h\} = [\mathbf{T}][\Phi]\{\mathbf{F}_a\} \tag{3.16}$$

$\{\mathbf{h}\}$	is the structural deformation at each aerodynamic box
$\{\mathbf{L}_h\}$	is the resultant aerodynamic force vector at each aerodynamic box due to **h**
$[\mathbf{T}]$	is the spline matrix relating aerodynamic dof's to structural dof's
$[\Phi]$	is the modal transformation matrix

and $[\overline{\mathbf{B}}]$, $[\overline{\mathbf{F}}]$, and $[\overline{\mathbf{D}}]$ are all complex matrices containing the steady mean flow conditions and normal vector components, and are a function of reduced frequency. Eq (3.14) is defined for the degrees-of-freedom at the aerodynamic grid points and must be interpolated to the structural grid points through a spline matrix, then transformed to modal coordinates before it can be included in the *g*-method eigenvalue equation. For a more rigorous derivation of the AIC matrix, refer to Ref [36] chapter 3.7.

3.3 Flutter Solution Methods

There are three basic methods for calculating the flutter boundary from the aeroelastic equations of motion: the *k*, *p*-*k*, and *g*-methods. The common thread among these methods is the assumption that, at the flutter boundary, one of the natural modes of the system will become neutrally stable, producing simple harmonic motion, while the other modes remain stable. By assuming this type of solution to the generalized equations of motion, one need only look for the flight conditions that produce such a solution [19].

The flutter matrix equation in the Laplace domain is constructed by combining Eqs (3.2) and (3.13-3.15) and substituting for $\mathbf{F}_a$ in Eq (3.3), corresponding to the aerodynamic forcing function, (the viscous damping term is left out for simplicity):

$$\left[s^2\mathbf{M} + \mathbf{K} - q_\infty \mathbf{Q}\left(\frac{sL}{V}\right)\right]\mathbf{q} = 0 \tag{3.17}$$

where:

$\mathbf{Q}(\frac{sL}{V})$ is the generalized aerodynamic force matrix in the Laplace domain

By applying the simple harmonic motion assumption, Eq (3.17) is transformed to the frequency domain where the aerodynamic force matrix becomes the AIC matrix, $\mathbf{Q}(i\mathrm{k})$, a function of reduced frequency, $k = \frac{\omega b}{V}$, where b is half the wing root chord length [36]:

$$[-\omega^2\mathbf{M} + \mathbf{K} - q_\infty \mathbf{Q}(ik)]\mathbf{q} = 0 \tag{3.18}$$

Eq (3.18) is the basic form of the flutter equation that will be solved for the flutter roots. This equation is a nonlinear, parametric complex eigenvalue (PCE) equation. That is, it depends parametrically on velocity directly through q_∞ and indirectly through M_∞ and k. The eigenvalues are in general complex, because $\mathbf{Q}$ is complex, however the desired flutter root has no real part and the PCE problem is nonlinear because $\mathbf{Q}$ depends on ω through k.

3.3.1 The k-Method. The assumptions that produce the flutter matrix equation in the frequency domain imply the solution is only valid when the damping of the system is zero. In order to allow for complex roots to Eq (3.18), an artificial structural damping term multiplying the stiffness matrix is added:

$$[-\omega^2\mathbf{M} + (1 + ig_s)\mathbf{K} - q_\infty \mathbf{Q}(ik)]\mathbf{q} = 0 \tag{3.19}$$

Substituting

$$q_\infty = \frac{1}{2}\rho V^2 = \frac{1}{2}\rho\left(\frac{\omega L}{k}\right)^2 \tag{3.20}$$

and dividing Eq (3.19) through by -ω^2 yields the k-method flutter equation:

$$\left[\mathbf{M} + \frac{\rho}{2}\left(\frac{L}{k}\right)^2 \mathbf{Q}(ik) - \lambda\mathbf{K}\right]\mathbf{q} = 0 \tag{3.21}$$

which is solved for the complex eigenvalue:

$$\lambda = \frac{(1 + ig_s)}{\omega^2} \tag{3.22}$$

The eigenvalue, λ, consists of pairings of ω and g which can be plotted versus V, q_∞, $\frac{1}{k}$, Mach number, etc. These plots of damping versus airspeed are often used to indicate the margin of instability near the flutter boundary (i.e. the steepness of the slope at the zero crossing) [19]. For the k-method, however, the artificial structural damping term merely indicates, for a particular value of ω, the level of damping required to produce harmonic motion, and hence has no physical significance. For this reason, a modification to the k-method was developed.

3.3.2 The p-k Method. Since the k-method predicts only the onset of instability, the modal coupling predictions at points other than $g_s = 0$ are not representative of the system's true behavior [19]. Modal coupling information near the flutter point is very important in the design process because it can lead to methods for delaying flutter onset. In response to this need, the p-k method for flutter analysis was developed, and in 1971, Hassig [18] clearly showed that the p-k method more accurately predicted the modes involved in flutter for lightly damped modes (which are typically the modes of greatest interest in flight vehicles). In the p-k method, Eq (3.17) is recast in terms of a nondimensional Laplace parameter, p,

defined as:

$$p = \frac{sL}{V} = (\gamma k \pm ik) \tag{3.23}$$

where γ is the transient decay rate coefficient [36]. The flutter matrix equation in terms of p now becomes:

$$\left[\left(\frac{V^2}{L^2}\right)\mathbf{M}p^2 + \mathbf{K} - q_\infty \mathbf{Q}(ik)\right]\mathbf{q} = 0 \tag{3.24}$$

There is, however, an inconsistency with the p-k method described above. The parameter, p, describes damped harmonic motion, whereas the AIC matrix, $\mathbf{Q}(ik)$ was developed based on undamped harmonic motion. To overcome this problem, Rodden [32] introduced an aerodynamic damping matrix into Eq (3.24) by splitting $\mathbf{Q}(ik)$ into real and imaginary parts, yielding:

$$\left[\left(\frac{V^2}{L^2}\right)\mathbf{M}p^2 + \mathbf{K} - q_\infty \frac{\mathbf{Q}^I}{k} g - q_\infty \mathbf{Q}(ik)\right]\mathbf{q} = 0 \tag{3.25}$$

The solutions to Eq (3.25) are found by iterating on k until Eq (3.23) satisfies Eq (3.25). That is, for a given k, $\mathbf{Q}(ik)$ is calculated and used to solve Eq (3.25) for the complex root, p. If the imaginary part of p does not match the given k, then k is updated, and the process repeated until convergence. The p with the largest real part is the critical root. The velocity is varied parametrically to determine the speed at which the critical root's real part becomes zero. At this flutter speed and for this critical root, the flutter mode, $\mathbf{q}$, can be determined from Eq (3.25). This modification of the p-k method produces more realistic results than the k-method, but still has some shortcomings. Notably, the additional term introduced in Eq (3.25) has been shown to be valid only for small values of k or linear $\mathbf{Q}(ik)$, otherwise unrealistic results may still be reported [36].

3.3.3 The g-Method. The g-method is essentially a generalization of Rodden's modification of the p-k method. Chen [7] shows that by examining a damping

perturbation of $\mathbf{Q}(ik)$ for small values of g,

$$\mathbf{Q}(p) \approx \mathbf{Q}(ik) + g\left(\frac{\partial \mathbf{Q}(p)}{\partial g}\right)_{g=0} \tag{3.26}$$

and

$$\left(\frac{\partial \mathbf{Q}(p)}{\partial g}\right)_{g=0} = \frac{d\mathbf{Q}(ik)}{d(ik)} = \mathbf{Q}'(ik) \tag{3.27}$$

Through the use of this damping perturbation technique, the flutter equation becomes:

$$\left[\left(\frac{V^2}{L^2}\right)\mathbf{M}p^2 + \mathbf{K} - q_\infty \mathbf{Q}'(ik)g - q_\infty \mathbf{Q}(ik)\right]\mathbf{q} = 0 \tag{3.28}$$

and by substituting $p = g + ik$ into Eq (3.28), the g-method equation is formed:

$$[g^2\mathbf{A} + g\mathbf{B} + \mathbf{C}]\mathbf{q} = 0 \tag{3.29}$$

where:

$$\begin{aligned}
\mathbf{A} &= \left(\frac{V}{L}\right)^2 \mathbf{M} \\
\mathbf{B} &= 2ik\left(\frac{V}{L}\right)^2 \mathbf{M} - q_\infty \mathbf{Q}'(ik) \\
\mathbf{C} &= -k^2\left(\frac{V}{L}\right)^2 \mathbf{M} + \mathbf{K} - q_\infty \mathbf{Q}(ik)
\end{aligned}$$

By equating Eq (3.25) to Eq (3.28), and expanding $\mathbf{Q}(ik)$ in a Taylor series about $ik = 0$, the additional aerodynamic damping matrix introduced by Rodden in the p-k method is shown to correspond to $\mathbf{Q}'(ik)$ only when $\mathbf{Q}(ik)$ is a linearly varying function of reduced frequency, k. Thus, the g-method extends the validity of the flutter equation to the first order of g and for all values of k [7]. Solution of Eq (3.29) involves iterating on values of k, searching for the condition $Im(g) = 0$. This is done by searching for a sign change in the imaginary part of each eigenvalue between k and $|k + \Delta k|$. When the sign change is found, $Im(g) = 0$ is calculated by linearly

interpolating between k values. A predictor-corrector scheme is used for eigenvalue tracking to ensure the correct mode is followed across the flutter boundary [7].

3.4 ZTAIC Nonlinear Formulation

The analysis discussed in sections 3.1, 3.2, and 3.3 described the methodology used to predict flutter in a linear formulation. In the transonic regime, however, nonlinearities introduced by shock waves and wing thickness effects become much more important and linear theory breaks down. To account for these nonlinearities, the potential, Φ, in the TSD equation can once again be separated into steady and unsteady potentials, ϕ_0 and ϕ_1, as was done in Eq (3.5). In the transonic formulation, however, the nonlinear terms are included in Eqs (3.7) and (3.8) as follows:

$$[(1-M_\infty^2)-(\gamma+1)M_\infty^2\phi_{0x}]\phi_{0xx}+\phi_{0yy}+\phi_{0zz}=0 \tag{3.30}$$

$$(1-M_\infty^2)\phi_{1xx}-(\gamma+1)M_\infty^2(\phi_{0x}\phi_{1x})_x+\phi_{1yy}+\phi_{1zz}-\frac{1}{a_\infty^2}\phi_{1tt}-\frac{2M_\infty}{a_\infty}\phi_{1xt}=0 \tag{3.31}$$

Based on work done by Liu, Kao and Fung [23] and Oyibo [30], Eqs (3.30) and (3.31) can be solved by separating the flow into sectional and spanwise components. This method, termed the transonic equivalent strip (TES) method, employs two corrections to the linear pressure distributions generated by ZONA6/7. First, the sectional mean flow characteristics are adjusted to account for wing thickness effects and shock structure, then a spanwise phase correction is added to account for the spanwise pressure phase lag. This is accomplished by separating the potential, ϕ_1, into a 2-D (sectional) component, which is corrected by a spanwise decaying function [36]:

$$\phi_1(x,y,z,t)=\psi_1(x,z,t)F(y_i,\lambda_i) \tag{3.32}$$

where:

ψ_1 is the 2-D unsteady solution at spanwise section $y = y_i$

F is Oyibo's spanwise decaying function

λ_i is the decay parameter

The 2-D steady solution, ϕ_0 is calculated via an inverse airfoil design scheme [36]. Steady C_p data, generated by CFD solution or experiment, is supplied to the software and an Inverse Approximate Factorization scheme (IAF2) [14] is used to generate the slope of the airfoil thickness. This solves for the steady flowfield corresponding to the steady C_p data for each spanwise strip. This mean steady flow solution satisfies the 2-D version of Eq (3.30) and is coupled to the unsteady potential through Eq (3.31) to calculate ψ_1.

Using the separability principle, the corrections yield the following relation [9]:

$$\Delta C_{p3}^N = \Delta C_{p3}^l + f_n(\delta, \mu) \tag{3.33}$$

where:

ΔC_{p3}^N is the 3-D nonlinear unsteady pressure

ΔC_{p3}^l is the 3-D linear unsteady pressure

$\delta = \delta(\Delta C_{p2}^N, \Delta C_{p3}^l)$ is the sectional correction function

$\mu = \mu(\Delta C_{p3}^l, \Delta C_{p2}^l)$ is the spanwise phase-correction function

ΔC_{p2}^N is the nonlinear 2-D sectional transonic pressure

ΔC_{p2}^l is the linear 2-D sectional unsteady pressure

The steady mean flow solution is then used in an internal 2-D TES solver named ZTRAN to generate ΔC_{p2}^N. The correction functions, δ and μ, are then calculated and used to generate f_n, which is then added to the linear 3-D unsteady pressures (generated by ZONA6/7) to generate the nonlinear, transonic 3-D unsteady pressure, ΔC_{p3}^N, via Eq (3.33). With ΔC_{p3}^N known, a modal transonic AIC is constructed as

described next for use in the g-method flutter equation, Eq (3.29), to find the flutter boundary.

3.4.1 ZTAIC Modal AIC. Section 3.2.2 discussed the generation of an AIC matrix, containing purely aerodynamic information, relating the aerodynamic forces to the structural deformation of the wing. Creating an AIC matrix containing purely aerodynamic information following the formulation described above is a much more daunting task, however. An expedient method for deriving a transonic AIC matrix is discussed by Chen, et. al., in reference [9]. This approach defines a 2-D AIC matrix that relates the structural deformations, $\mathbf{h}$, to the aerodynamic forces, $\mathbf{F}_h$ at each section:

$$\{\mathbf{F}_h\} = q_\infty [AIC]\{\mathbf{h}\} \tag{3.34}$$

This transonic AIC is based upon five baseline modal vectors (not to be confused with the structural modes of the wing). These five baseline modes describe the local structural deformations at each section based on the aspect ratio of the wing and whether there are any leading or trailing edge devices [36]. Using these modes and applying the amplitude linearization principle ("the linearization of the aerodynamics for an aeroelastic system in any flow regime can be assured if the modal amplitude is kept sufficiently small."), a sectional incremental pressure matrix,

$$[\mathbf{P}] = [\{C_p\}_1, \cdots, \{C_p\}_5] \tag{3.35}$$

can be considered the result of a linear operator acting on the baseline modes. Each column of $[\mathbf{P}]$ is a vector of pressure coefficients acting on each box in the current spanwise section due to the structural deformation corresponding to each baseline mode. The structural deformation, $\mathbf{h}$, of each section can also be given as a combination of the baseline modes with a set of coefficients found through a least-squares fit:

$$\{\mathbf{h}\} = [\Phi]\{\mathbf{a}\} \tag{3.36}$$

where:

$$\{\mathbf{a}\} = [[\Phi^T\Phi]^{-1}\Phi^T]\{\mathbf{h}\} \tag{3.37}$$

and Φ now represents the baseline modal matrix, not the structural modal matrix of Eq (3.2) or velocity potential of Eq (3.4). Using Eq (3.37) to eliminate the least-squares coefficients and combining Eqs (3.35) and (3.36), the linear pressure coefficient operator is defined as the modal AIC:

$$\{C_p\} = [MAIC]\{\mathbf{h}\} \tag{3.38}$$

where:

$$[MAIC] = \mathbf{P}[\Phi^T\Phi]^{-1}\Phi^T \tag{3.39}$$

Finally, the AIC relating the aerodynamic forces to the structural displacement in Eq (3.34) is identified as:

$$[AIC] = [\overrightarrow{n}][AREA][MAIC] \tag{3.40}$$

where $[AREA]$ is the diagonal matrix containing the area of each aerodynamic box. Figure 3.2 diagrams the entire solution procedure for both the linear and nonlinear formulations.

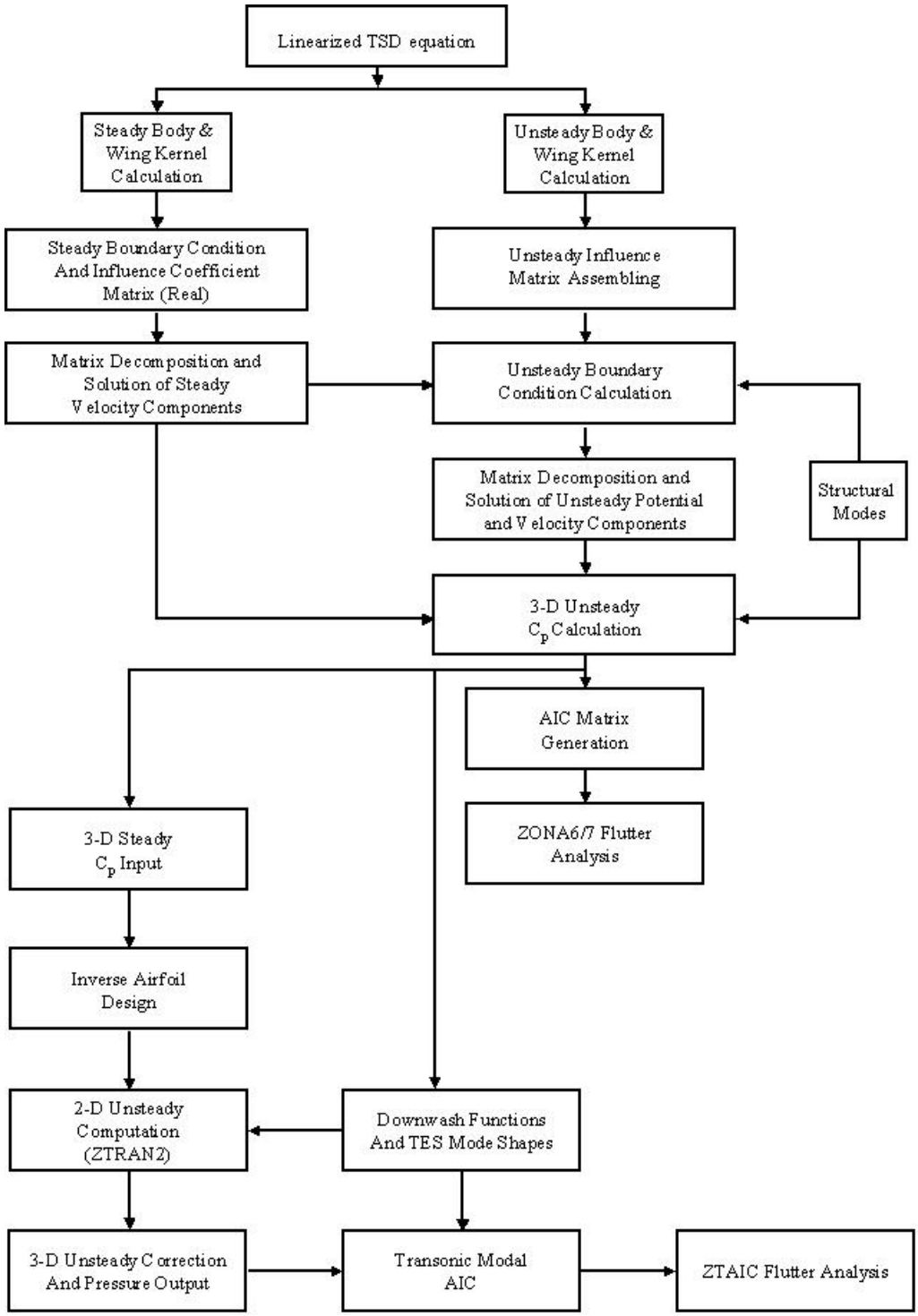

Figure 3.2 Flow Chart for Linear and Nonlinear Flutter Analysis [36]

IV. Methodology

Flutter prediction for the F-16 has always relied on linear analysis without regard to the aerodynamic effects of stores or structural damping. Also, the UFAP methodology is a "non-matched point" analysis. In other words, the freestream mach number is set at .95 Mach and the density is set at sea level. Then, when solving the eigenvalue problem (using the k-method), Eq (3.21), the velocity is varied until the flutter point is found. This may result in an airspeed that, when converted to Mach, does not match the input freestream condition. In order to conduct a matched point analysis, the initial freestream conditions would be varied until both the input condition and the flutter speed matched. Unfortunately, with UFAP, this would be a time consuming process; however, non-matched point analyses have little physical significance. Fortunately, ZAERO automates the match pointing process, and provides the opportunity to include nonlinearities, the aerodynamic effects of stores, and structural damping. This section discusses the process used to validate the structural and aerodynamic models, as well as test the flutter solution's sensitivity to the aforementioned effects.

4.1 Test Cases

Two test cases were selected for this study due to their unique LCO characteristics. Both cases were previously flight tested and analyzed using both UFAP [12] and MSC/NASTRAN [21]. The Lockheed-Fort Worth Company (LFWC) also independently analyzed both configurations. Both cases exhibited LCO from the transonic through supersonic regimes, with one case reaching an LCO flight test limit, while the second case exhibited an LCO "hump" mode (the aircraft was able to fly through the LCO condition).

The two cases, designated SCL007 and SCL008, were configured as shown in Figs 4.1 and 4.2 with the corresponding station/store combinations listed in Table

4.1. Stations are numbered sequentially from one to nine starting from the left wingtip station to the right wingtip station. The LAU-129 is the launch rail used for the AIM-120 Advanced Medium Range Air-to-Air Missile (AMRAAM) and the three letter identifiers after each fuel tank indicate the fuel status of each of the three bladders within the fuel tank (i.e. FEF means Full/Empty/Full or a tank that is half full).

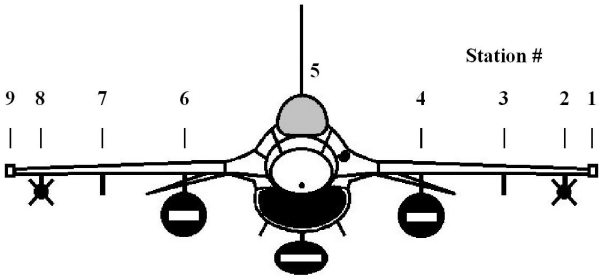

Figure 4.1 SCL007 Configuration

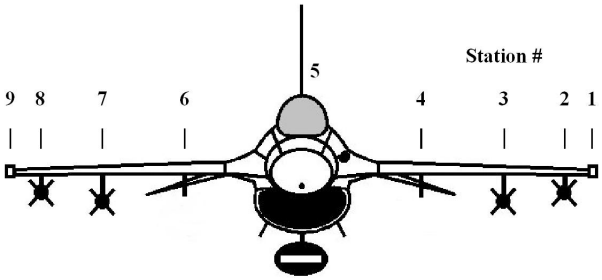

Figure 4.2 SCL008 Configuration

Station	Configuration	
	SCL007	**SCL008**
1, 9	LAU-129	LAU-129
2, 8	LAU-129 + AMRAAM	LAU-129 + AMRAAM
3, 7	Empty	LAU-129 + AMRAAM
4, 6	370 Gal Tank (FEF)	Empty
5	300 Gal Tank (EEE)	300 Gal Tank (EEE)
Wing Fuel	Full	Empty

Table 4.1 Summary of Store Configurations

4.2 Simulation Models

In order to carry out a flutter prediction using ZAERO, two separate models of the aircraft are required. First, a finite-element structural model is required for calculating the normal modes of the aircraft. These modes are then passed to the aerodynamic panel model via a spline matrix, both of which are contained in the ZAERO software.

4.2.1 Structural Models. Many structural finite-element models of the F-16 are being used in various forms of research, however the Lockheed-Fort Worth model is considered to be the most accurate [21]. The models used in this research, one for each of the two configurations investigated (SCL007/008), were the latest updated models available for the F-16 C/D Block 40 aircraft from LFWC (Figs 4.3 and 4.4). A half aircraft model was used due to the symmetry of the store configuration. AFSEO also uses the same models for supersonic flutter analysis in conjunction with UFAP, however UFAP itself uses a different structural model.

This research compares results from three different sources for the linear, subsonic flutter analysis, so it is important to understand the background of each model. While the latest LFWC model is used here, an earlier form of the F-16 model from LFWC, circa 1994, was used as a baseline in tests conducted at AFSEO [12] and by Johnson [21]. The 1994 LFWC model was not available to Johnson, however, so he tuned his own NASTRAN model to match the LFWC test results. Lastly, UFAP does not use a finite-element model (FEM); the input to UFAP consists of modified mass and flexibility matrices generated by the LFWC model.

4.2.2 Aerodynamic Models. A flutter analysis requires compatibility between the aerodynamic panel model and the structural model. In the previous research by LFWC, AFSEO, and Johnson, the same aerodynamic panel model was used. This model consisted simply of the wing planform with tip missile launcher

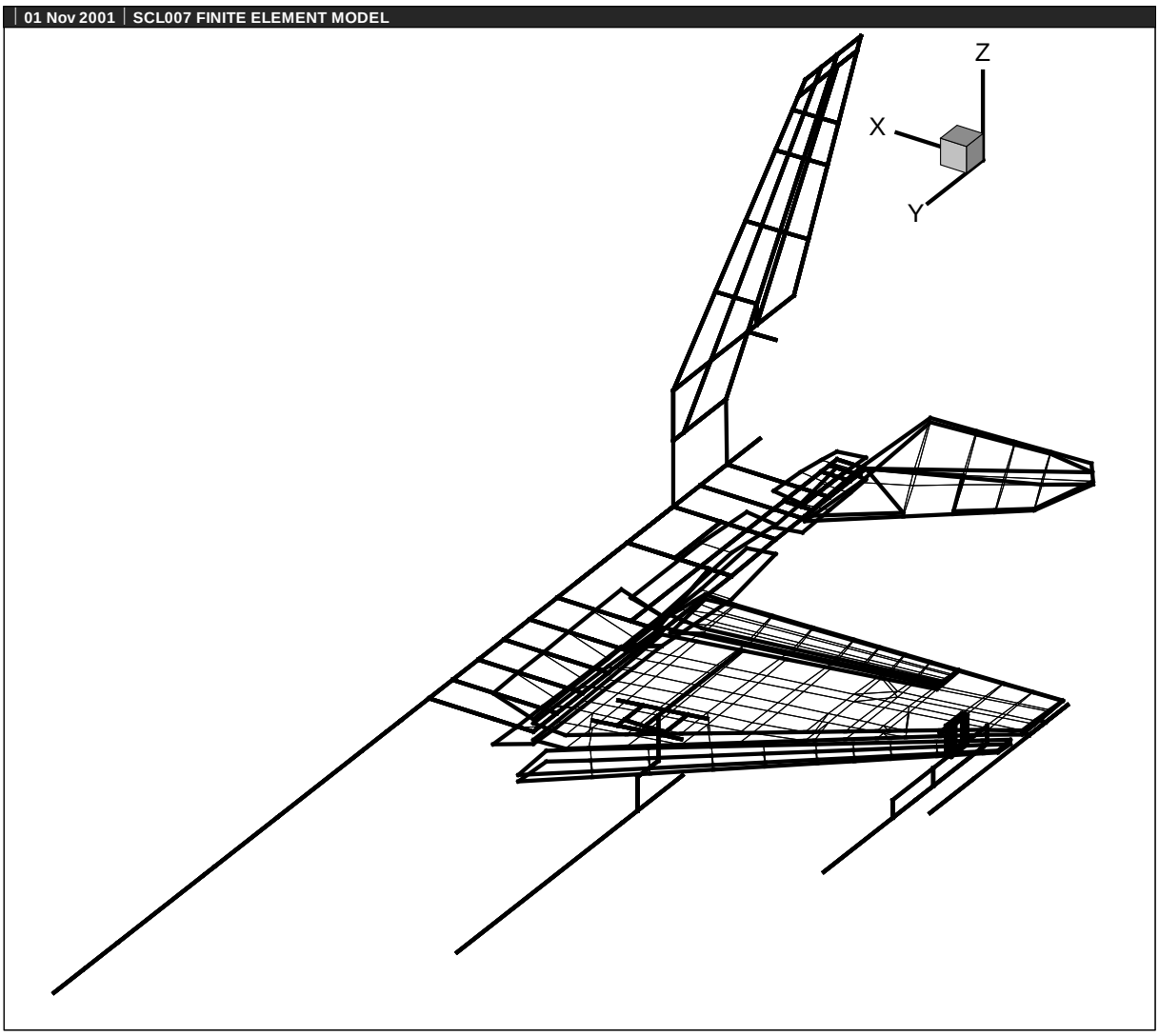

Figure 4.3 SCL007 Finite Element Model

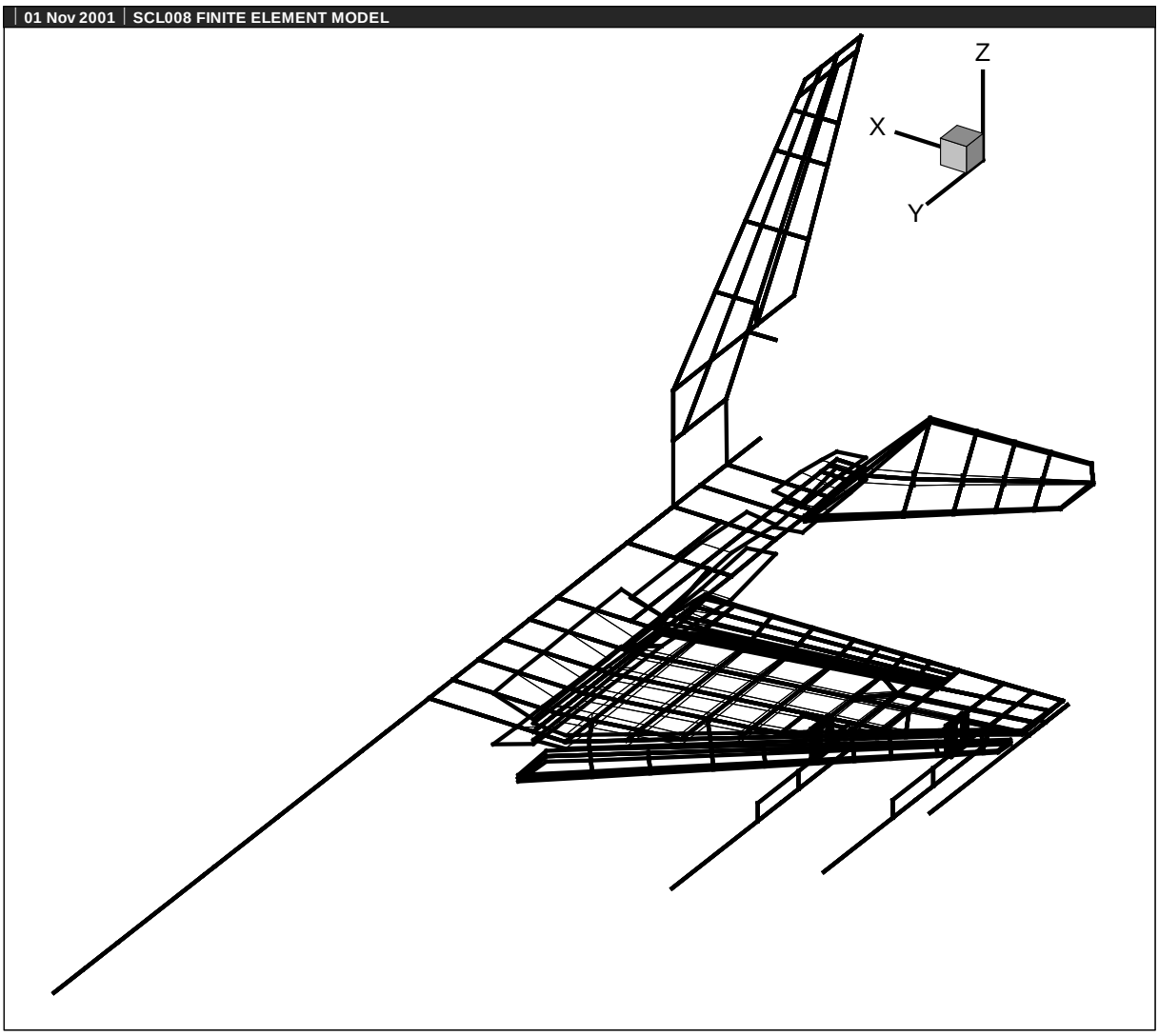

Figure 4.4 SCL008 Finite Element Model

and a portion of the fuselage equal to the length of the wing root, all modeled as flat plate elements for use with the Doublet-Lattice Method (DLM) [1]. The aerodynamic effects of underwing stores was considered to be negligible, and the DLM had no provision for including body-type elements in the flutter analysis. For this thesis, however, determining the aerodynamic effects of underwing stores was one of the goals, therefore the aerodynamic panel model had to include body-type elements and the solution method had to be able to deal with interference effects. ZONA Technologies had already conducted some aeroelastic analyses on the F-16 and had a panel model available for a different store configuration than SCL007/008. This model was modified for the two configurations of interest as shown in Figs 4.5 and 4.6, and once again a half aircraft model was used due to symmetry. The bulk data for the ZAERO code is contained in Appendix C.

4.2.3 Spline Methods. The aerodynamic loads generated by an aircraft in flight cause the structure to deform. The two models, however, are discretized differently, one via the finite-element method (FEM) and the other via an aerodynamic panel method, leading to different degrees-of-freedom for each model. Transferring the aerodynamic loads and forces to the structure and vice versa, requires a method for interpolating between degrees-of-freedom (dof). The method used for this interpolation is called splining. Five splining methods are available in ZAERO for flexibility [37]: a zero displacement spline, infinite plate spline, beam spline, thin plate spline, and rigid attachment. The zero displacement spline imposes a zero displacement condition on an aerodynamic panel and is primarily available for modeling wind tunnel walls. The infinite plate spline is used to interpolate between wing-like elements of the panel model and plate-type elements of the FEM using only the translational dof's. The beam spline is used to interpolate between body-like elements in the panel model and beam-type elements in the FEM, and includes both translational and rotational dof's. The thin plate spline is a 3-D splining method that can relate FEM grid points in 3-D space to either body-like or wing-like elements of

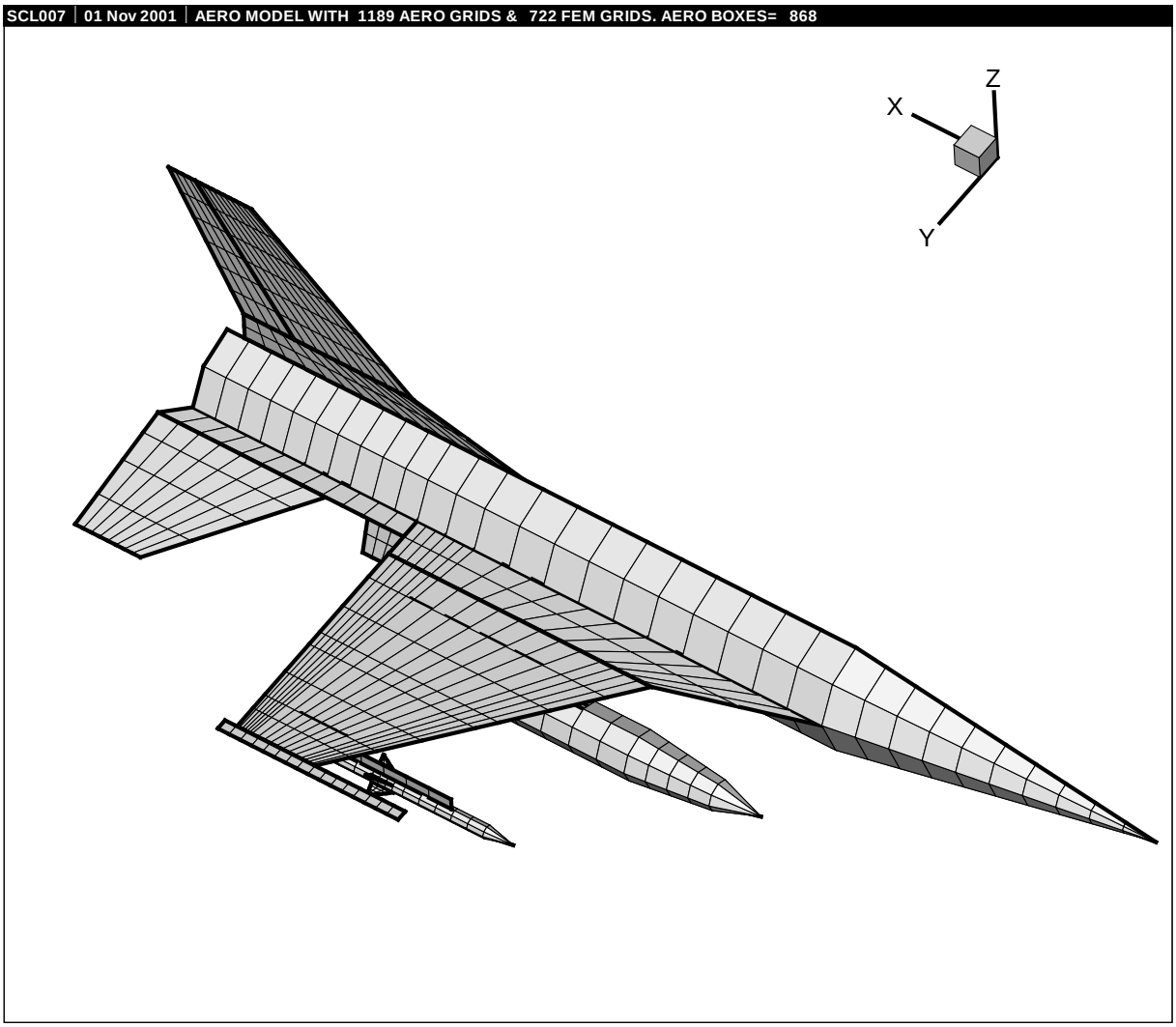

Figure 4.5 SCL007 Aerodynamic Panel Model

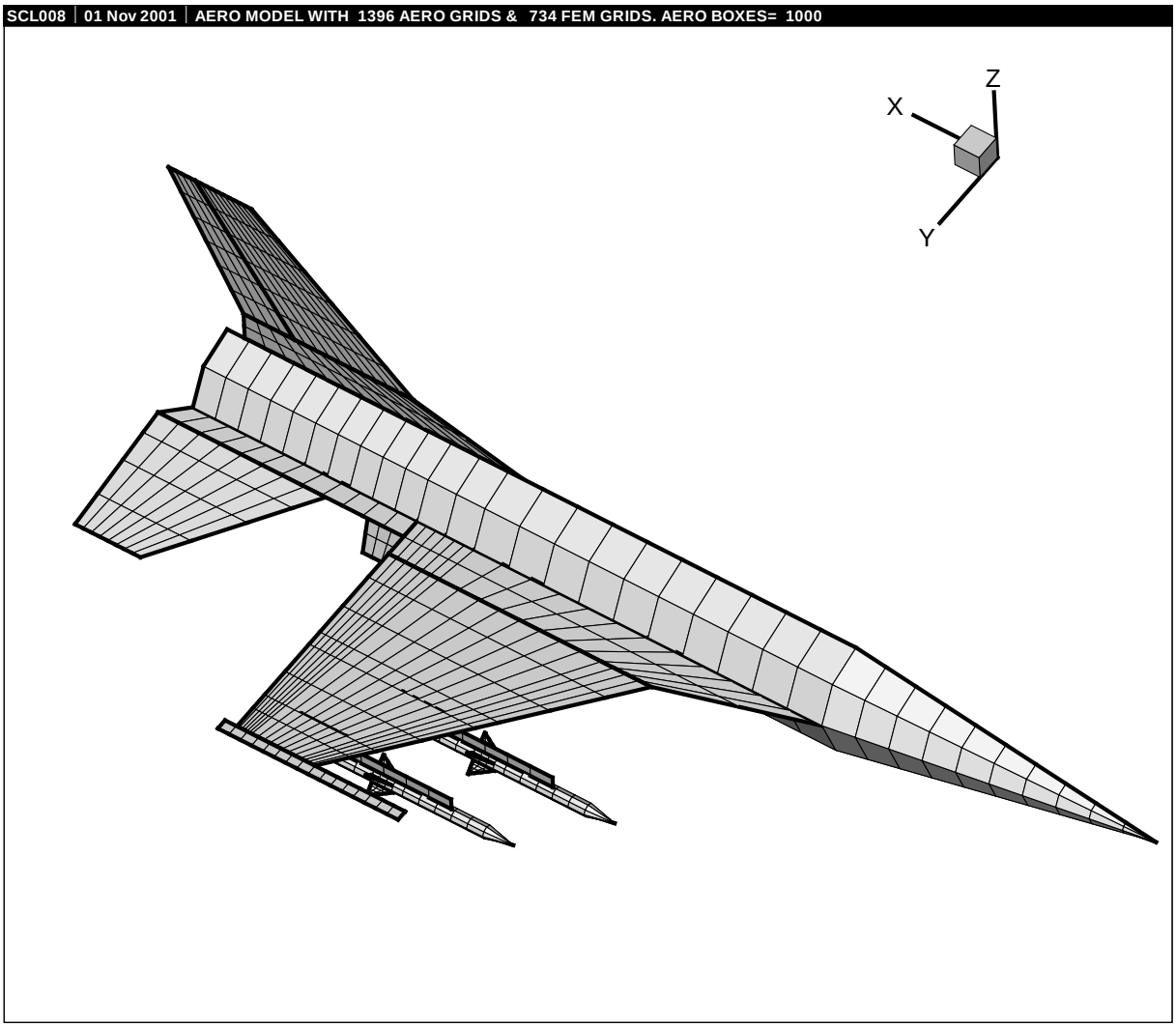

Figure 4.6 SCL008 Aerodynamic Panel Model

the panel model. Lastly, the rigid attachment enables a series of aerodynamic boxes (either wing-like or body-like) to be attached to, and move with, a single structural grid point.

Since splining takes place for each grid point in both models, a matrix is generated which relates the two grid systems. To ensure the overall spline between models is correct, ZAERO provides a means for visualizing the spline by creating a model with both aero and FEM grid points that can be viewed on a number of post-processing packages such as TECPLOT, FEMAP, ANSYS, etc.

4.3 Model Validation

4.3.1 FEM Validation. Before any flutter analysis was run, the structural model needed to be validated against previous research. Although the structural model used in this thesis was deemed to be the most accurate available, the results of a normal modes analysis were compared to the modes found in refs [12] and [21]. In this analysis, both the Modified-Givens and Lanczos eigenvalue extraction methods incorporated into MSC/NASTRAN were used to calculate the natural frequencies of each mode under both symmetric and antisymmetric boundary conditions. A cutoff of 25 Hz was used to limit the number of modes generated (modes above 25 Hz were assumed to contribute little to the flutter mode, as evidenced in ref [5]).

4.3.2 Panel Model Validation. Similar to the FEM, the panel model needed to be validated for convergence of the mesh. This study was conducted on the SCL007 configuration without the stores modeled aerodynamically (Fig 4.7). For simplicity, only the wing panel and horizontal tail panel meshes were adjusted in the study, since the wing is typically the main contributor to aircraft flutter. The horizontal tail was also adjusted because the spanwise divisions of the horizontal tail must match those of the wing. The mesh was refined by a factor of two in first the spanwise, then chordwise direction and solved using the ZONA6/7 linear

method by holding altitude constant at sea level and match pointing across Mach numbers. A tolerance level of two percent in flutter speed and one percent in flutter frequency was set to define convergence of the solution. As an additional check of the mesh, the procedure outlined in chapter 5.4.1 of the ZAERO User's Manual [37] was accomplished to determine the Mach and reduced frequency range over which the mesh was valid.

4.4 ZONA6/7 Analysis

With the validation of both the structural and aerodynamic models complete, the next step was to begin the linear analysis to correlate ZAERO with previous research ([12], [21]). First, a matched point analysis of SCL007, under antisymmetric boundary conditions, was accomplished for three cases with the external stores modeled aerodynamically: sea level, 5000 feet, and 15000 feet, between 0.5 and 1.1 Mach. Antisymmetric boundary conditions were imposed on all flutter analyses conducted in this thesis, since flutter appears as a predominantly antisymmetric condition [4, 28]. Sensitivity to aerodynamic modeling of the stores was accomplished at sea level by first removing the store panel models (Fig 4.7) and accomplishing a matched point analysis between the same Mach numbers as used for the fully modeled cases. Stores were then added sequentially to determine effects due to individual stores as well as store locations (the stores were still accounted for in the aerodynamic model via the structural modes, generalized mass and stiffness matrices from the structural model). Once the matched point solution was found, a non-matched point run was conducted at the match point to generate the V-g and V-ω plots, as well as an animation of the flutter mode on the aerodynamic panel model. The same procedure was followed for SCL008 without conducting a store sensitivity analysis.

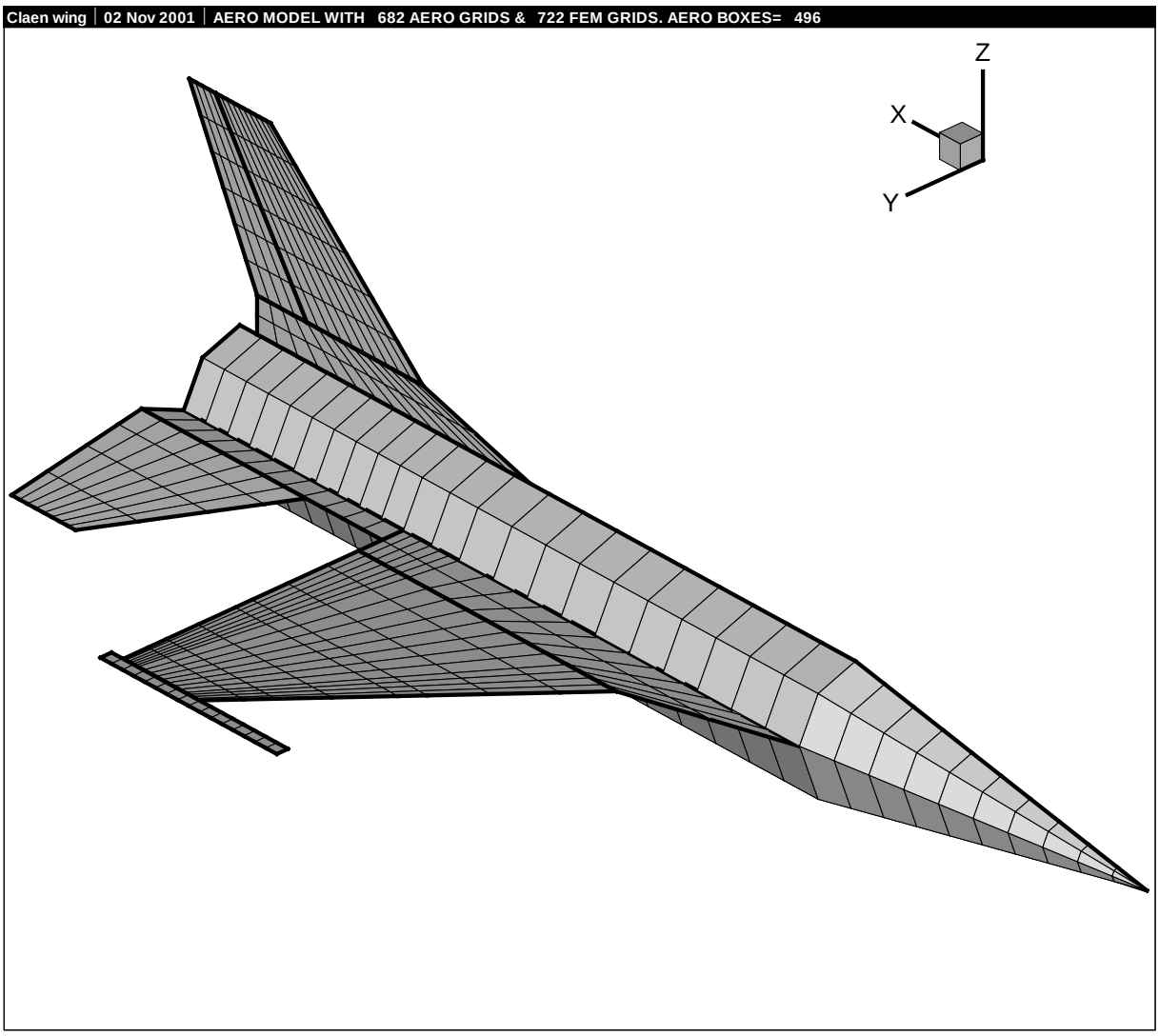

Figure 4.7 Clean Wing Aerodynamic Panel Model

4.5 ZTAIC Analysis

Following the linear analysis, nonlinear effects were studied through the use of ZAERO's ZTAIC module. Steady C_p data is required as a function of Mach number in the case of rigid C_p's; when flexible C_p data is used, it must be generated at specific Mach number/density pairs. This C_p data is required for each wing-like element, however, to reduce the complexity of the model and the amount of C_p data required, only pressure data for main wing was used; the elements that did not have pressure data input reverted to linear analysis. Again, since the wing is the primary lifting surface involved in flutter, the effects of a linear analysis on the remaining portion of the model were considered to be negligible. For these cases, what amounted to an altitude match point analysis was conducted. By fixing the Mach number and varying the altitude, only one set of steady C_p data was required. The objective was to find where the nonlinear analysis predicted flutter to occur at sea level, 5000 feet, and 15000 feet in the case of SCL007, and at sea level, 5000 feet, and 10000 feet in the case of SCL008. Again, once the matched point solution was found, a non-matched point run was conducted at the match point to generate the V-g and V-ω plots, as well as an animation of the flutter mode on the aerodynamic panel model. The same procedure was used for SCL008, however, only rigid C_p data was investigated.

4.5.1 Sensitivity to C_p Type. The C_p data used in this thesis was provided by Dr. Reid Melville, AFRL/VAAC, from an inviscid, fully-implicit CFD code. Dr. Melville provided both rigid and flexible C_p data at each Mach number or Mach number/density pair. The data generated by Dr. Melville comes from an F-16 model configured with an empty tip missile launcher and no underwing stores. To generate flexible data, the symmetric eigenvectors calculated in the normal modes analysis must be input to the system (this accounts for any underwing stores inertially and structurally). Then, for a given freestream Mach number/density pair, the model is allowed to deform under air loads until a converged, deflected position is found.

The C_p data is then extracted for this condition. In the case of rigid C_p's, no modal information is required, and the solution is independent of density. Before this data could be used however, it had to be interpolated from the fine mesh used in the CFD solution to the coarse mesh used in the ZTAIC module. ZTAIC requires data at the center of each spanwise strip in the aerodynamic model. For example, the models used in this research had nine spanwise divisions on the wing, resulting in eight strips. The CFD mesh, on the other hand, used 61 divisions in the flow direction (not purely x-direction flow, the CFD mesh allowed for spanwise components to the flow). A MATLAB code was written to interpolate the CFD data to data that could be used by ZAERO and is included in Appendix D. Figures 4.8 and 4.9 depict CFD and interpolated pressure distributions for both rigid and flexible C_p data (larger C_p plots are included in Appendix B for reference).

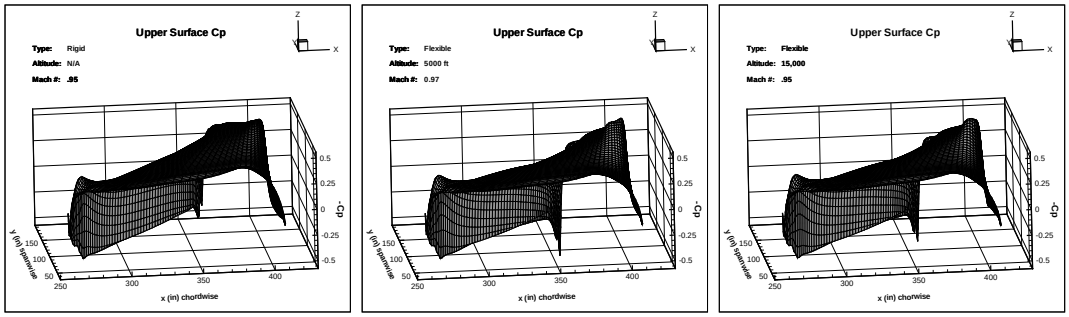

Figure 4.8 CFD Upper Surface Pressure Distributions

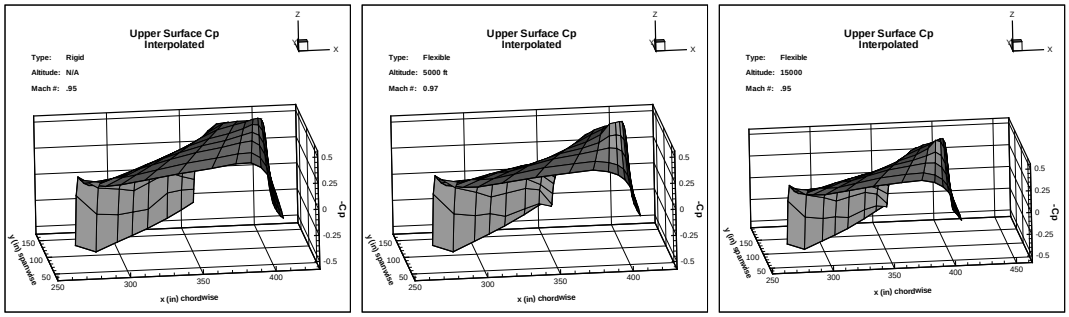

Figure 4.9 Interpolated Upper Surface Pressure Distributions

In order to investigate the sensitivity of the solution to C_p type, altitude matched point runs were conducted at sea level, 5000 feet, and 15000 feet for SCL007, and sea level, 5000 feet, and 10000 feet for SCL008 using both rigid and flexible data.

4.5.2 Sensitivity to Structural Damping. The last analysis undertaken was to determine the sensitivity of the flutter solution to structural damping. ZAERO includes the effects of representative amounts of aerodynamic damping (ranging from 0.5 to 4.0% of critical damping) in every flutter analysis in the form of a table in the output file. To calculate this effect, ZAERO simply looks for the flutter crossing at some percentage of g, i.e. to determine the effect of 1% aerodynamic damping, instead of finding where the damping curve crosses 0%, the speed/frequency are calculated where the damping curve crosses 1%.

It was thought that this method was not capturing the effects of structural damping however, since structural damping was not thought to be simply an additive effect. To test this, ZAERO allows for inclusion of damping through the use of a modal damping table [37]. Through this table, modal damping values are set as a function of frequency. Three types of damping values are available: CRIT (a fraction of critical damping), g (structural damping), or Q (amplification/quality factor) where:

$$\begin{aligned} CRIT &= \frac{C}{C_0} \\ g &= 2\left(\frac{C}{C_0}\right) \\ Q &= \left\{ \begin{array}{c} \frac{1}{\left(\frac{2C}{C_0}\right)} \\ \frac{1}{g} \end{array} \right\} \end{aligned}$$

For the damping sensitivity, values of g between 0.5 and 2.5% were set across the modal frequency range, 0 to 25 Hz, and a flutter analysis was accomplished. The data were compared by matching the percentage of aerodynamic damping from

the flutter prediction without structural damping included, to the 0% aerodynamic damping column from the flutter prediction for a set percentage of structural damping. For example, when g was set to 1%, the data for 1% aero damping from an analysis without g included was compared to the data for 0% aero damping from an analysis with 1% g included.

V. Results and Analysis

This chapter presents the results and analysis of both the linear and nonlinear flutter analyses of F-16 configurations SCL007 and SCL008 using the ZAERO method. Section 5.1 details the validation of the new LFWC finite-element model (designated L-model) with the old LFWC model (Baseline), UFAP model, and the tuned F-16 model from ref [21] (J-model). The convergence study on the panel model of configuration SCL007 is briefly discussed in section 5.2. Flutter analysis results begin in section 5.3, where the ZAERO linear results are presented along with flutter solution sensitivity to aerodynamic store modeling. Nonlinear results, including sensitivities to steady C_p type and structural damping are presented in section 5.4. All results, both linear and nonlinear, are compared to the linear analyses of refs [12, 21]. The linear and nonlinear predictions are then compared with flight test data from the original flight test conducted in 1992 [5]. Lastly, an additional section discusses results of structural tuning on the SCL007 FEM conducted after the bulk of this study was completed.

5.1 FEM Validation

The finite-element model delivered by AFSEO for this analysis is an update of the LFWC model used by Denegri [12] and represents the most current F-16 FEM available. A normal modes analysis was accomplished using both the Lanczos and Modified-Givens eigenvalue extraction methods to ensure accuracy of the model with previous versions. By contrast, UFAP uses the Power method, while Johnson used the Modified-Givens method for his analysis. No difference, however, was found in the natural frequencies between the two extraction methods. Results for both symmetric and antisymmetric modal analyses are presented for the first 10 modes for SCL007 and the first nine modes for SCL008. Since the flutter mode is generally

composed of the first few natural modes, this discussion will focus on the lower frequency modes.

5.1.1 SCL007. The results for both the symmetric and antisymmetric boundary conditions are shown in Tables 5.1 through 5.4. In the symmetric case, the UFAP model matches the baseline model quite well for the first four modes, as does the L-model with the exception of mode 1, which is 6% stiffer than the baseline. Also, with the exception of mode 1, all of the low frequency modes (modes 1-4) of the L-model correlate better than the J-model. Since mode 1, which is first wing bending, is stiffer than the baseline model, this could lead to a higher predicted flutter speed if mode 1 plays a dominant role. The higher frequency modes all correlate quite well with the exception of the modes which contain first wing bending. These modes show the greatest discrepancies from the baseline, all being stiffer.

	Description				
Mode	**Wing**	**Sta 1**	**Sta 2**	**Sta 4**	**Remarks**
1	1^{st} bending				
2	1^{st} torsion	pitch	pitch	pitch	
3	2^{nd} torsion	pitch	pitch	yaw	
4	1^{st} torsion	pitch	yaw	yaw	sta 2/4 out of phase
5	2^{nd} bending		yaw		
6	1^{st} bending		yaw	yaw	sta 2/4 out of phase, 2^{nd} fuselage bending
7	2^{nd} bending		yaw	yaw	sta 2/4 out of phase
8	1^{st} torsion	pitch			
9	slight 1^{st} bending				horiz tail bending
10	1^{st} bending		yaw	yaw	sta 2/4 in phase, 3^{rd} fuselage bending, ht bending

Table 5.1 SCL007 Symmetric Mode Shapes

Mode	**Frequency (Hz)**				**Comparison**		
	Baseline	**UFAP**	**J-model**	**L-model**	**UFAP / Baseline**	**J-model / Baseline**	**L-model / Baseline**
1	4.92	4.95	5.00	5.22	1.006	1.016	1.061
2	6.87	6.90	6.78	6.90	1.004	0.987	1.004
3	7.79	7.85	7.71	7.73	1.008	0.990	0.992
4	8.11	8.11	8.01	8.07	1.000	0.988	0.995
5	9.18	8.89	9.20	9.22	0.968	1.002	1.004
6	10.87	10.95	10.56	10.96	1.007	0.971	1.008
7	12.74	12.46	12.70	12.85	0.978	0.997	1.009
8	14.86	14.69	14.58	14.62	0.989	0.981	0.984
9	17.10	17.88	17.88	18.18	1.046	1.046	1.063
10	18.18	18.55	18.48	18.80	1.020	1.017	1.034

Table 5.2 Normal Mode Analysis SCL007 Symmetric

In the antisymmetric case, there is much better agreement with the baseline model for both UFAP and the L-model. Again the greatest difference in the L-model is among the first wing bending modes, however it only amounts to 1.7% stiffer in the worst case. The L-model also agrees with both UFAP and the baseline better, in general, than the J-model which appears to be more flexible than either the L-model or baseline.

Mode	Description				
	Wing	**Sta 1**	**Sta 2**	**Sta 4**	**Remarks**
1	bending/torsion	pitch	yaw	yaw	sta 2/4 out of phase
2	1^{st} torsion	pitch	yaw		
3	slight bending		yaw	pitch/yaw	
4	1^{st} bending		yaw	pitch	sta 2 yaw in phase w/ vert tail
5	1^{st} bending		yaw	pitch	sta 2 yaw out of phase w/ vert tail
6	slight bending	pitch	yaw		vert tail bending
7	2^{nd} bending	pitch	yaw	yaw	sta 2/4 out of phase
8	1^{st} torsion				
9	2^{nd} bending	pitch	yaw	yaw	sta 2/4 out of phase, vert tail bending
10	2^{nd} bending	pitch	yaw	yaw	sta 2/4 in phase, horiz/vert tail bending

Table 5.3 SCL007 Antisymmetric Mode Shapes

Mode	Frequency (Hz)				Comparison		
	Baseline	**UFAP**	**J-model**	**L-model**	**UFAP / Baseline**	**J-model / Baseline**	**L-model / Baseline**
1	6.66	6.72	6.47	6.62	1.009	0.971	0.994
2	7.19	7.25	7.26	7.30	1.008	1.010	1.015
3	8.07	8.09	7.97	8.01	1.002	0.988	0.993
4	8.44	8.45	8.47	8.58	1.001	1.004	1.017
5	9.58	9.26	9.51	9.59	0.967	0.993	1.001
6	12.46	12.45	12.37	12.57	0.999	0.993	1.009
7	13.40	13.09	12.83	13.50	0.977	0.957	1.007
8	14.93	14.90	14.31	14.70	0.998	0.958	0.985
9	15.83	15.72	14.78	15.92	0.993	0.934	1.006
10	17.34	17.42	17.26	17.44	1.005	0.995	1.006

Table 5.4 Normal Mode Analysis SCL007 Antisymmetric

5.1.2 SCL008. For the symmetric case, UFAP matched modes 1 and 2 well, but was too flexible in modes 3 and 4 (the results for both the symmetric and antisymmetric boundary conditions are shown in Tables 5.1.2 through 5.1.2). The J-model and L-model were nearly equal for the first four modes and very close to the baseline configuration. For the remaining modes, UFAP was, in general, slightly stiffer whereas both the J-model and L-model were more flexible. There is one glaring

discrepancy between all the models with the baseline. Mode 9 (mostly horizontal tail bending) is stiffer in all three models (similar to SCL007) which suggests that the original model's horizontal tail was too flexible.

Mode	Description				
	Wing	**Sta 1**	**Sta 2**	**Sta 3**	**Remarks**
1	1^{st} bending				
2	1^{st} torsion				
3	2^{nd} bending		yaw	yaw	sta 2/3 out of phase
4			yaw	yaw	sta 2/3 in phase
5	2^{nd} torsion		yaw	pitch	sta 2/3 out of phase, 2^{nd} fuselage bending
6	2^{nd} torsion		pitch	pitch	sta 2/3 out of phase, 2^{nd} fuselage bending
7	2^{nd} bending	yaw			
8	1^{st} torsion		yaw		3^{rd} fuselage bending, horiz tail bending
9	2^{nd} bending		yaw		3^{rd} fuselage bending, horiz tail bending
10	2^{nd} bending		yaw	yaw	sta 2/3 out of phase, 3^{rd} fuselage bending, ht bending

Table 5.5 SCL008 Symmetric Mode Shapes

Mode	Frequency (Hz)				Comparison		
	Baseline	**UFAP**	**J-model**	**L-model**	**UFAP / Baseline**	**J-model / Baseline**	**L-model / Baseline**
1	4.99	5.00	5.06	5.08	1.002	1.014	1.018
2	7.09	7.20	7.07	7.07	1.016	0.997	0.997
3	9.16	8.87	9.20	9.19	0.968	1.004	1.003
4	9.50	9.13	9.43	9.43	0.961	0.993	0.993
5	10.58	10.67	10.27	10.54	1.009	0.971	0.996
6	11.59	11.72	11.28	11.45	1.011	0.973	0.988
7	14.32	14.39	14.17	14.11	1.005	0.990	0.985
8	16.87	17.96	18.11	18.16	1.065	1.074	1.076
9	18.19	18.48	18.50	18.46	1.016	1.017	1.015

Table 5.6 Normal Mode Analysis SCL008 Symmetric

The antisymmetric case is very similar to the symmetric. Once again, Mode 9 and, in this case, Mode 10 are much stiffer than the baseline. These modes are the primary modes for horizontal tail bending. Through the first ten modes, the L-model is, in general, stiffer than the baseline for the SCL007 configuration and more flexible for the SCL008 configuration. However, for the low frequency modes, both cases are very similar to the baseline. Since the lower frequency modes tend to dominate the flutter mode, a similar linear flutter analysis should produce similar results.

Mode	Description				
	Wing	**Sta 1**	**Sta 2**	**Sta 3**	**Remarks**
1	1^{st} torsion				
2	1^{st} bending		yaw	yaw	sta 2/3 in phase
3	2^{nd} bending		yaw	yaw	sta 2/3 out of phase
4	1^{st} bending		yaw	yaw	sta 2/3 in phase
5	2^{nd} torsion		pitch	pitch	sta 2/3 out of phase
6	1^{st} torsion		yaw		
7	1^{st} torsion		yaw	yaw	sta 2/3 out of phase
8	1^{st} torsion		yaw	yaw	2^{nd} fuselage yaw bending
9	2^{nd} bending		yaw		horiz tail bending
10	2^{nd} bending		yaw	yaw	sta 2/3 out of phase, horiz tail bending

Table 5.7 SCL008 Antisymmetric Mode Shapes

Mode	Frequency (Hz)				Comparison		
	Baseline	**UFAP**	**J-model**	**L-model**	**UFAP / Baseline**	**J-model / Baseline**	**L-model / Baseline**
1	7.03	7.16	7.01	7.02	1.018	0.997	0.999
2	7.98	8.01	8.15	8.16	1.004	1.021	1.023
3	9.39	9.06	9.35	9.35	0.965	0.996	0.996
4	9.68	9.36	9.55	9.57	0.967	0.987	0.989
5	11.53	11.66	11.30	11.35	1.011	0.980	0.984
6	12.89	12.98	12.71	12.88	1.007	0.986	0.999
7	14.86	14.79	13.34	14.58	0.995	0.898	0.981
8	15.30	15.42	14.67	15.45	1.008	0.959	1.010
9	17.02	17.69	17.57	17.60	1.039	1.032	1.034
10	18.65	19.64	20.48	20.50	1.053	1.098	1.099

Table 5.8 Normal Mode Analysis SCL008 Antisymmetric

5.2 Convergence Study

Similar to the finite-element models, the aerodynamic panel model for this study had to be checked to ensure convergence of the mesh. Table 5.9 displays the results of the constant altitude, Mach number match point solutions at 0% structural/aerodynamic damping using ZONA6/7. It was expected that refining the mesh in the chordwise direction would result in a different solution, whereas the spanwise direction should not make much difference. The chordwise mesh, however, was already relatively fine with 21 divisions and, after doubling the number of cuts, only showed a 0.86% change in flutter speed. The spanwise direction was not as fine, though. It had only nine divisions and when the mesh was doubled, the solution changed by 0.38% in flutter speed. The differences in frequency were negligible at 0.01% and 0.03% respectively. This was within the criteria established for convergence (2% in speed, 1% in frequency), therefore the original mesh was considered converged. The convergence of the mesh was also verified using the criteria defined in

Case	**Description**	**Flutter Speed (fps)**	**% Change**	**Flutter Frequency (Hz)**	**% Change**
1	Baseline SCL007 w/o aero stores	1068.5		7.025	
2	2x chordwise cuts	1073.2	0.38	7.026	0.01
3	2x spanwise cuts	1078.2	0.86	7.023	-0.03

Table 5.9 Convergence Study Results

chapter 5.4.1 of the ZAERO User's Manual [37]. This criteria was used to determine the maximum chord length for each aerodynamic box of the mesh as a function of Mach number and reduced frequency. For the mesh used in this thesis, the largest chord length of a wing box was 9.4 inches. Table 5.10 shows that for all Mach numbers below 0.98 and above 1.02 the mesh was converged.

5.3 ZONA6/7 Linear Analysis

Once the models had been validated, the linear analysis using ZONA6/7 was accomplished for comparison with Denegri [12] and Johnson [21], as well as to provide a benchmark for the nonlinear analysis. In the comparisons, it must be noted that

Mach	k	Max Box Chord Length (in)
0.90	0.222	33.7
0.92	0.219	30.1
0.94	0.217	26.6
0.96	0.208	13.0
0.98	0.204	6.44
1.02	0.196	6.31
1.04	0.192	12.5
1.06	0.188	18.6
1.08	0.185	24.6
1.10	0.181	30.4

Table 5.10 Solution Convergence Criterion

the data from LFWC, UFAP, and the J-model are all non-matched point analyses. In the case of the LFWC model, the input conditions were 0.9 Mach at sea level, whereas for UFAP and the J-model, input conditions were 0.95 Mach at sea level. By comparison, all the data for the L-model were matched point calculations at various altitudes depending on configuration. Both loading conditions were run at sea level to provide a comparison to previous data, as well as at altitudes matching those of the flight test. Since LCO in the F-16 is known to be primarily an antisymmetric phenomenon [4, 28], only the antisymmetric cases were investigated.

5.3.1 SCL007. The L-model flutter results for SCL007 at sea level were very similar to those of the J-model; both were higher than the predictions using UFAP or the LFWC model (Table 5.11), and both overpredicted the LCO onset speed observed in flight test (Table 5.12). The discrepancy between the L-model and UFAP/LFWC models can be explained partly by the latter two not being match point solutions, and partly by the fact that the flutter engineers at AFSEO are constantly adjusting their model to correlate to flight test, producing a more refined structural model. Better agreement was expected though, given that the structural modes were very close to those of the UFAP/LFWC models. Obviously this discrepancy cannot be attributed to the structural model alone (in fact, the J-model was, in general, more flexible than the L-model, yet both produced similar flutter results using two different methodologies). A more probable source of the discrepancy involves

the panelling method and solution technique. UFAP uses the DLM to generate subsonic AIC's, and the Laguerre iteration technique (a variation of the k-method) to solve for the complex eigenvalues [12]). The J-model also used the same panelling scheme, however it was solved using the p-k method available in MSC/NASTRAN. Lastly, the L-model panelling scheme was much different, incorporating body elements and interference effects in a higher order method than DLM, and used the g-method to compute the complex eigenvalues.

Model	**Mach**	**Flutter Speed (KCAS)**	**Flutter Frequency (Hz)**
L-model	0.90	595	6.9
J-model	0.95	630	7.0
UFAP	0.73	481	7.1
LFWC	0.65	428	7.1

Table 5.11 SCL007 Flutter Results (Sea Level, 0% Damping)

	Flutter Speed (Mach)			**Flutter Frequency (Hz)**		
Altitude (ft)	**Flight Test**	**L-model**	**% Difference**	**Flight Test**	**L-model**	**% Difference**
5,000	0.80	0.95	15.8	6.8	6.9	1.5
15,000	0.90	1.09	21.1	6.8	6.9	1.5

Table 5.12 SCL007 Flutter Flight Test Comparison

The critical mode for this case was composed primarily of mode 2, the first wing torsion mode, and mode 1, a combination of first wing bending and torsion (Table 5.13). Modes 1 and 2 show yaw at station 2, while only mode 1 shows yaw additionally at station 4. This matches well with the actual flutter mode, Fig 5.3, which appears as primarily torsion with very little yaw at station 4 as compared to station 2. The V-g/V-ω plots show a relatively benign crossing at 0.9 Mach, with modes 1 and 2 beginning to coalesce, but not actually merging until well past the flutter condition (Fig 5.1).

The effects of altitude/airspeed on flutter mode composition are depicted in Table 5.13. As altitude/airspeed increase, the modal composition changes from

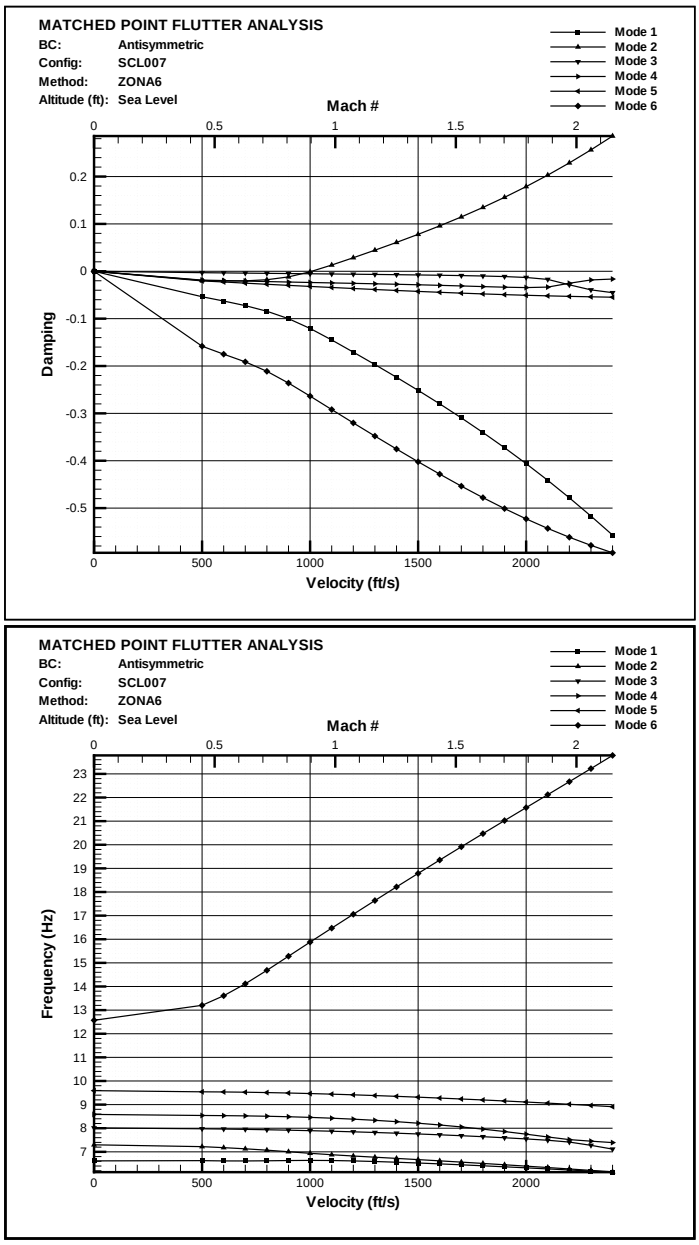

Figure 5.1 SCL007 Flutter Damping and Frequency Curves (Sea Level, 0% Damping)

primarily mode 2 to primarily mode 1 at 15,000 feet. This effect may be related more to the Mach crossing than to altitude changes. Also of note in the V-g/V-ω plots is the steeper crossing of the unstable damping mode, and the coalescence of modes 1 and 2 occurring nearer the flutter point (Fig 5.2). The changes in the flutter

mode are subtle and difficult to see with a static image presented in Fig 5.3, though it is possible to see that the wing node line moves forward at the wingtip and the station 2 AMRAAM displays less yaw.

Altitude	**Modal Participation (%)**									
(ft)	**1**	**2**	**3**	**4**	**5**	**6**	**7**	**8**	**9**	**10**
0	26.8	68.0	0.1	1.9	1.5	0.6	0.0	0.6	0.0	0.3
5,000	29.4	65.8	0.0	1.7	1.5	0.5	0.0	0.6	0.0	0.3
15,000	64.3	30.4	0.1	1.3	1.4	1.0	0.0	0.6	0.3	0.6

Table 5.13 SCL007 Flutter Mode Participation Factors (0% Damping)

5.3.2 SCL008. For the SCL008 loading, the comparison with UFAP/LFWC were opposite that seen with SCL007; the L-model prediction was at a lower speed than those of UFAP/LFWC, while the J-model once again was similar to the L-model. All of the predictions, however, overestimated the flutter onset speed seen during flight test by a significant margin. The sea level prediction data is shown in Table 5.14. Again, the disparity in results between the L/J-models and the UFAP/LFWC models cannot be explained by the structural model alone since the modes agree to within 3% for all modes except mode 10, and may be the result of differences in solution methods and not match pointing the solutions.

The flutter mode at sea level in this case is composed primarily of mode 1, first wing torsion, followed by mode 2, first wing bending and out of phase yaw (and pitch) among stations 2 and 3 (Table 5.15). The influence of mode 1 increases with increasing altitude to 10,000 feet. Although it is hard to visualize in a static image (Fig 5.4), the flutter mode shows this combination well, with the missiles being more out of phase in the pitch axis than in the yaw axis.

The flight test results for this configuration are very interesting. At both altitudes investigated, this configuration showed a "hump" mode, i.e. the aircraft was able to fly through the LCO condition. Also, the onset and termination of LCO occur at roughly the same airspeeds (termination of LCO occurred between 1.25

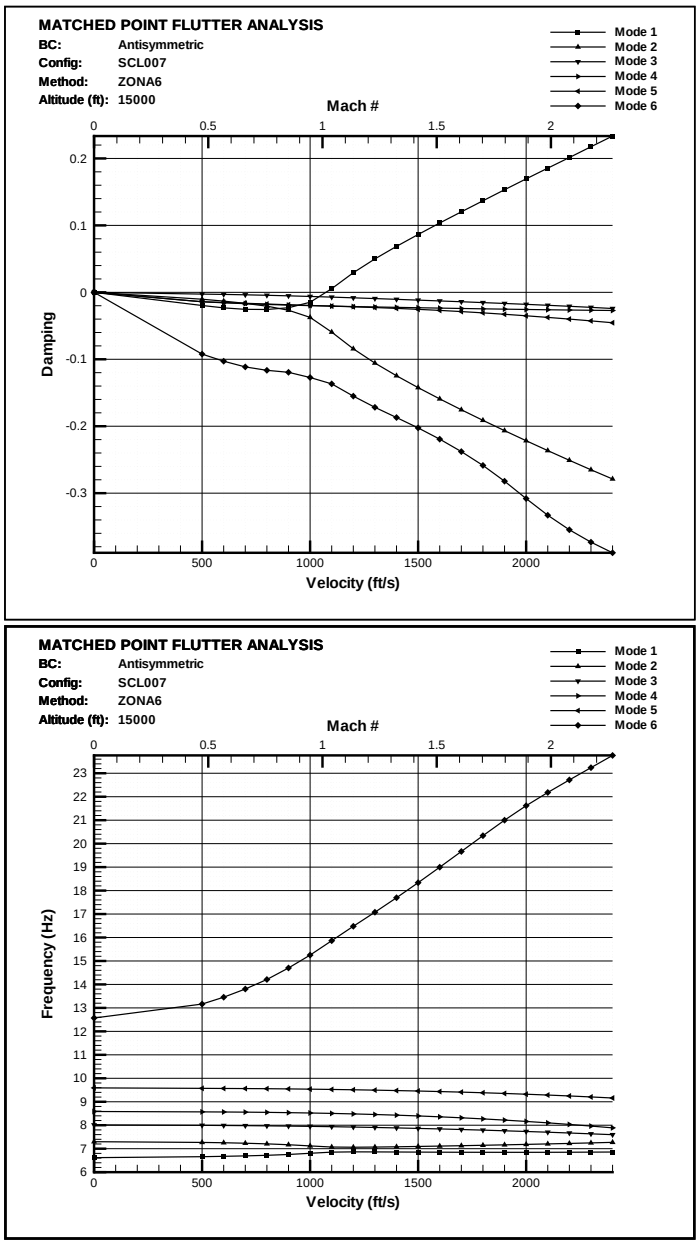

Figure 5.2 SCL007 Flutter Damping and Frequency Curves (15,000 ft, 0% Damping)

and 1.30 Mach) for both altitudes investigated. Typically, as altitude increases, the flutter onset speed increases, which is indicated in the results of Table 5.16. The appearance of the hump mode should be visible in the V-g/V-ω plots of Fig 5.5 and Fig 5.6, and although at 10,000 feet the V-g plot of the critical mode appears

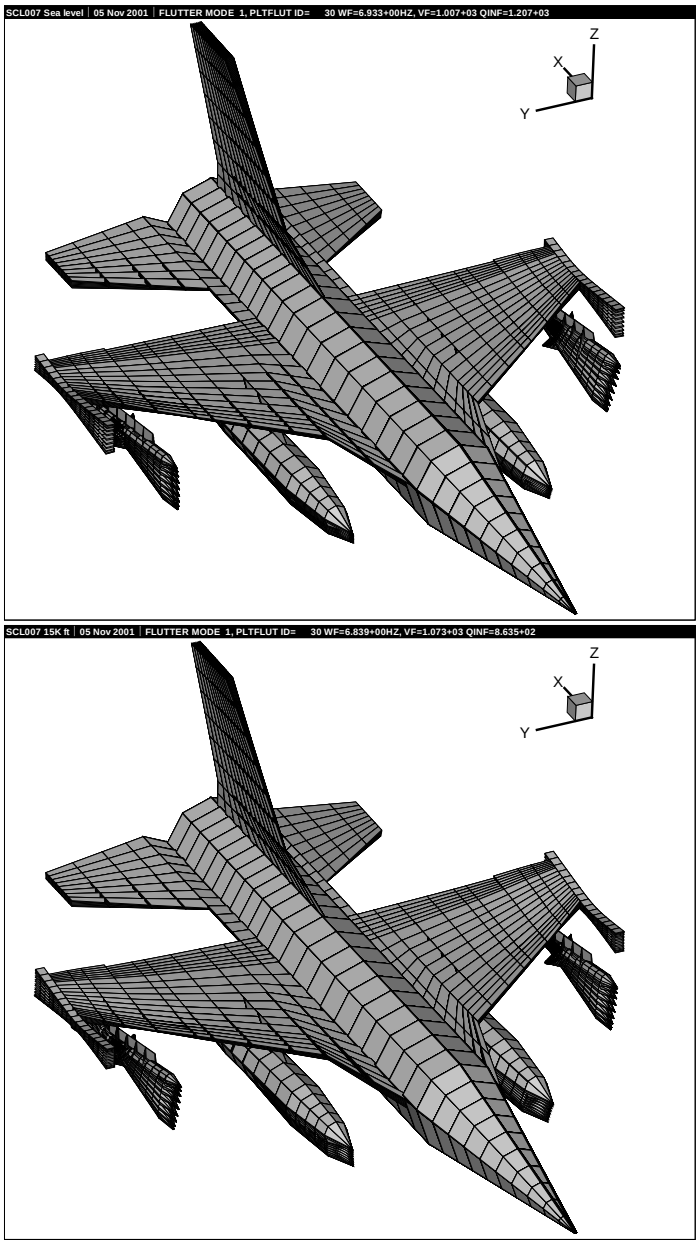

Figure 5.3 SCL007 Flutter Mode (Sea Level & 15,000 ft, 0% Damping)

as if it may begin to show a hump mode, the plots do not show definitively the presence of a hump mode. Another indicator of a possible hump mode in the V-g plots is a relatively shallow zero crossing for the critical mode. This was seen in the SCL007 plots, but for SCL008 the opposite is true, especially at 10,000 feet. The zero crossing is more abrupt than SCL007 at sea level and very rapid at 10,000 feet;

Model	Mach	Flutter Speed (KCAS)	Flutter Frequency (Hz)
L-model	1.18	784	7.6
J-model	1.13	748	7.9
UFAP	1.36	900	7.8
LFWC	1.31	869	7.8

Table 5.14 SCL008 Flutter Results (Sea Level, 0% Damping)

Altitude (ft)	Modal Participation (%)									
	1	2	3	4	5	6	7	8	9	10
0	53.2	39.8	0.8	0.1	2.0	1.5	1.0	0.1	0.7	0.9
5,000	62.8	30.9	0.4	0.3	1.6	1.3	1.3	0.1	0.6	0.7
10,000	63.0	28.5	0.5	0.3	1.3	1.8	1.8	0.2	1.2	0.5

Table 5.15 SCL008 Flutter Mode Participation Factors (0% Damping)

	Flutter Speed (Mach)			Flutter Frequency (Hz)		
Altitude (ft)	Flight Test	L-model	% Difference	Flight Test	L-model	% Difference
5,000	0.95	1.25	31.6	7.4	7.7	4.1
10,000	0.95	1.42	49.5	7.4	7.8	5.4

Table 5.16 SCL008 Flutter Flight Test Comparison

just the opposite of what would be expected were a hump mode present. Similar to the SCL007 frequency plots, for SCL008 at sea level, the modes do not quite merge, but at 10,000 feet, the modal frequencies merge just prior to the flutter onset speed and remain so.

5.3.3 Stores Sensitivity Analysis. To date, no research has been accomplished quantifying the effects of modeling underwing stores aerodynamically (to be fair, with the exception of high order CFD methods, in which grid generation with stores is extremely complex, no panel method existed until recently for creating body-like elements and including their interference effects). The structural and inertial properties are always included in the normal modes analysis, however, the aerodynamic influence has always been assumed to be negligible. To determine

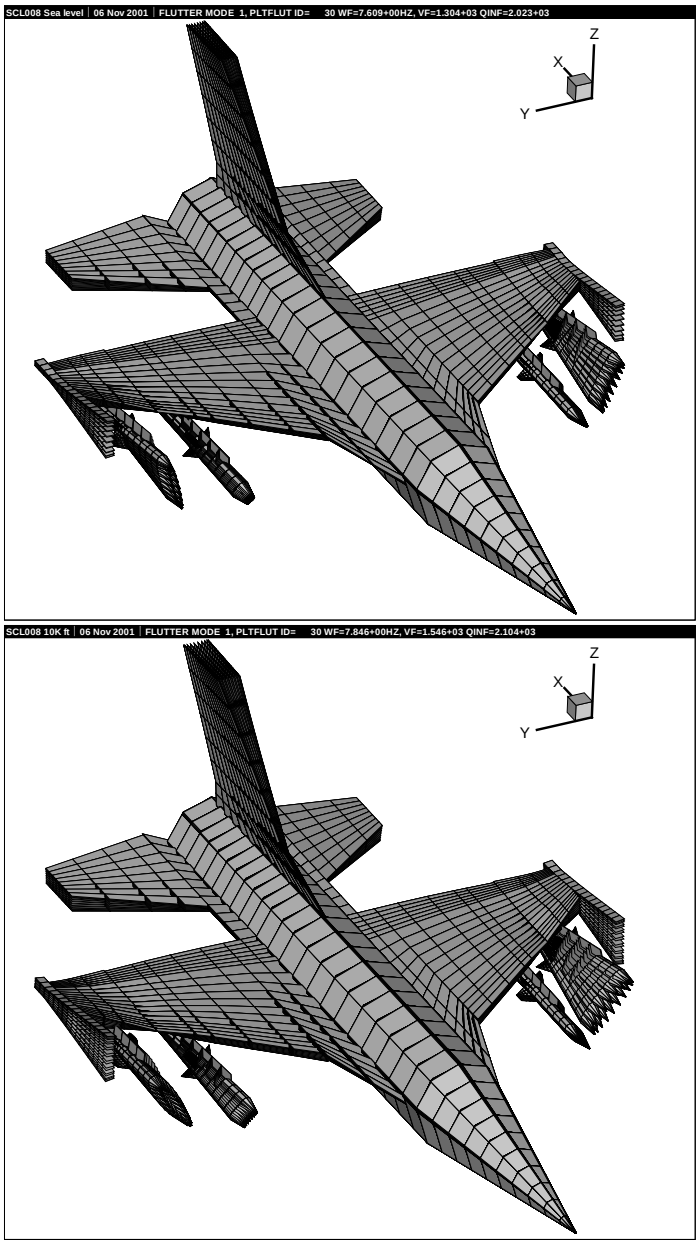

Figure 5.4 SCL008 Flutter Mode (Sea Level & 10,000 ft, 0% Damping)

whether this was indeed the case or not, a sensitivity analysis was conducted to measure the influence of adding the underwing stores to the aerodynamic panel model. The flutter point was first found for a clean wing configuration in a match point run at sea level. Stores were then added individually until the complete configuration

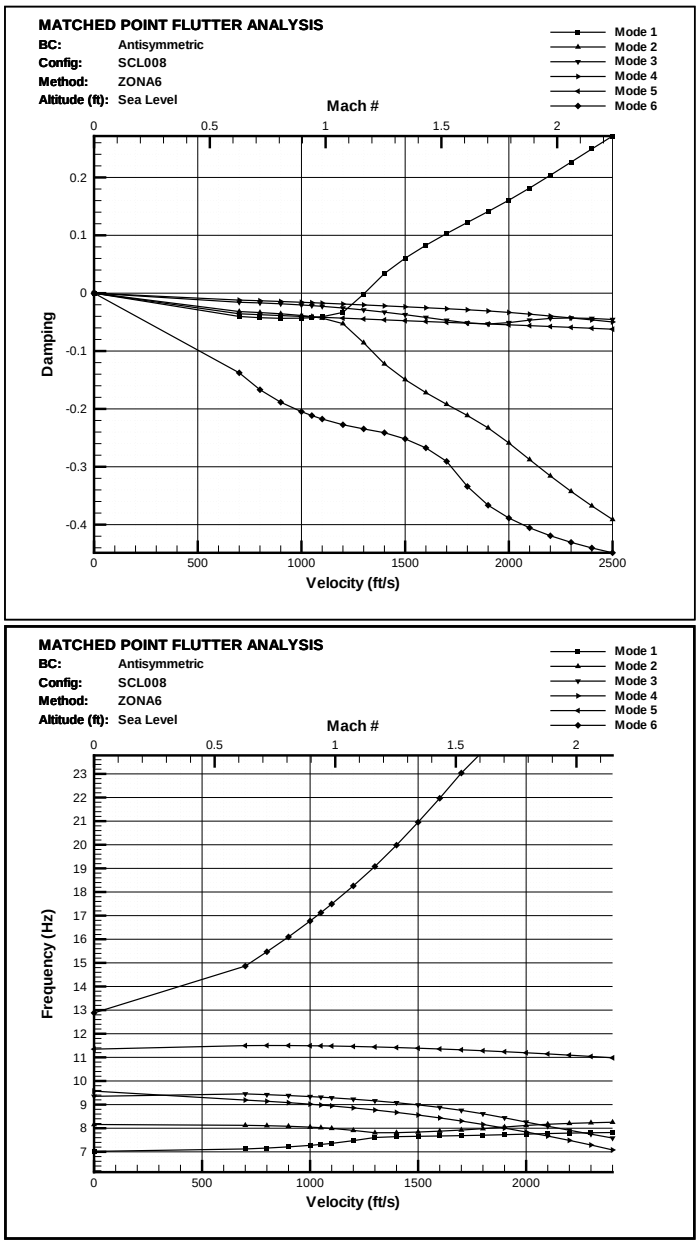

Figure 5.5 SCL008 Flutter Damping and Frequency Curves (Sea Level, 0% Damping)

was built. The results of this analysis are presented in Table 5.17 for SCL007 and Table 5.18 for SCL008.

For the SCL007 case, the addition of the AMRAAM at station 2 caused the clean wing flutter speed to drop from 0.97 Mach to 0.88 Mach, with only a slight

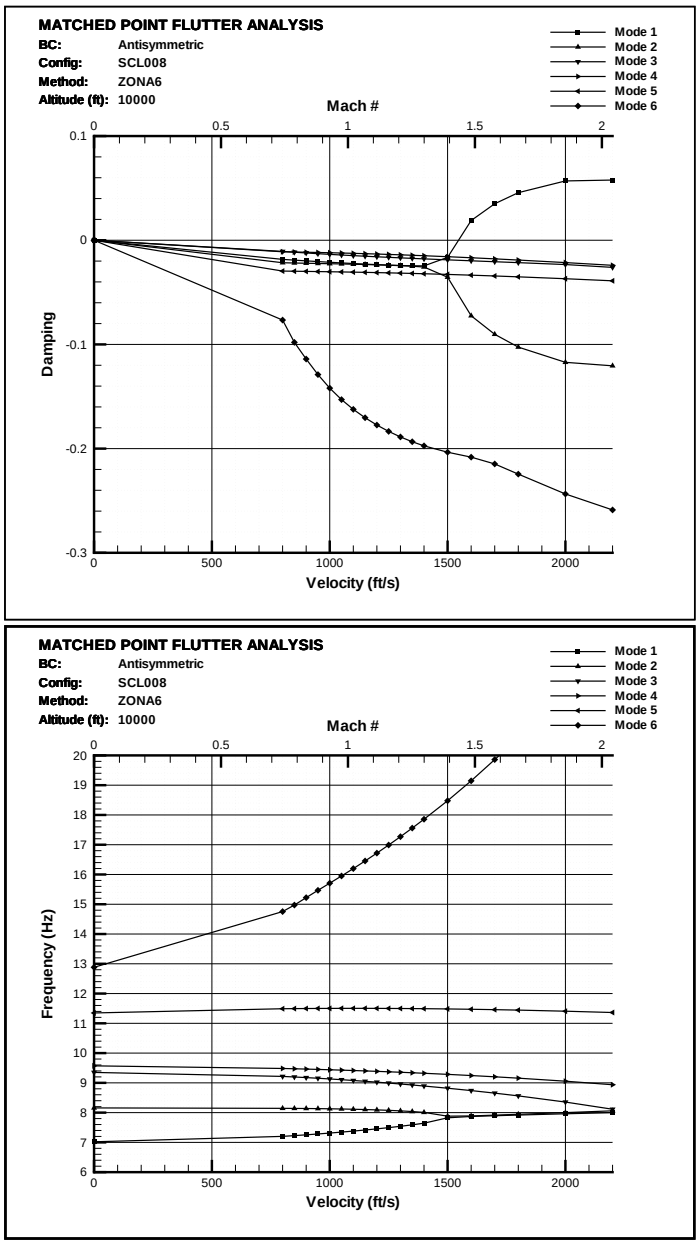

Figure 5.6 SCL008 Flutter Damping and Frequency Curves (10,000 ft, 0% Damping)

drop in frequency. This large drop in flutter speed is indicative of a decrease in aerodynamic damping. With the fuel tank only, however, the flutter speed increased slightly to 0.98 Mach (frequency increasing slightly), indicating an increase in aerodynamic damping. Most compelling though, is the effect of the full configuration

Case	Description	Flutter Speed (Mach)	Flutter Frequency (Hz)
1	Clean wing	0.965	7.02
2	AMRAAM sta 2	0.882	6.97
3	Fuel tank sta 4	0.982	6.98
4	SCL007	0.898	6.94

Table 5.17 SCL007 Store Sensitivity Analysis

Case	Description	Flutter Speed (Mach)	Flutter Frequency (Hz)
1	Clean wing	1.097	7.65
2	AMRAAM sta 2	1.208	7.62
3	AMRAAM sta 3	1.062	7.54
4	SCL008	1.168	7.61

Table 5.18 SCL008 Store Sensitivity Analysis

on flutter speed and frequency. With a speed/frequency of 0.90 Mach/6.94 Hz, this demonstrates that the presence of a missile on the outboard wing stations significantly alters the aerodynamic damping properties of the system, to the point of practically negating the effect of a half full fuel tank on the inboard station.

The same effect continues with SCL008, only in the opposite direction. The addition of the station 2 AMRAAM seems to stiffen the system aerodynamically, resulting in a relatively large increase in the flutter speed from 1.10 Mach to 1.21 Mach. The station 3 AMRAAM provides slightly more aerodynamic flexibility to the system over that of the clean wing, while the complete SCL008 configuration is more stiff overall. The effect of a missile on the outboard wing stations is again demonstrated as significant in this configuration.

5.4 ZTAIC Nonlinear Analysis

The theory behind the ZTAIC method is to include wing thickness and shock effects in the flutter solution to produce a more accurate estimation of the onset speed, frequency, and modal composition of flutter. Damping predictions using ZTAIC have been shown to correlate well with flight test data for characterizing one

of three types of instability as described by Denegri: classical flutter, typical LCO, and non-typical LCO [13]. Typical LCO is described as LCO in which the amplitude continues to grow with increasing airspeed, while non-typical LCO is described as LCO where the amplitude will increase to a point, then decrease and vanish at some higher speed. The shape of the damping curve of the critical mode produced by ZTAIC can be used to predict one of these types. An indication of classical flutter occurs when the damping curve continues to grow past the flutter point. For typical LCO, this curve will eventually show a zero slope, and for non-typical LCO, the slope of the curve will eventually become negative [10].

According to Chen [6], there are two primary effects that the ZTAIC method attempts to capture:

1. In the absence of a strong shock, the thickness effect introduced by ZTAIC will cause the flutter speed to increase.
2. When a strong shock is present, its effect (which is greater than the thickness effect) will drive the flutter speed back down.

This section will discuss the effects of the nonlinear analysis of the two test configurations using the ZTAIC module of ZAERO. The additional data required for ZTAIC, above that needed for a linear analysis, is the steady C_p distribution (either rigid or flexible) on the wing at the midline of each spanwise strip. This data was generated by an inviscid 3-D CFD code, using the symmetric modal eigenvectors from the normal modes analysis, and interpolated from the CFD grid to the panel model via a MATLAB interpolation routine. Examples of the CFD C_p distributions and interpolated C_p distributions, as well as the additional bulk data input required for ZTAIC are shown in Appendices B and C. Using the C_p data, a similar analysis as that outlined in sec 5.3 was undertaken. In order to keep the generation of pressure data to a minimum, rather than match point at a constant altitude across various Mach numbers, the match point technique used here was to hold the Mach number

constant and match point across altitudes. In this method, only one set of steady pressure data was needed per run, and multiple runs were carried out to find where the flutter altitudes matched those of Tables 5.13 and 5.15 for each configuration. Parallel to this analysis, a sensitivity analysis on the effects of C_p type, rigid versus flexible, was undertaken on the SCL007 configuration. Finally, a sensitivity analysis on the effects of adding structural damping to the system was investigated, again on the SCL007 configuration, at 0.9 Mach with flexible C_p data.

5.4.1 SCL007 Results. Flutter onset speed and frequency predictions using the ZTAIC method are presented in Tables 5.19 and 5.20 and compared with both the linear analysis and flight test data. Clearly, with respect to flutter onset speed, the data shows that the ZTAIC method (using either rigid or flexible C_p data) did not yield significantly better predictions than the ZONA6/7 method. In fact, the nonlinear analysis seems to have simply reproduced the linear results. In terms of flutter frequency, the data appear slightly better for the nonlinear analysis, but not significantly, as both methods are within 1.5% of the frequency observed in flight.

These results obviously did not meet expectations, and much thought and research went into possible explanations. First, the two primary effects of the ZTAIC method, wing thickness and shock strength/location, must be investigated. The prediction at 5,000 feet shows a slight increase in flutter speed over that of the linear method for both the rigid and flexible C_p's. This suggests that the thickness effect is playing a slightly greater role than the shock effect, possibly due to the shock not being strong enough to overcome the thickness effect. The upper surface C_p data for this condition is shown in Fig 5.7 for both the rigid and flexible conditions [1]. In each of these cases, a shock is clearly present near the trailing edge of the wing, however it's strength is difficult to quantify. The C_p data was generated using an inviscid method, therefore the shock shown will be stronger and more defined than

[1]Larger C_p plots are included in Appendix B for reference

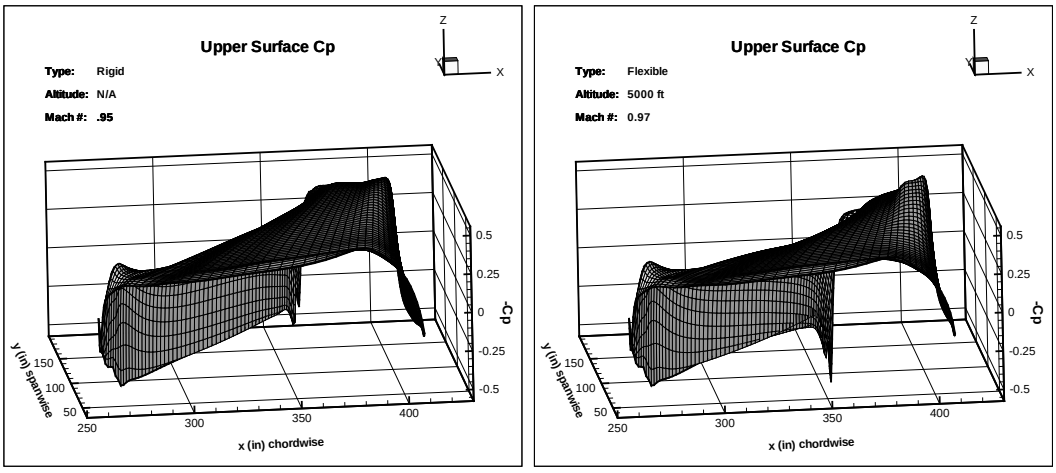

Figure 5.7 SCL007 Upper Surface Rigid/Flexible C_p Data (5,000 feet)

the actual shock during flight. Also, the stores were not modeled aerodynamically in the CFD solution used to generate the C_p data, suggesting that the shock location and strength may not be completely accurate. As was seen in the store sensitivity analysis, a missile on the outboard wing stations significantly effects the flutter solution, and this effect may carry over to the upper surface C_p distribution through interference effects.

At 15,000 feet, ZTAIC does show a reduction in the flutter onset speed of between 4% and 7% over the linear prediction. This does not negate the previous discussion though, it may simply mean that at this condition the C_p data produced a strong enough shock to overcome the thickness effect.

Altitude	**Flutter Speed (Mach)**				**Comparison**			
		ZTAIC		**Flight**	**Rigid**	**Flex**	**Rigid**	**Flex**
(ft)	**ZONA6/7**	**Rigid**	**Flex**	**Test**	**ZONA6/7**	**ZONA6/7**	**Flt Test**	**Flt Test**
5,000	0.95	0.97	0.97	0.80	1.021	1.021	1.213	1.213
15,000	1.09	1.04	1.01	0.90	0.954	0.927	1.156	1.122

Table 5.19 SCL007 ZTAIC V_f Results and C_p Sensitvity

The composition of the flutter mode predicted by ZTAIC shows good agreement with the linear prediction especially at 5,000 feet, where the difference is on the order of fractions of a percent. ZTAIC also captured the change in flutter mode

Altitude (ft)	Flutter Frequency (Hz)				Comparison			
		ZTAIC		Flight	Rigid	Flex	Rigid	Flex
	ZONA6/7	Rigid	Flex	Test	ZONA6/7	ZONA6/7	Flt Test	Flt Test
5,000	6.95	6.85	6.91	6.80	0.986	0.994	1.007	1.016
15,000	6.90	6.88	6.88	6.80	0.997	0.997	1.012	1.012

Table 5.20 SCL007 ZTAIC ω_f Results and C_p Sensitvity

Mode	Modal Participation (%)					
	5,000 ft			15,000 ft		
	ZONA6/7	Rigid C_p	Flexible C_p	ZONA6/7	Rigid C_p	Flexible C_p
1	29.4	28.4	30.8	64.3	73.2	72.4
2	65.8	65.2	62.6	30.4	21.0	21.9
3	0.0	0.1	0.0	0.1	0.1	0.1
4	1.7	2.6	2.5	1.3	1.5	1.6
5	1.5	1.9	2.0	1.4	1.6	1.6
6	0.5	0.3	0.6	1.0	1.2	0.9
7	0.0	0.0	0.1	0.0	0.0	0.0
8	0.6	0.8	0.9	0.6	0.9	0.8
9	0.0	0.0	0.0	0.3	0.0	0.0
10	0.3	0.5	0.3	0.6	0.5	0.5

Table 5.21 SCL007 ZTAIC Flutter Mode Participation Factors (0% Damping)

composition at 15,000 feet, but predicted approximately an 8% stronger mode 1 influence and a correspondingly weaker mode 2 influence (Table 5.21). Although this difference may seem important, mode 1 is already a combination of bending and torsion, and the animation of the flutter mode is indistinguishable from the linear prediction.

Lastly, the V-g/V-ω plots generated using ZTAIC again show only minor differences in the critical mode from the ZONA6/7 results. Figures 5.8 and 5.9[2] show the ZONA6/7 and ZTAIC V-g/V-ω plots for both 5,000 and 15,000 feet. The key feature to note is that the damping curve for the critical mode using ZTAIC shows a continuous positive slope, indicating that in flight, this configuration should show classical flutter. The flight test, however, showed a phenomenon closer to typical LCO. At 5,000 feet, an LCO limit was reached at 0.95 Mach, whereas at 15,000 feet, the LCO stabilized at $\pm$ 2 G's and the test was stopped before either a limit was reached or the LCO condition abated.

[2]All V-g/V-ω charts are reprinted individually in Appendix A

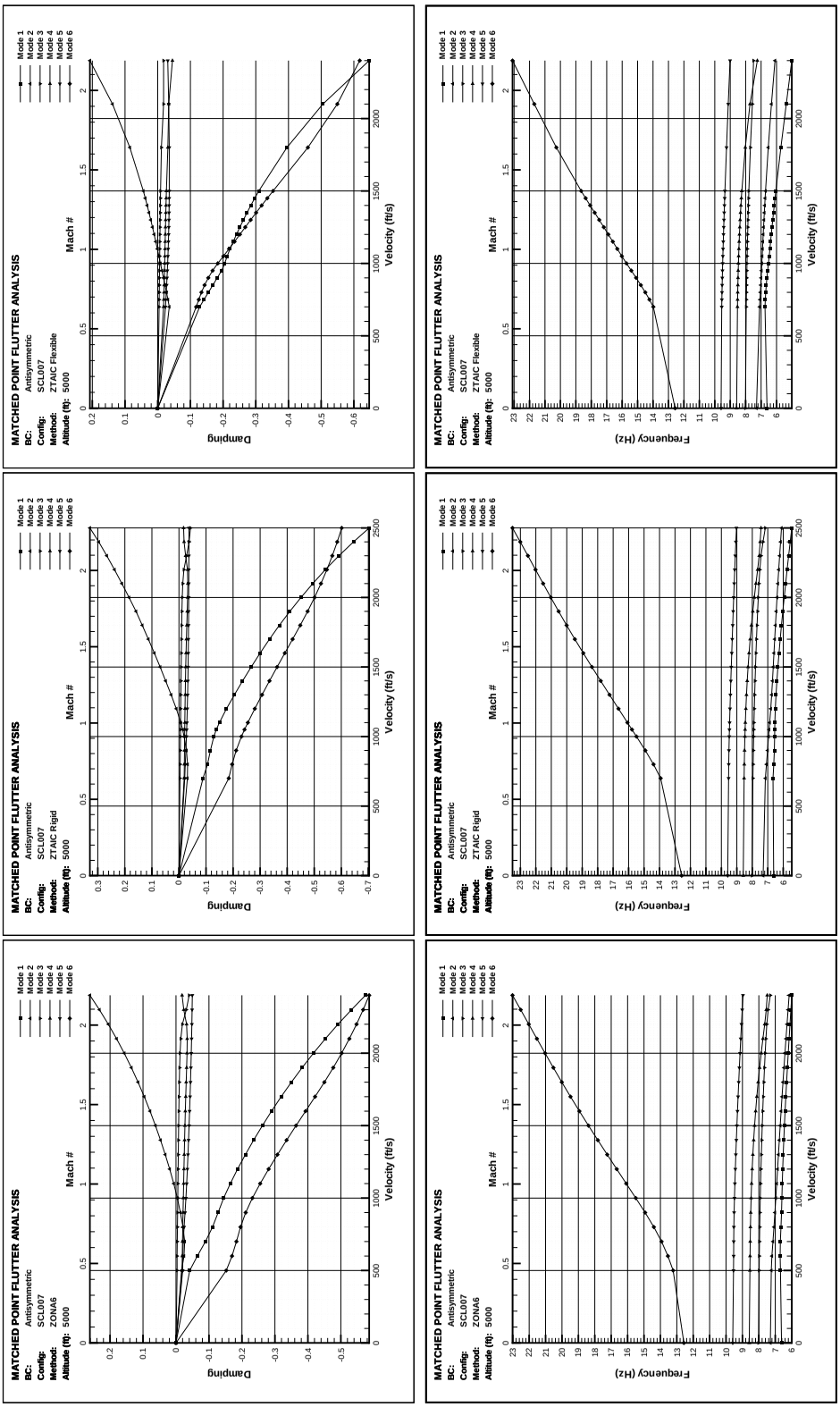

Figure 5.8 SCL007 Flutter Damping and Frequency Curves (5,000 ft, 0% Damping)

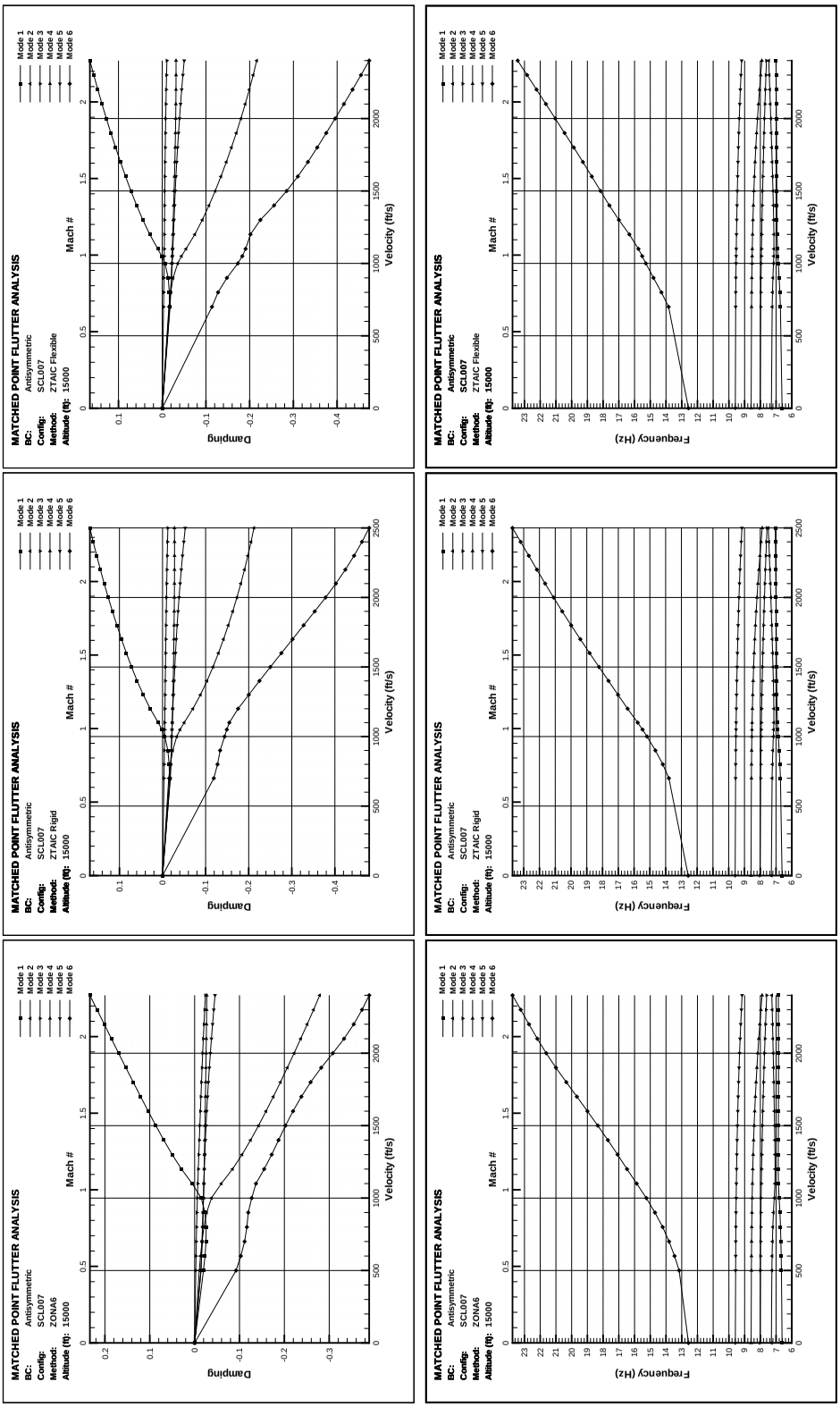

Figure 5.9 SCL007 Flutter Damping and Frequency Curves (15,000 ft, 0% Damping)

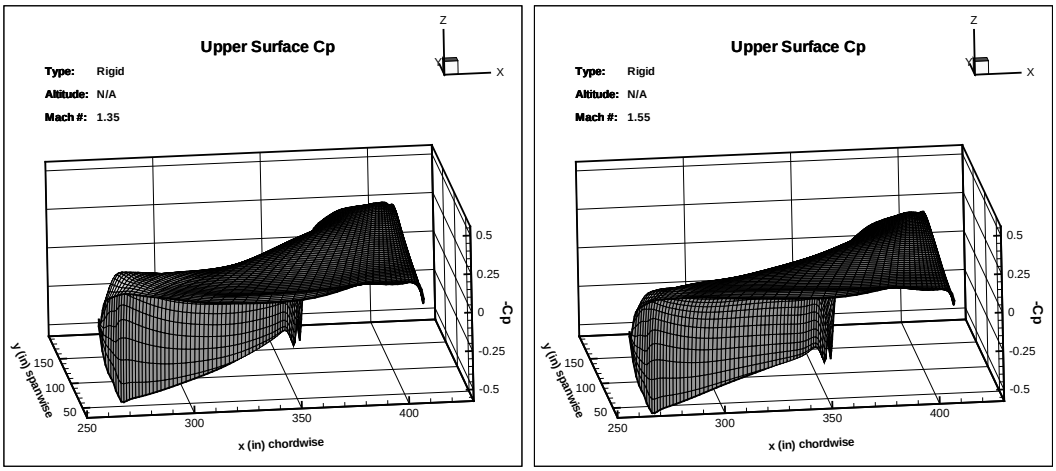

Figure 5.10 SCL008 Upper Surface Rigid C_p Data (5,000/10,000 feet)

5.4.2 SCL008 Results. The SCL008 results presented in Tables 5.22 and 5.23 are much more readily explained by the ZTAIC thickness effect. The onset speeds predicted for this case are approximately 9% higher than those predicted by ZONA6/7, and by examining the upper surface C_p distributions at each condition, the reason is evident. Figure 5.10 shows the pressure distributions at both 5,000 and 10,000 feet for SCL008 and clearly shows a weaker (than SCL007) shock now attached to the trailing edge of the wing. Accordingly, the thickness effect will dominate to drive the flutter speed above the linear prediction.

Altitude (ft)	**Flutter Speed (Mach)**			**Comparison**	
	ZONA6/7	**ZTAIC Rigid**	**Flight Test**	**$\frac{\text{Rigid}}{\text{ZONA6/7}}$**	**$\frac{\text{Rigid}}{\text{Flt Test}}$**
5,000	1.25	1.36	0.95	1.316	1.432
10,000	1.42	1.55	0.95	1.495	1.632

Table 5.22 SCL008 V_f ZTAIC Results

Altitude (ft)	**Flutter Frequency (Hz)**			**Comparison**	
	ZONA6/7	**ZTAIC Rigid**	**Flight Test**	**$\frac{\text{Rigid}}{\text{ZONA6/7}}$**	**$\frac{\text{Rigid}}{\text{Flt Test}}$**
5,000	7.7	7.8	7.4	1.041	1.054
10,000	7.8	7.9	7.4	1.054	1.068

Table 5.23 SCL008 ω_f ZTAIC Results

The ZTAIC method also predicts a large change in modal participation of modes 1 and 2 for the flutter mode (Table 5.24). In both altitude cases, more of mode 2, first wing bending with yaw at stations 2 and 3, is comprising the flutter mode. This is particularly evident in the flutter animation at 10,000 feet (Fig 5.11).

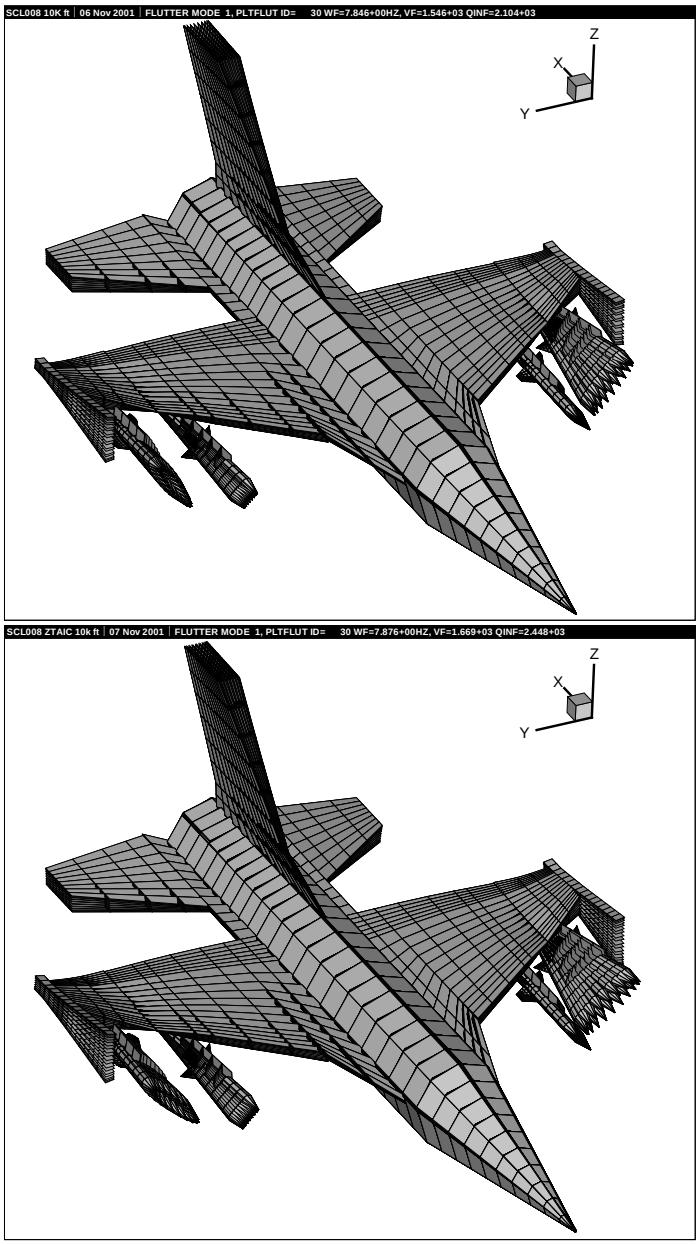

Figure 5.11 SCL008 Flutter Mode: ZONA6/7 vs. ZTAIC (10,000 ft, 0% Damping)

Most important, though, is the change in the damping and frequency curves. Figures 5.12 and 5.13 show that the ZONA6/7 prediction of the damping of the critical mode continues to increase with speed for the 5,000 foot case, whereas for the 10,000 foot case it levels off. In the ZTAIC prediction, however, the damping curve reverses direction between 1.9 and 2.2 Mach. This is an indicator of non-typical LCO, which is precisely what was seen during flight test [12].

	Modal Participation (%)			
	5,000 ft		**10,000 ft**	
Mode	**ZONA6/7**	**Rigid C_p**	**ZONA6/7**	**Rigid C_p**
1	62.8	50.4	63.0	45.7
2	30.9	38.3	28.5	41.4
3	0.4	0.6	0.5	1.6
4	0.3	0.4	0.3	1.2
5	1.6	2.7	1.3	2.0
6	1.3	3.2	1.8	4.4
7	1.3	1.8	1.8	1.2
8	0.1	0.2	0.2	0.2
9	0.6	1.7	1.2	1.8
10	0.7	0.8	0.5	0.6

Table 5.24 SCL008 ZTAIC Flutter Mode Participation Factors (0% Damping)

5.4.3 C_p Sensitivity Analysis. In order to determine precisely what type of steady C_p data (rigid or flexible) was required to produce the most accurate results using ZTAIC, a sensitivity study on steady pressure type was conducted. It was thought that flexible pressure data (pressure data generated from CFD solutions of a deflected wing using symmetric normal mode data) was required in order to recreate the correct shock location and strength, since rigid pressure data did not match any physical phenomenon (rigid data was produced by subjecting the wing to the same flow conditions that produced the flexible data, but the wing was not allowed to deform). The results of the sensitivity analysis, however, did not confirm this assumption. Tables 5.25 and 5.26 (discussed earlier in the text and recreated here for comparison) show, for SCL007, there was a negligible difference in flutter onset between the rigid and flexible pressure data. For SCL007, this insensitivity is also found in the flutter mode composition (Table 5.21) and V-g/V-ω plots (Figs 5.8 and 5.9).

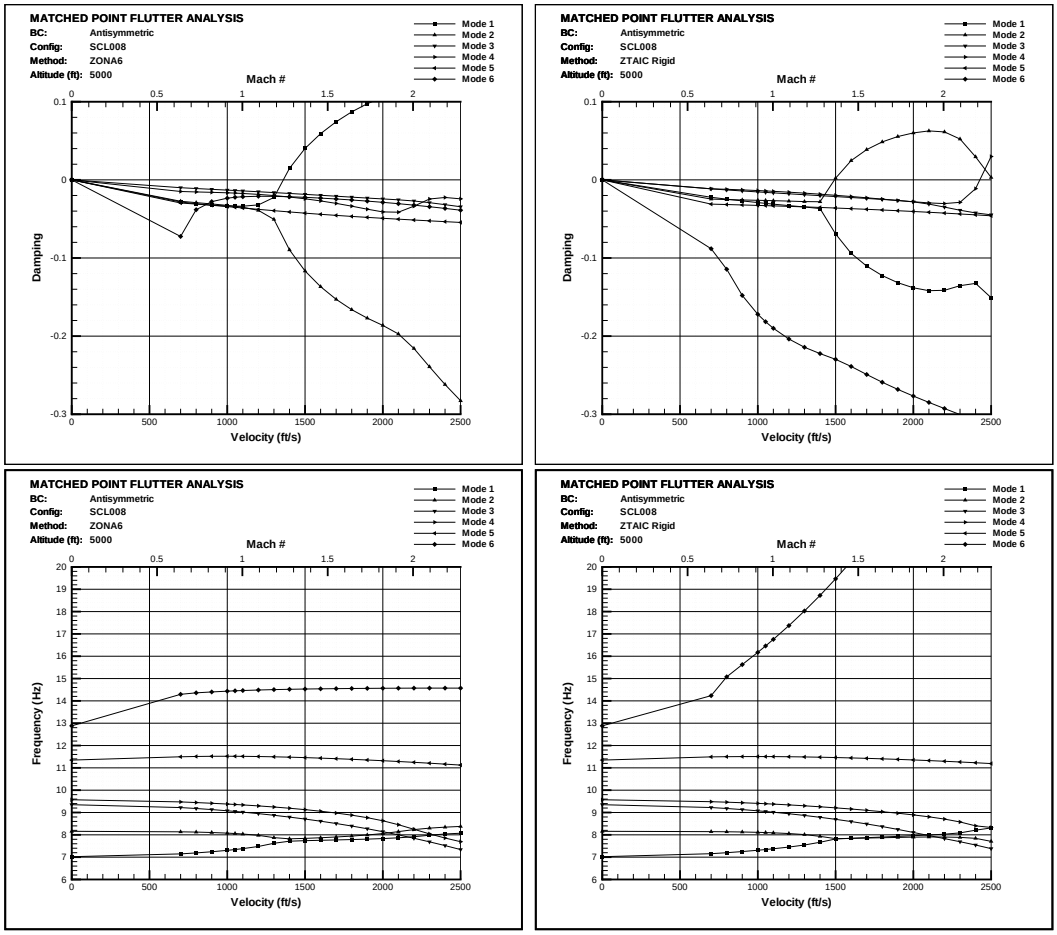

Figure 5.12 SCL008 Flutter Damping and Frequency Curves (5,000 ft, 0% Damping)

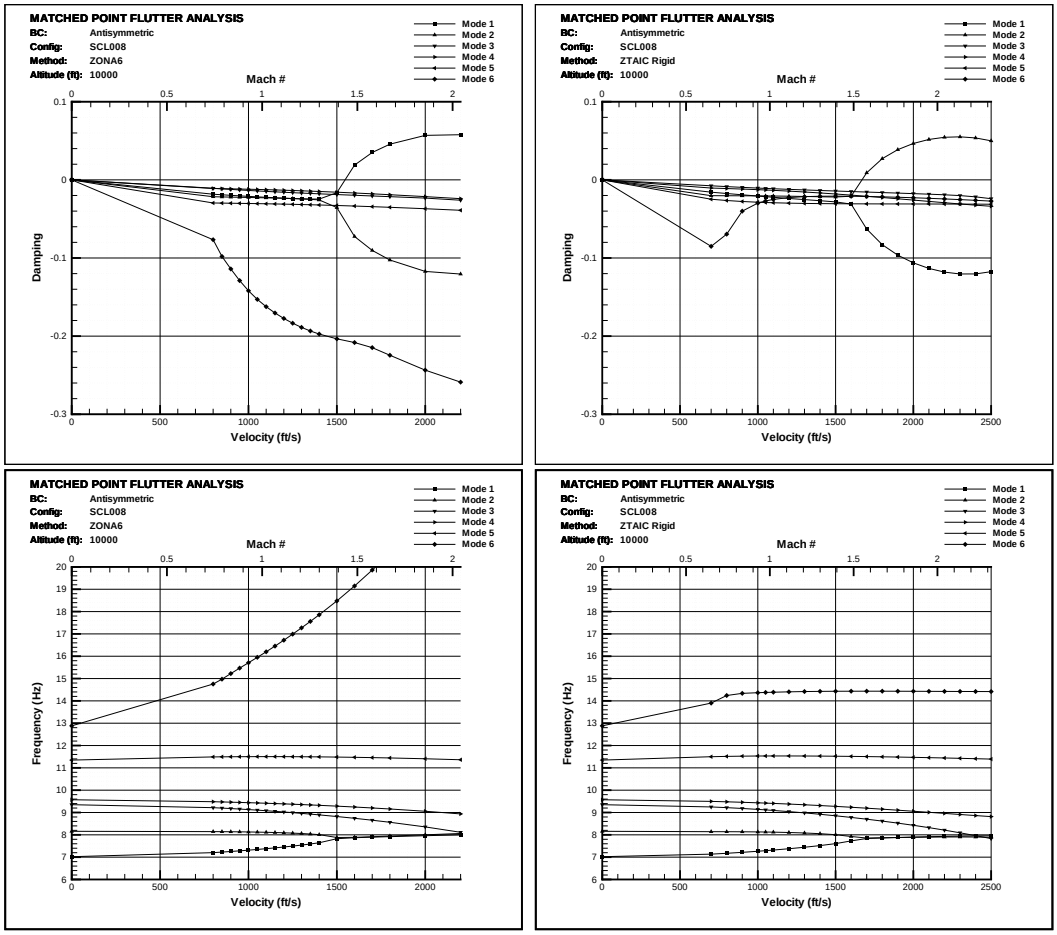

Figure 5.13 SCL008 Flutter Damping and Frequency Curves (10,000 ft, 0% Damping)

In order to try to develop a greater feel for the effects of steady pressure type, an additional comparison was made. The flutter altitude versus airspeed chart (Fig 5.14) depicts rigid versus flexible C_p effects. It must be noted though, that the flexible data is truly only accurate for the altitude and Mach number that it was generated for. However, this chart does imply that, in the region between 0.95 and 1.05 Mach, there is little difference between using rigid or flexible steady pressure data. These findings must be taken with caution however, since only one case was studied, and this effect may be an anomaly.

Altitude (ft)	Flutter Speed (Mach)				Comparison			
		ZTAIC		Flight	Rigid	Flex	Rigid	Flex
	ZONA6/7	Rigid	Flex	Test	ZONA6/7	ZONA6/7	Flt Test	Flt Test
5,000	0.95	0.97	0.97	0.80	1.021	1.021	1.213	1.213
15,000	1.09	1.04	1.01	0.90	0.954	0.927	1.156	1.122

Table 5.25 SCL007 ZTAIC V_f Results and C_p Sensitvity

Altitude (ft)	Flutter Frequency (Hz)				Comparison			
		ZTAIC		Flight	Rigid	Flex	Rigid	Flex
	ZONA6/7	Rigid	Flex	Test	ZONA6/7	ZONA6/7	Flt Test	Flt Test
5,000	6.95	6.85	6.91	6.80	0.986	0.994	1.007	1.016
15,000	6.90	6.88	6.88	6.80	0.997	0.997	1.012	1.012

Table 5.26 SCL007 ZTAIC ω_f Results and C_p Sensitvity

5.4.4 Structural Damping Sensitivity Analysis. A damping sensitivity analysis was conducted to determine whether the g-method for extracting the complex eigenvalues of the flutter equation could indeed provide valuable damping predictions at values other than 0%. The g-method implies that a level of aerodynamic damping (as a percentage of critical damping) shown on the V-g plot for 0% structural damping will correspond to an equivalent level of structural damping at 0% aerodynamic damping. In other words, the flutter speed predicted by choosing a level of damping from the V-g plot (say 2%), with no structural damping included in the analysis, will be the same as that predicted by including 2% structural damping at the 0% V-g crossing. Figure 5.15 shows the results of a constant Mach, altitude match point case for the SCL007 configuration. Holding Mach at 0.90, this data was generated

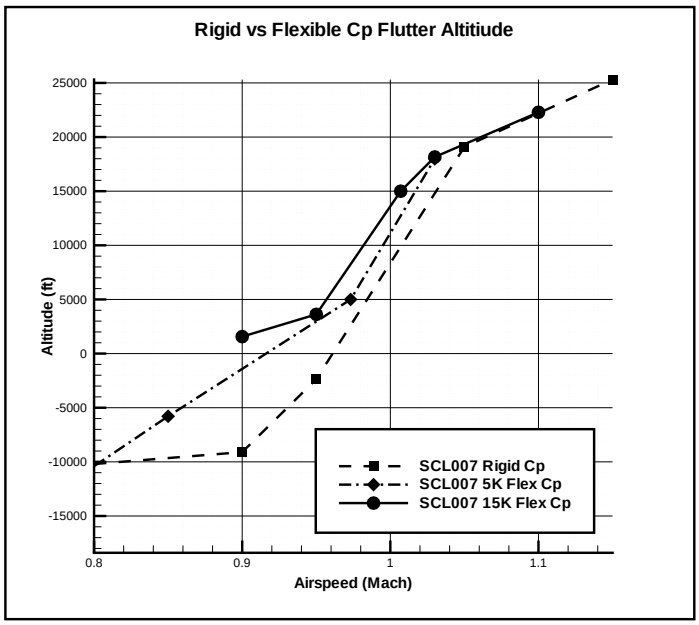

Figure 5.14 SCL007 Flutter Altitude Curves (0% Damping)

by adding structural damping at levels from 0.5% to 2.5% and calculating the corresponding flutter onset altitude. As the data indicates, the g-method assumptions prove to hold for damping values away from 0%.

5.4.5 SCL007 GVT Tuning Results. After the bulk of the current research was accomplished, ground vibration testing (GVT) results were obtained for the F-16 configuration depicted in Figure 5.16 below, labelled the A-model. The FEM for this configuration was obtained and was tuned (via the MSC/NASTRAN SOLUTION 200 optimization algorithm) to match the GVT data, focusing on the fuel tank pitch and hook spring stiffnesses, four outboard wing element thicknesses, and the station 2 LAU-129 beam stiffnesses. The resulting changes in element properties are shown below in Table 5.27. Most notable are differences in the pitch and hook spring stiffnesses and the PSHEAR element.

After optimizing and tuning the A-model, the new element properties were inserted into the SCL007 FEM and an antisymmetric normal modes analysis was conducted. Table 5.28 highlights the changes to the A-model as well as the changes

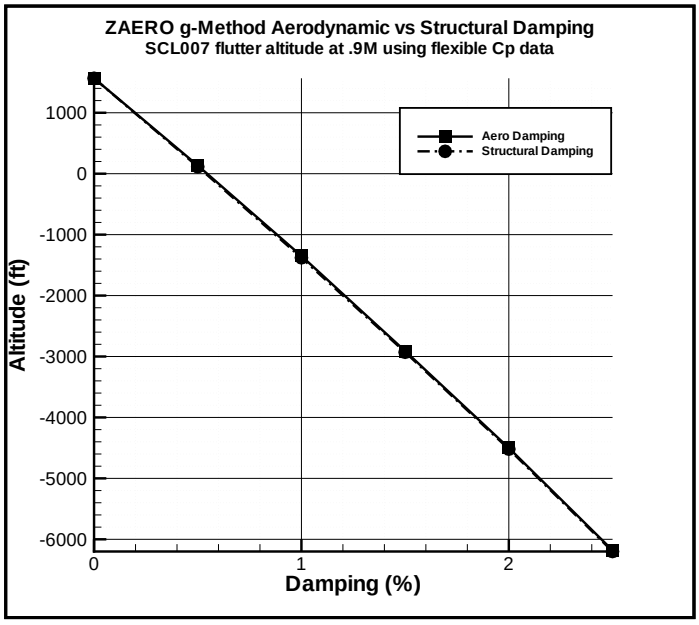

Figure 5.15 SCL007 Flutter Altitude vs Damping Curve (0.9 Mach)

Element Type	Element Number	Field	Initial Value	Final GVT Tuned Value	% Diff
PSHELL	647	T	0.400	0.400	0.00
PSHELL	648	T	0.400	0.440	9.09
PSHELL	649	T	0.400	0.420	4.76
PSHEAR	650	T	0.038	0.049	22.01
PELAS	3414	K1	1.52E+08	2.55E+08	40.58
PELAS	3415	K1	1.72E+08	2.42E+08	28.87

Table 5.27 Optimization Results - Element Properties

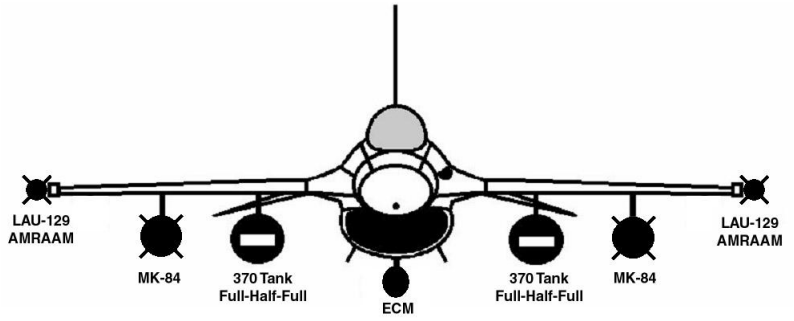

Figure 5.16 F-16 A-Model Configuration

that occurred in the L-model after tuning. These changes resulted in the first natural mode of the wing becoming 1.45% stiffer, while the second natural mode became 0.46% more flexible. In essence, the first two modes went from 0.68 Hz apart to 0.55 Hz apart. Modes four and five also showed increased flexibility of 1.3 and 2.3% over the original model. Although the modal frequencies did change, the mode shapes were virtually indistinguishable from the pre-tuned mode shapes.

Modal Frequencies (Hz)					
Mode	**A-Model**	**Tuned A-Model**	**GVT Data**	**L-Model**	**Tuned L-Model**
1	4.61	4.64	4.64	6.62	6.79
2	5.24	5.30	5.35	7.30	7.27
3	7.29	7.31	7.10	8.01	8.02
4	7.42	7.49	7.40	8.58	8.68
5	7.81	8.34	7.62	9.59	9.58
6	9.00	9.03	8.78	12.57	12.60
7	10.89	10.90	12.17	13.50	13.51
8	11.73	11.74	12.57	14.70	14.76

Table 5.28 Optimization Results - Modal Frequencies

While the differences in modal frequency seem almost negligible, they had a profound impact on the flutter onset speeds predicted by both the linear (ZONA6/7) and nonlinear (ZTAIC) codes. These results are presented in Tables 5.29 and 5.30 below. The primary mechanism for the reduction in flutter onset speed appears to be the reduction in the frequency difference between the first two natural modes of the system. These are the two modes that coalesce to form the flutter mode. Consequently, as the natural frequencies get closer together, a lower airspeed is

required to force the two modes to coalesce. Flutter frequency was overpredicted by 4.4% after tuning, however this difference is not as important as the change in flutter speed. Once again, the type of C_p did not seem to influence the flutter prediction significantly. However it is notable that at 5,000 feet the nonlinear code predicted an onset speed closer to that seen during flight test[3] than the linear code. But at 15,000 feet the linear code produced a better prediction.

Flutter Speed (Mach)									
Alt			L-Model			Tuned Model			Flight
				ZTAIC			ZTAIC		
(ft)	LFWC	UFAP	ZONA 6/7	Rigid	Flexible	ZONA 6/7	Rigid	Flexible	Test
SL	0.65	0.73	0.90	-	-	0.72	-	-	-
5,000	-	-	0.95	0.97	0.97	0.77	0.78	0.79	0.80
15,000	-	-	1.09	1.04	1.01	0.88	0.86	0.85	0.90

Table 5.29 SCL007 V_f Tuning Results

Flutter Frequency (Hz)									
Alt			L-Model			Tuned Model			Flight
				ZTAIC			ZTAIC		
(ft)	LFWC	UFAP	ZONA 6/7	Rigid	Flexible	ZONA 6/7	Rigid	Flexible	Test
SL	7.1	7.1	6.9	-	-	7.1	-	-	-
5,000	-	-	6.9	6.9	6.9	7.1	7.1	7.1	6.8
15,000	-	-	6.9	6.9	6.9	7.1	7.1	7.1	6.8

Table 5.30 SCL007 ω_f Tuning Results

Since the tuning appeared to produce better speed predictions for the flutter boundary, a more stable result was expected for the flutter mode. Indeed, the composition of the flutter mode shows good agreement across all solution techniques (linear versus nonlinear) and altitudes, unlike the pre-tuned results (see Table 5.21). Only slight changes in the primary flutter mechanism occur with the tuned model across altitudes, however the primary mode is always mode 2, 1^{st} torsion.

After verifying flutter speeds and the flutter mode, the V-g/V-ω plots generated using ZTAIC were evaluated. Only minor differences were noted in the critical mode crossing from the ZONA6/7 results and from the pre-tuned results. The figures in

[3]Flight test data were taken in 0.05 Mach increments. For a reported flutter speed of 0.8M, flutter onset may actually have occurred between 0.75 and 0.8M.

Mode	Modal Participation (%)						
	Sea Level	5,000 ft			15,000 ft		
	ZONA6/7	ZONA6/7	Rigid	Flexible	ZONA6/7	Rigid	Flexible
1	18.4	17.7	17.4	18.0	17.8	20.2	16.2
2	77.9	79.0	79.3	78.4	79.4	75.0	81.0
3	0.0	0.0	0.0	0.0	0.0	0.0	0.0
4	0.1	0.1	0.1	0.1	0.0	0.2	0.1
5	1.1	1.0	1.0	1.0	0.8	1.5	0.8
6	1.7	1.5	1.5	1.6	1.2	2.1	1.2
7	0.0	0.0	0.0	0.0	0.0	0.0	0.0
8	0.4	0.4	0.4	0.4	0.3	0.5	0.3
9	0.0	0.0	0.0	0.0	0.0	0.0	0.0
10	0.3	0.2	0.2	0.3	0.2	0.3	0.2

Table 5.31 Tuned SCL007 Flutter Mode Participation Factors (0% Damping)

Appendix A show the ZONA6/7 and ZTAIC V-g/V-ω plots for sea level, 5,000, and 15,000 feet. The key feature to note is that the V-ω plots show much better coalescing of the two primary flutter modes than the pre-tuned model did. Also, the damping curve for the critical mode after tuning shows a continuous positive slope (for all cases using both rigid and flexible C_p's except at 15,000 feet), however the slope is shallower than before tuning. This indicates that in flight classical flutter would be expected or that the onset of the instability would be fairly gradual. Flight testing showed a phenomenon closer to typical LCO; at 5,000 feet, LCO onset occured at 0.80 Mach and a limit was reached at 0.95 Mach. However, the V-g diagram for the flexible C_p case at 15,000 feet indicates a possible hump mode, and during flight test, the LCO stabilized at $\pm$ 2 G's. The test was stopped before either a limit was reached or the LCO condition abated. Again, ZTAIC seemed to capture the type of instability seen in flight testing. This result is the only major difference shown between using rigid and flexible C_p's throughout this study.

Lastly, the aerodynamic store sensitivity study was reinvestigated using the tuned model. Table 5.32 details the results of the pre-tuned and tuned study. The changes in predicted onset speed for the tuned model are not as significant as those seen with the pre-tuned model (3% for the tuned model, 7% for the pre-tuned model), however, the stores influence appears to be dependent on transonic effects. The results do show that the presence of an AMRAAM on Station 2/8 reduces the aero-

Case	Description	Flutter Speed (Mach)	
		L-Model	Tuned Model
1	Clean wing	0.965	0.736
2	AMRAAM sta 2	0.882	0.713
3	Fuel tank sta 4	0.982	0.742
4	SCL007	0.898	0.715

Table 5.32 Tuned SCL007 Aerodynamic Store Sensitivity

dynamic damping properties of the system enough to counter the presence of a half full fuel tank and should be accounted for aerodynamically.

VI. Conclusions and Recommendations

The research presented in this thesis was aimed at finding a transonic flutter prediction methodology for the F-16 that would more accurately predict the onset speed and frequency than that currently used by AFSEO. Additionally, this research set out to show that the aerodynamic effects of underwing stores on the flutter solution could not be ignored and that structural damping and steady C_p type also influenced the solution. The applicability of this research to AFSEO will be to provide a single package methodology for predicting flutter from the subsonic through the supersonic range, as well as providing a means for creating visualizations of the flutter phenomena.

6.1 Conclusions

The initial goal of this research was to try to provide a more accurate estimate of the flutter onset speed and frequency for various F-16 store configurations. This analysis (and many others) has shown that the frequency of flutter can be predicted quite well using linear methods, and the additional effort required for the nonlinear analysis does not justify the slight gain. The hoped for improvement in onset speed estimation was mixed as the nonlinear ZTAIC method showed improvement in the transonic region (after tuning the FEM), but worse predictions in the supersonic region. In the transonic case (below approximately 1.05 Mach), the C_p data never showed the presence of a strong shock on the wing, at least not strong enough to definitively overcome the thickness effects in the transonic small disturbance theory. Although the C_p data came from an inviscid solution method (which should result in a stronger, more defined shock than a viscous method), the lack of aerodynamically modeling the stores may have produced a shock too far aft on the wing or a shock that was too weak. Another possibility is that, although the panel model showed convergence for the linear analysis, the mesh may still have been too coarse in the

spanwise direction for the ZTAIC method, causing the spanwise correction of the TES theory to produce an inaccurate unsteady flowfield. Perhaps the most compelling result of this study was the sensitivity of the flutter speed solution to changes in the FEM. After tuning, the SCL007 onset speed results for both the linear and nonlinear codes were very close to flight test. However, for SCL008, the same tuning may not have significantly changed the predictions, since SCL008 had no wing tank or wing tank pylon. Obviously, the accuracy of the FEM for any configuration must be ensured before undertaking a flutter analysis.

Although the flutter onset speed predictions were mixed, a result of equal or perhaps greater value was found. ZTAIC's apparent ability to characterize the type of LCO/flutter that will occur in flight is invaluable, and should lead to a reduction in the number of cases that must be flight tested. The relationship between C_p type and ZTAIC's ability to characterize the type of LCO that will occur must be studied with more cases to ensure that rigid C_p data can indeed be used (since for SCL007 the only difference seen in characterizing the LCO was for the flexible data at 15000 feet). Additionally, ZAERO's output can be tailored to many post-processing software packages such as TECPLOT and FEMAP, giving the analyst an unprecedented capability to visualize various flutter results. By building a database of store models and AIC's, and combining the LCO characterization capability with ZAERO's output visualization, the total time for a clearance request to be approved should be reduced.

As alluded to earlier, most flutter prediction does not include the aerodynamic effects of underwing stores. For both cases investigated in this study, however, the aerodynamic effects of missiles on the outboard wing stations proved to effect the flutter onset speeds. The greatest influence of external stores seems to come from station 2/8. In this position, including the aerodynamic effect of the AMRAAM led to a 3.1% reduction in flutter speed for SCL007 (7% before tuning the FEM) and a 10% increase in flutter speed for the SCL008 configuration. Aerodynamically

modeling stores at stations inboard of station 2/8 seemed to have only a small impact on flutter speed both individually and when combined with the outboard stores. This result leads to the possibility that excluding the aerodynamic effects of outboard wing stores may effect the shock strength and location predicted by CFD analysis and, therefore, the ability of the ZTAIC module to produce a better onset estimate.

The necessity of using steady C_p distributions as input to the ZTAIC module requires an ability to generate those data. Pressure distribution data from either wind tunnel tests (rigid pressure data, typically) or CFD analysis may be used, however, for F-16 configuration studies, most often CFD data will be needed. In order to generate flexible pressure data, the symmetric normal modes must be used to generate a deflected wing position at each Mach number/density pair; this results in a large amount of data being required for each analysis. Rigid steady pressure data, on the other hand, does not require modal data, nor is it density dependent; this makes the generation of rigid steady pressures quicker and easier. Fortunately, the sensitivity analysis undertaken in this thesis has shown that, in the region between 0.95 and 1.05 Mach for the F-16 wing, rigid data produces nearly the same onset estimate as flexible data.

Finally, the g-method assumption of accurate damping prediction away from the 0% damping line was tested. Analysis showed that the g-method did indeed produce accurate damping predictions as far away as 2.5% of critical damping from the 0% crossing. The effect of structural damping on the flutter onset is to increase the flutter speed depending on the slope of the critical mode as it crosses 0% damping. A shallow crossing shows a large change in flutter speed for a given value of structural damping, while a steep crossing is relatively insensitive to changes in damping level. Fortunately, ZAERO automates the calculation of structural damping effects by creating a table of flutter speeds and corresponding frequencies for different damping levels.

6.2 Recommendations

Based on the above conclusions, four recommendations for future research and one recommendation for AFSEO methodology are made.

For future research:

1. The F-16 finite element model must be checked against all available GVT data (for as many configurations as possible). This will ensure each pylon, store, and launcher is modeled correctly and give more confidence in the results of any flutter analysis.
2. Conduct a convergence study on the aerodynamic panel model, specifically on the spanwise distribution of divisions, using the ZTAIC method. This will ensure that the spanwise correction taking place in the transonic equivalent strip method is not being extrapolated too far.
3. Perform a more rigorous sensitivity analysis on rigid versus flexible steady C_p data by "match-pointing" the flexible C_p's with flutter altitude predictions. In this way, a better understanding of the pressure distribution effects outside of the 0.95 to 1.05 Mach range can be developed. Also, the effect of C_p type on ZTAIC's ability to characterize LCO may be quantified.
4. Perform a sensitivity analysis on steady C_p data from CFD codes with the stores modeled aerodynamically (at least with a missile at station 2/8) versus data from CFD analysis without the stores aerodynamically modeled. This should confirm whether the predicted shock location and strength are influenced by underwing stores, and how sensitive ZTAIC is to shock location.

For AFSEO methodology:

1. Incorporate the use of ZAERO into flutter analyses for the F-16 to build a database of stores and AIC matrices, while continuing to use UFAP. Use the

ZTAIC method to attempt to characterize LCO/flutter for new test cases, and correlate old test cases to see if ZTAIC correlation holds across the spectrum.

Appendix A. V-g/V-ω Plots

A.1 SCL007 V-g/V-ω Plots

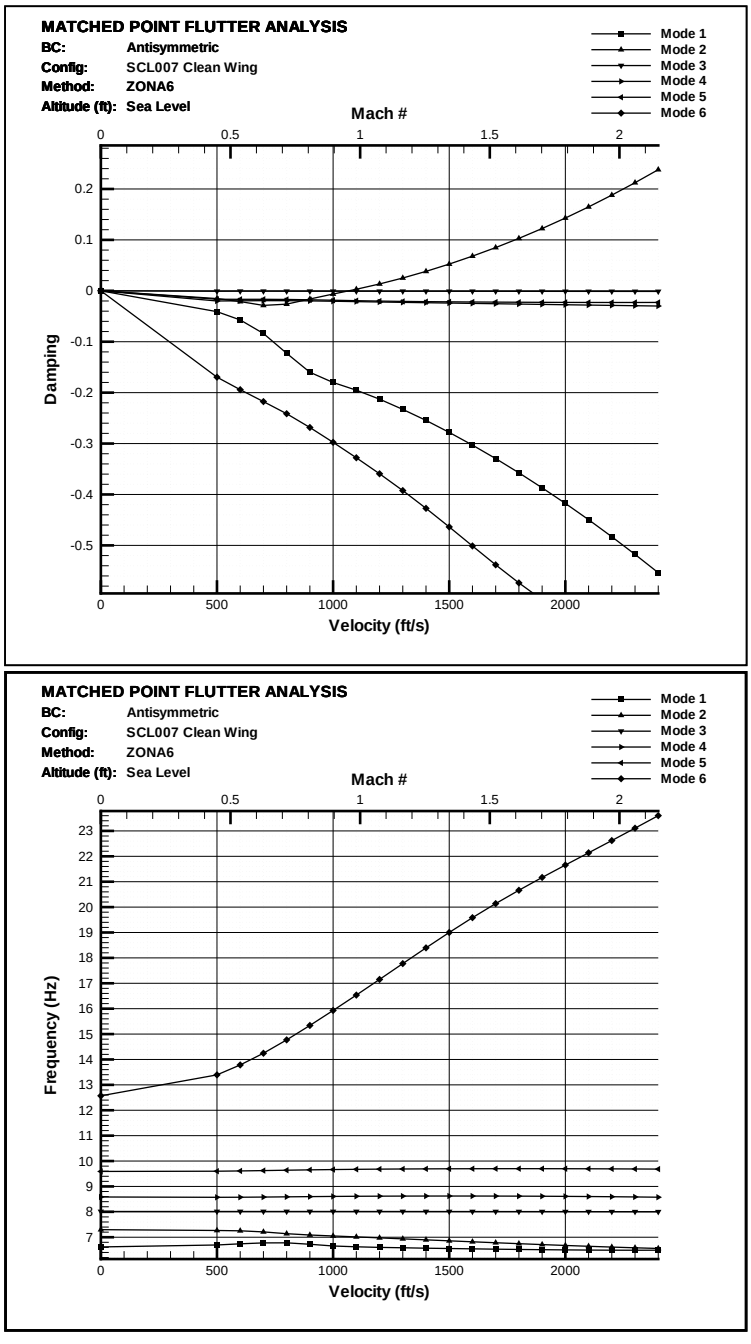

Figure A.1 SCL007 Clean Wing V-g/V-ω Plot (Sea Level, 0% Damping)

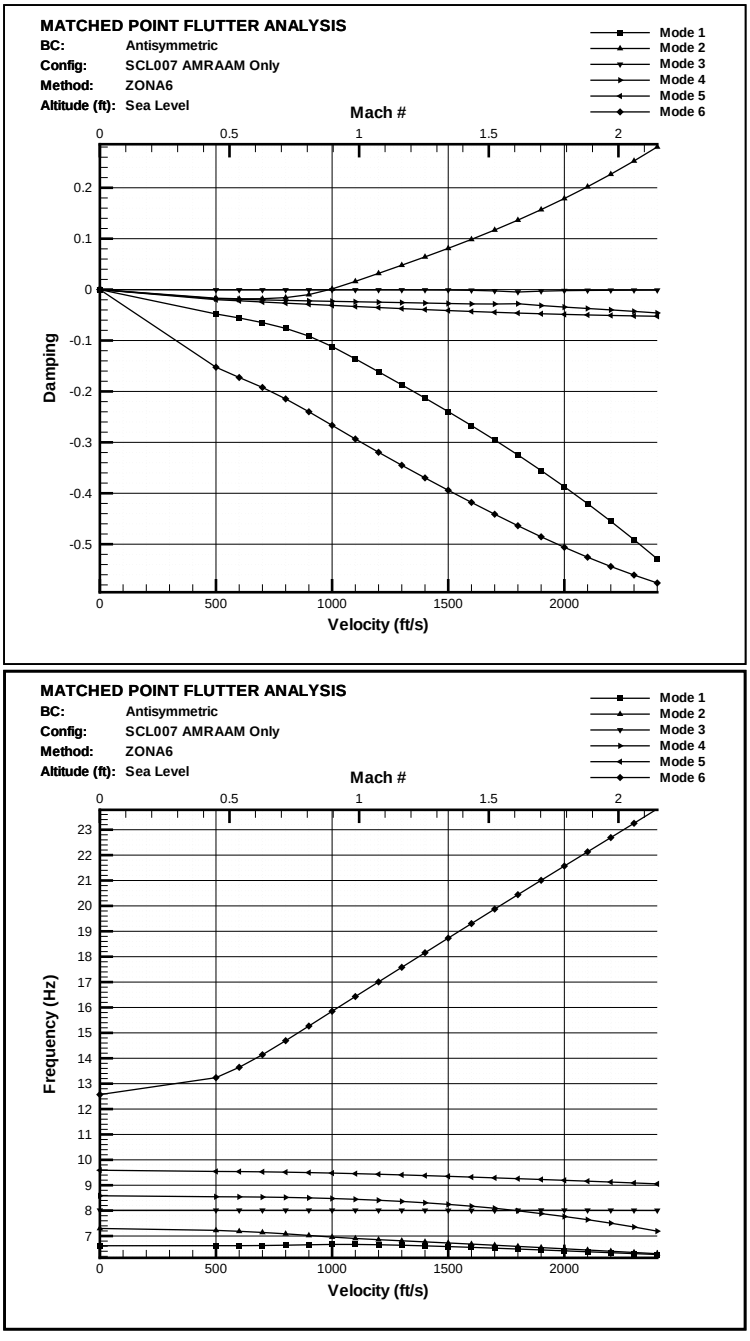

Figure A.2 SCL007 AMRAAM Only V-g/V-ω Plot (Sea Level, 0% Damping)

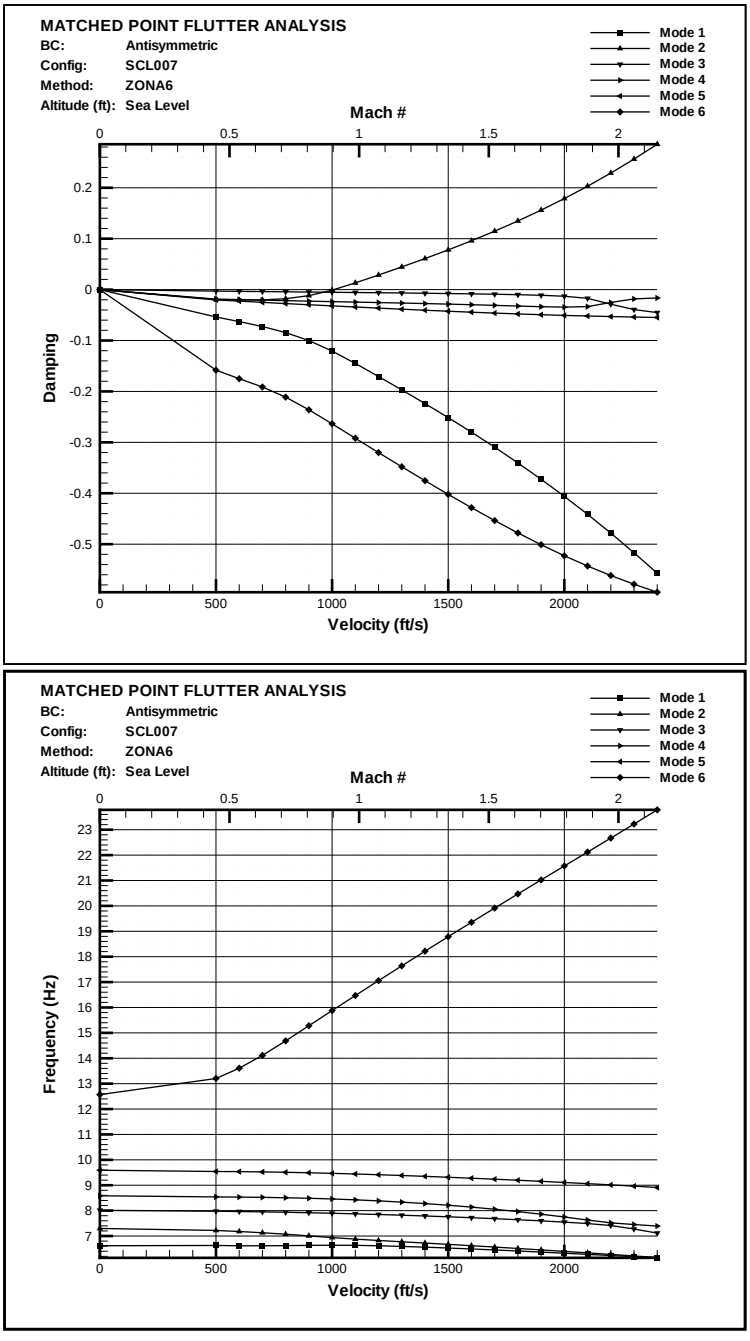

Figure A.3 SCL007 V-g/V-ω Plot (Sea Level, 0% Damping)

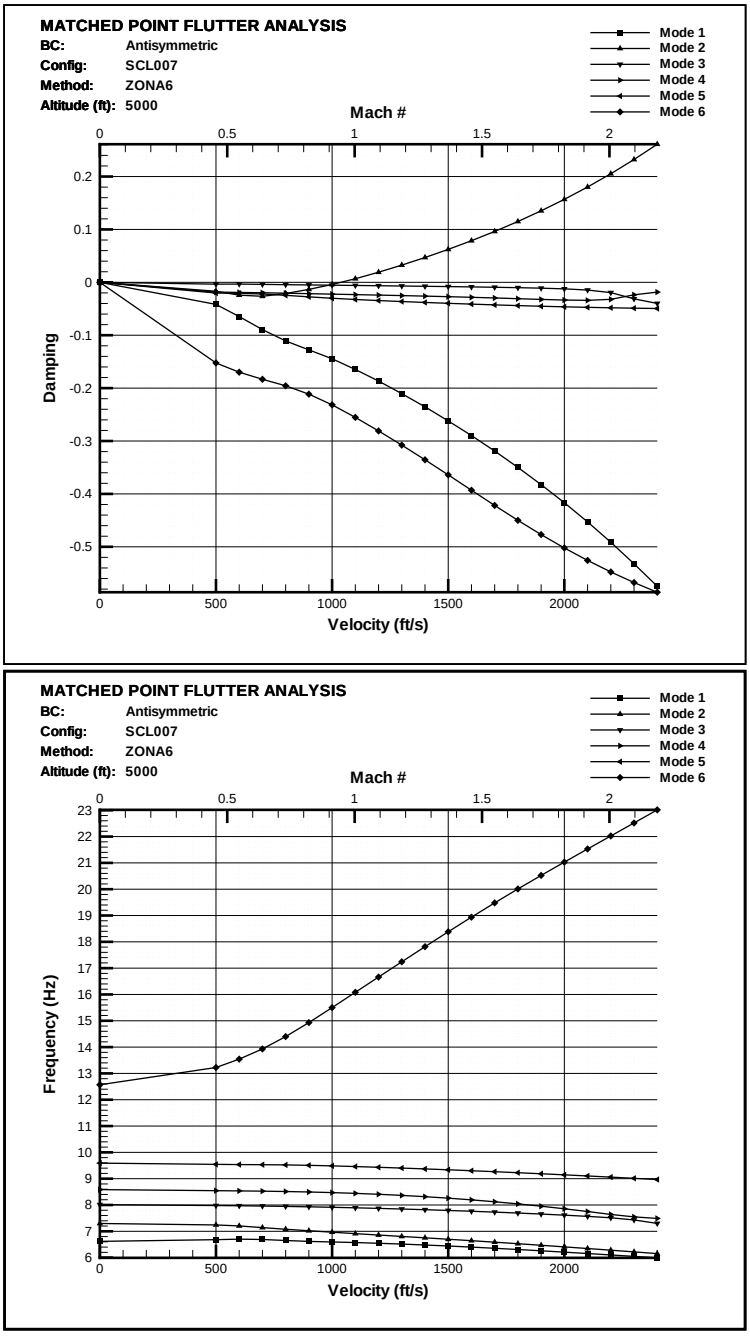

Figure A.4 SCL007 V-g/V-ω Plot (5000 ft, 0% Damping)

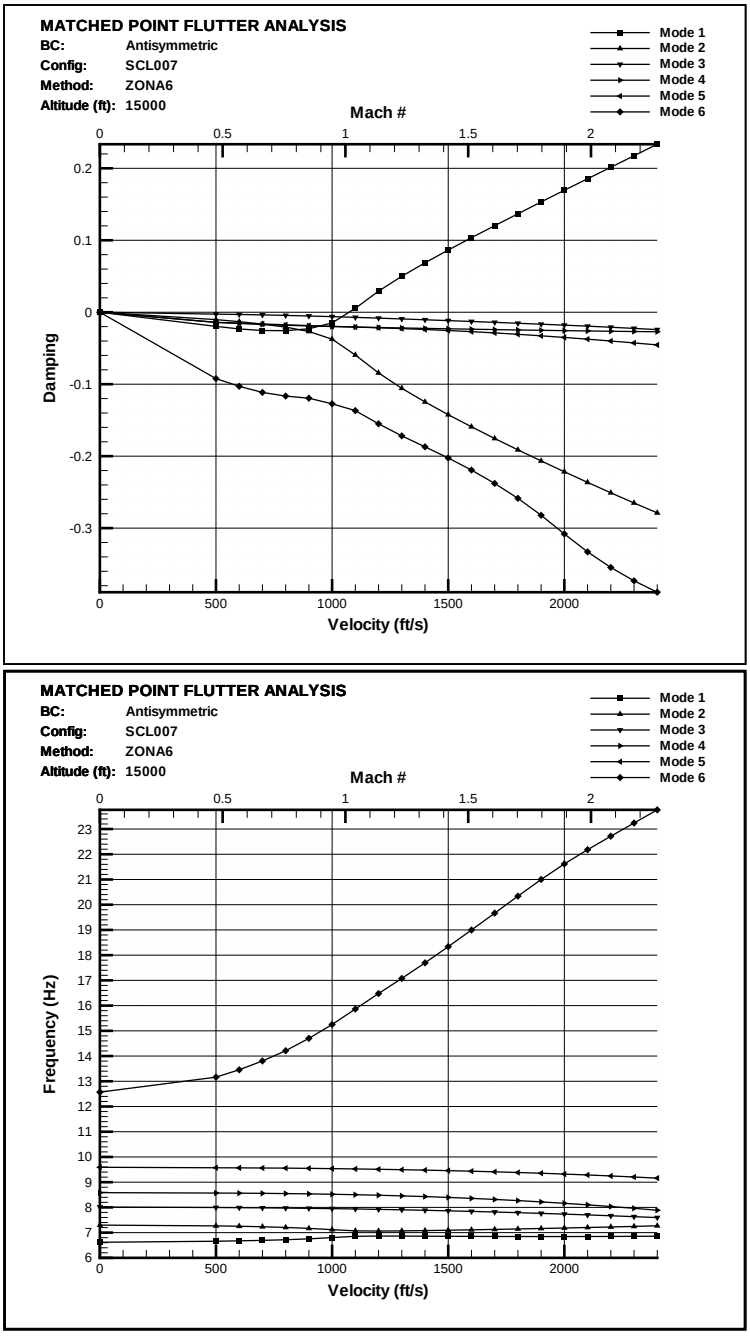

Figure A.5 SCL007 V-g/V-ω Plot (15000 ft, 0% Damping)

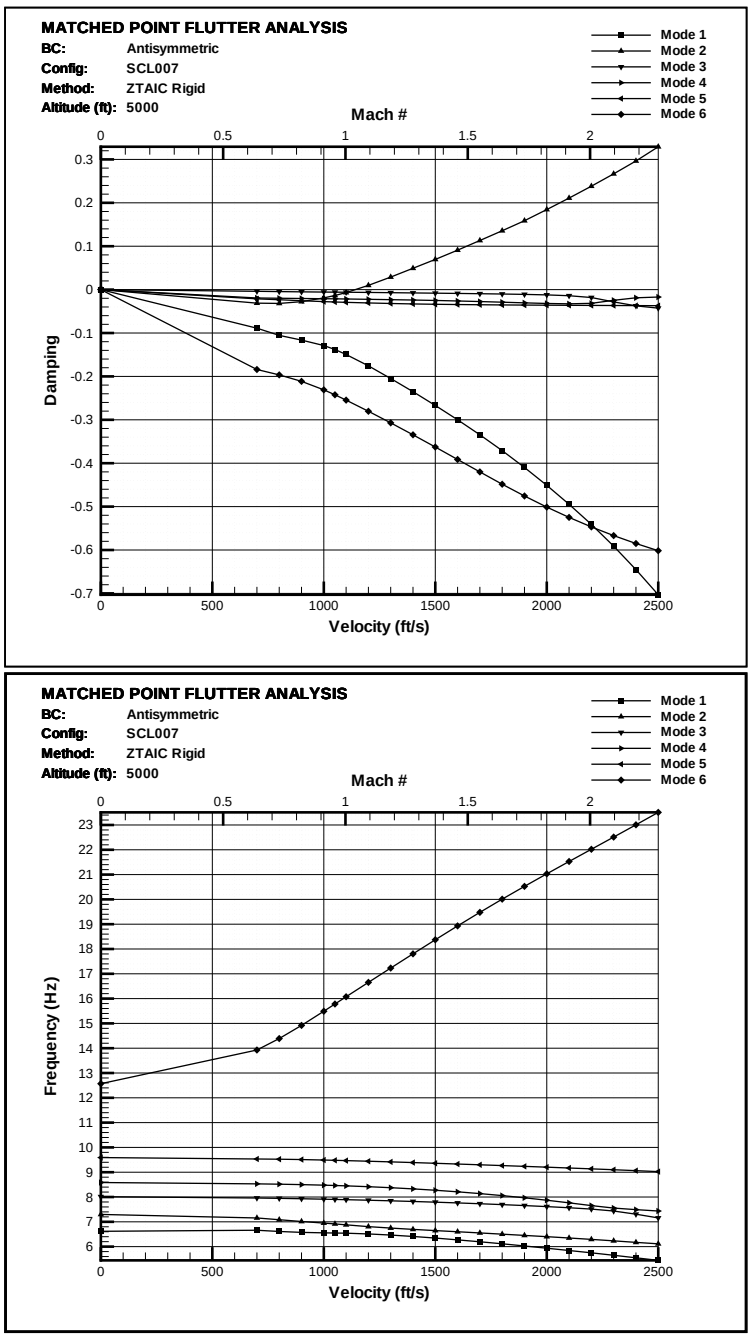

Figure A.6 SCL007 V-g/V-ω Plot Rigid C_p (5000 ft, 0% Damping)

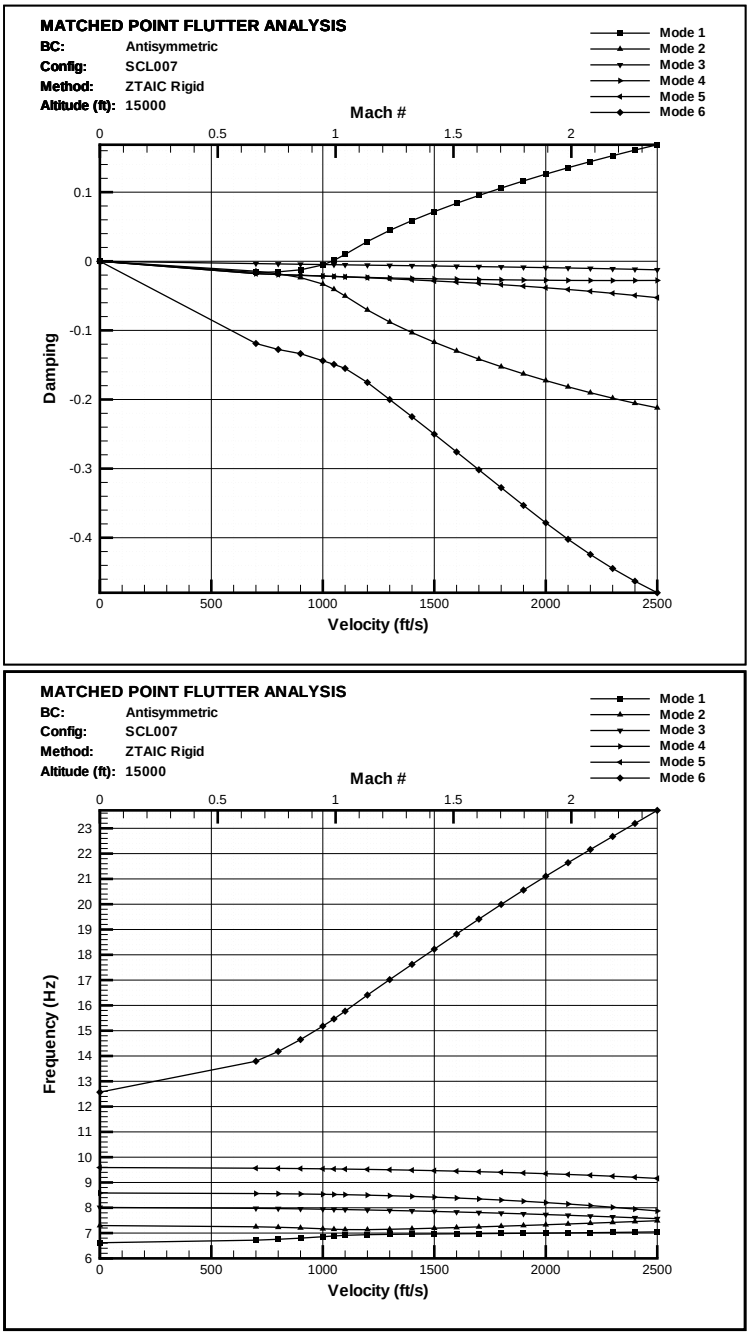

Figure A.7 SCL007 V-g/V-ω Plot Rigid C_p (15000 ft, 0% Damping)

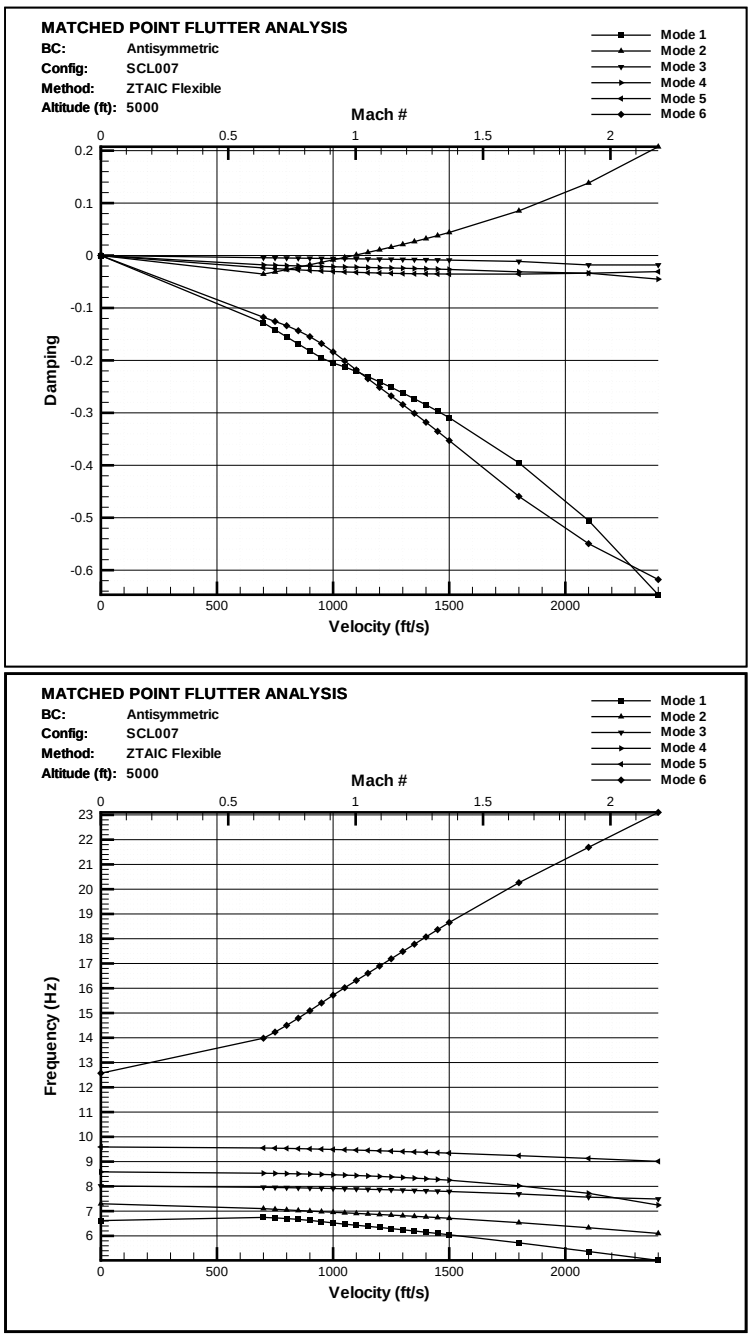

Figure A.8 SCL007 V-g/V-ω Plot Flexible C_p (5000 ft, 0% Damping)

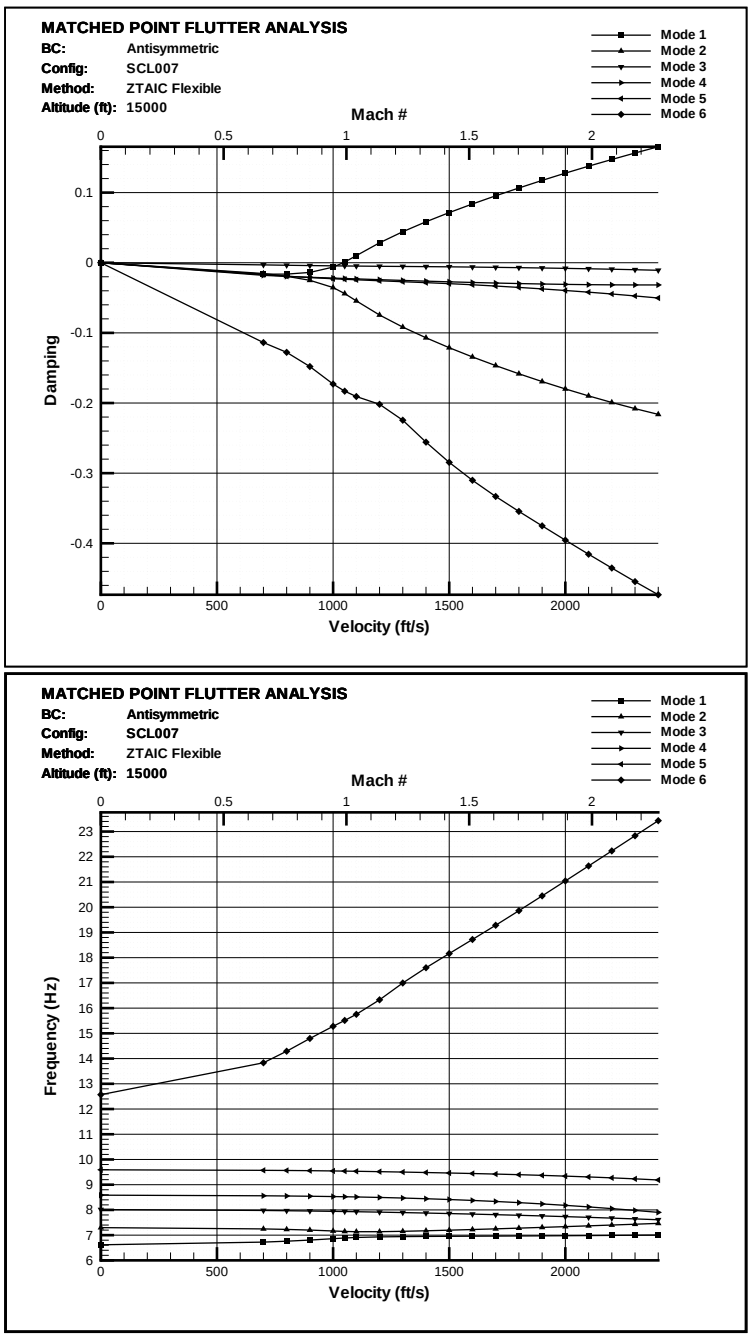

Figure A.9 SCL007 V-g/V-ω Plot Flexible C_p (15000 ft, 0% Damping)

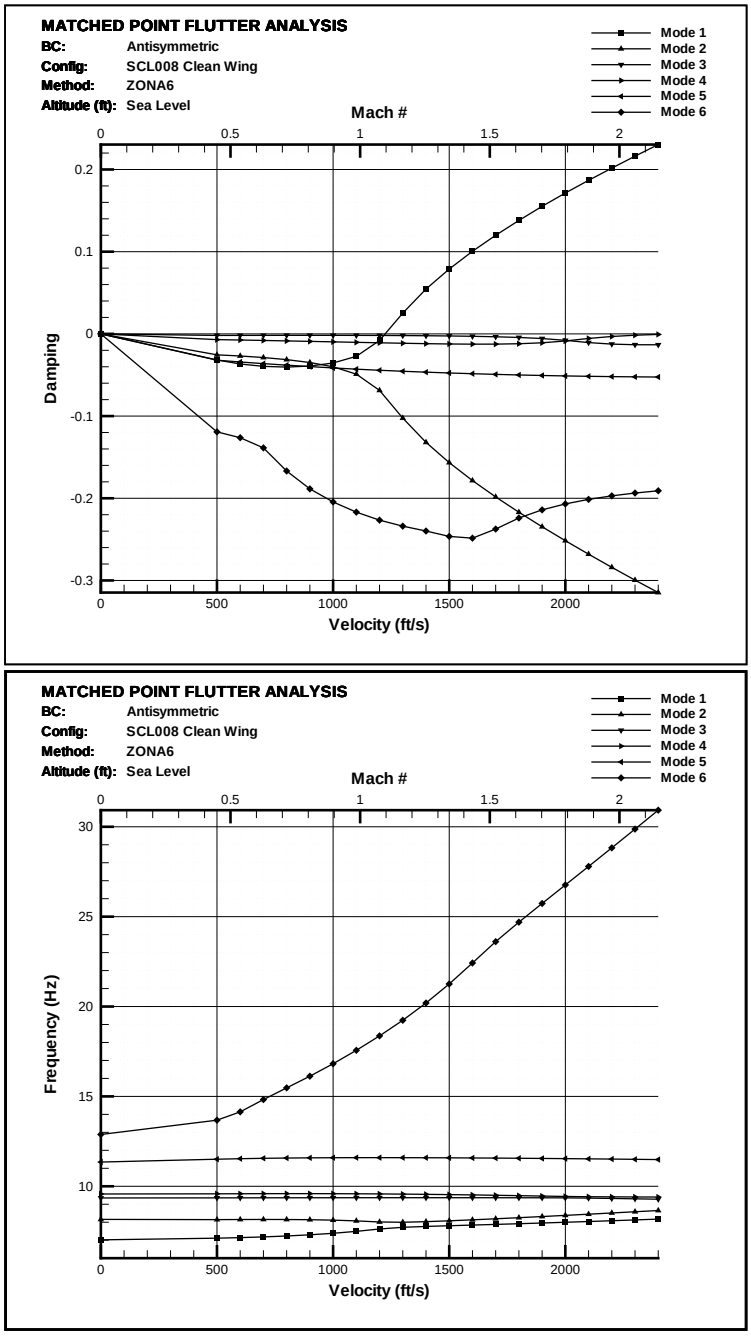

Figure A.10 SCL008 Clean Wing V-g/V-ω Plot (Sea Level, 0% Damping)

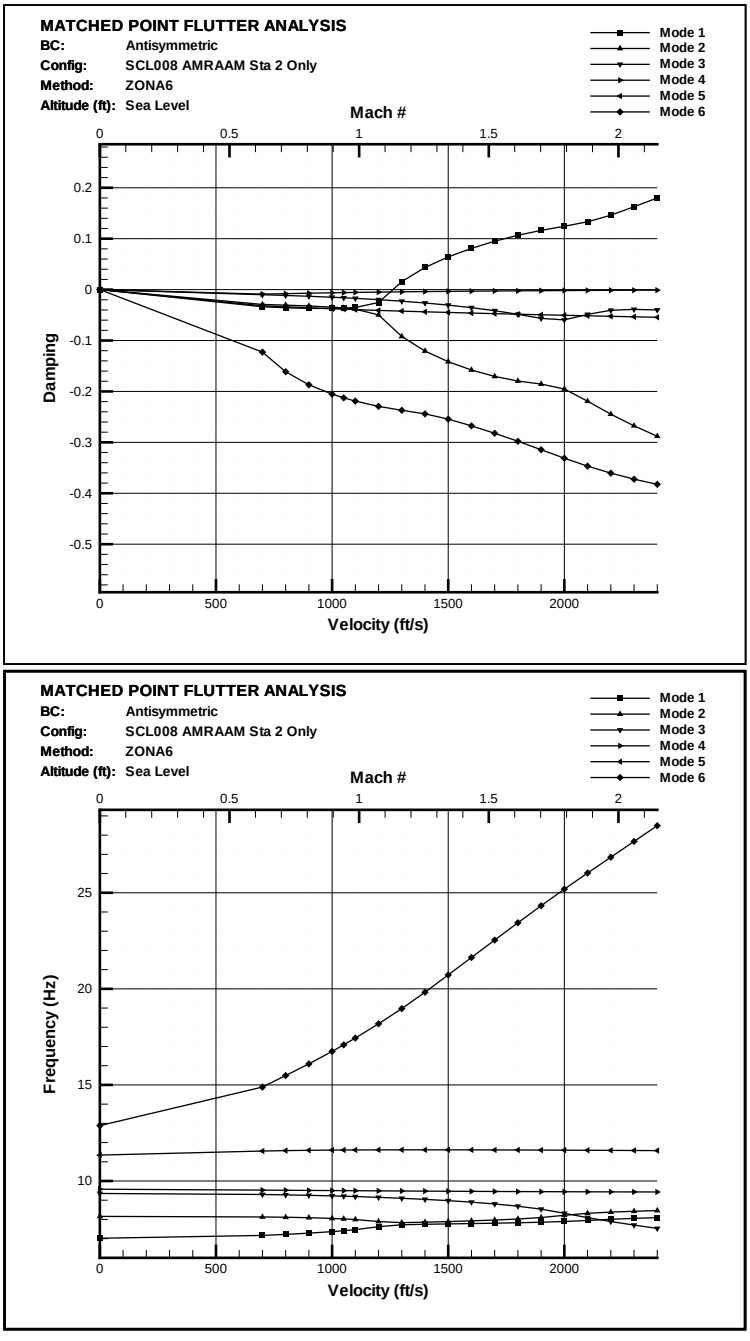

Figure A.11 SCL008 AMRAAM Sta 2 V-g/V-ω Plot (Sea Level, 0% Damping)

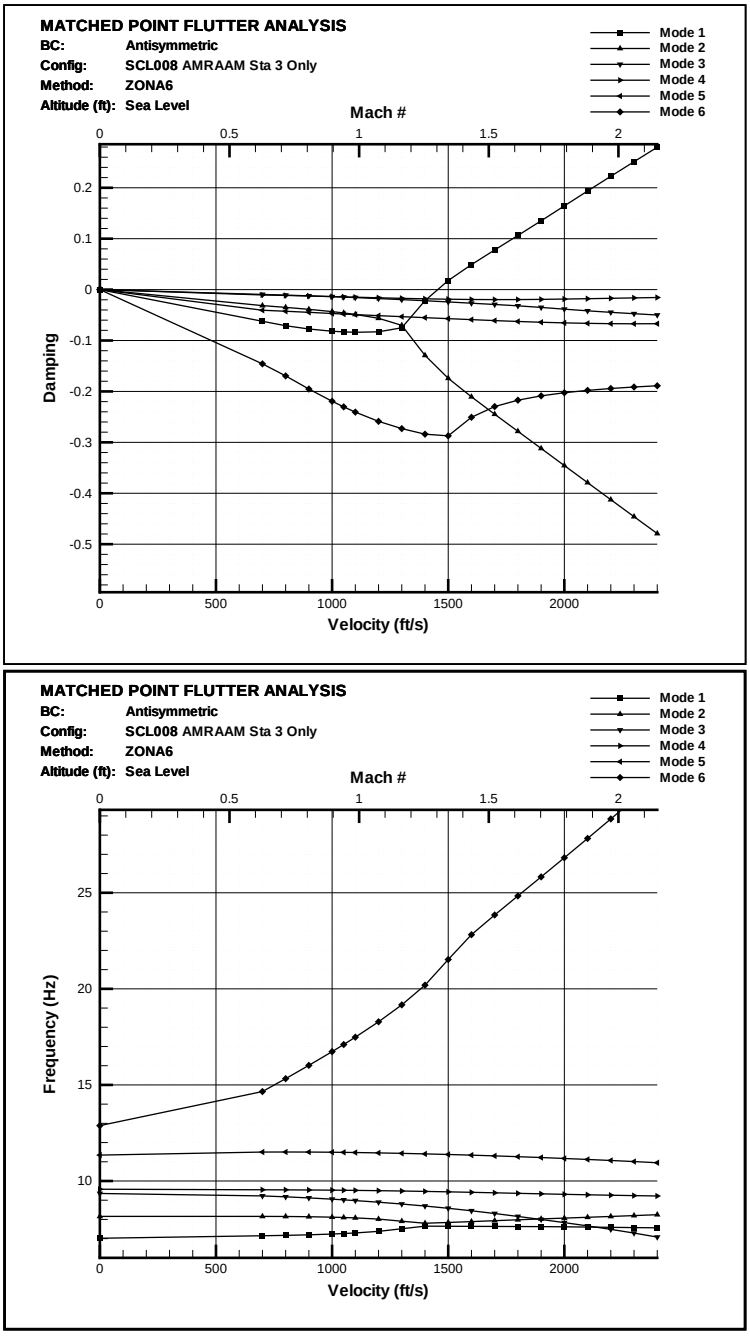

Figure A.12 SCL008 AMRAAM Sta 3 V-g/V-ω Plot (Sea Level, 0% Damping)

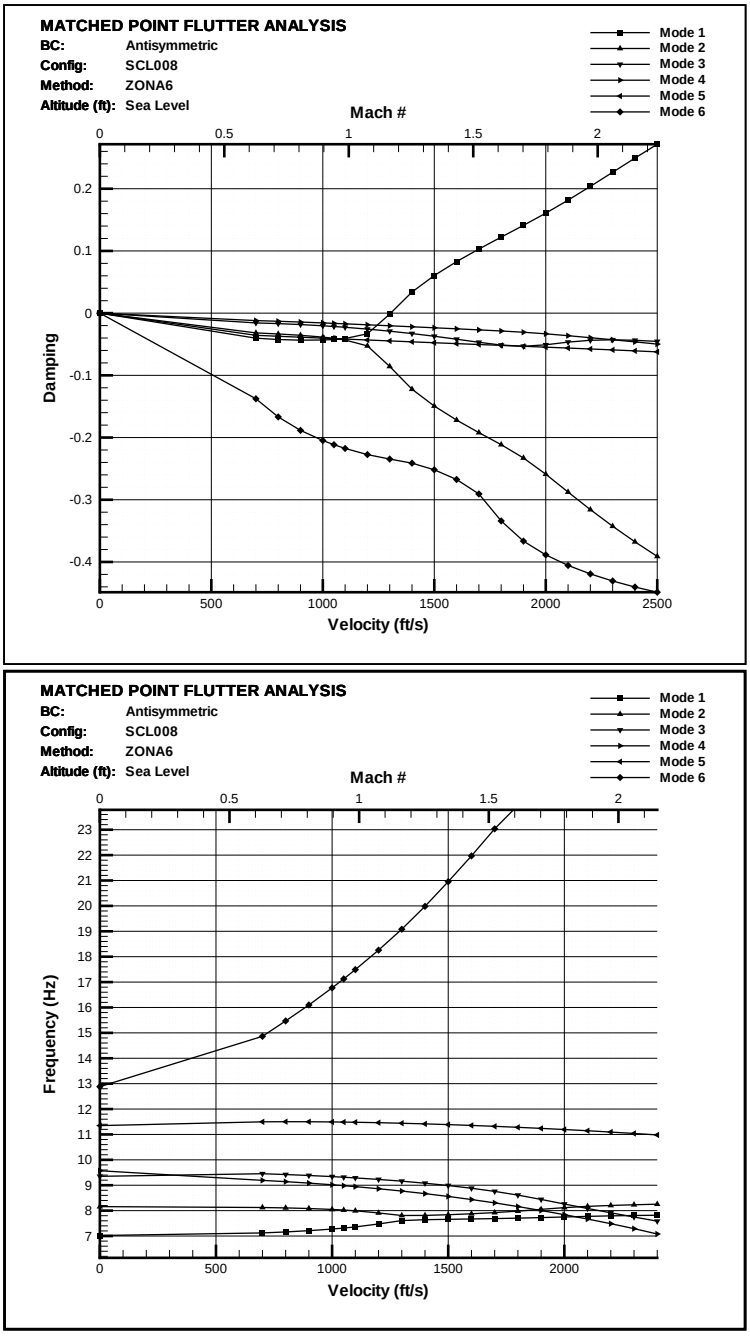

Figure A.13 SCL008 V-g/V-ω Plot (Sea Level, 0% Damping)

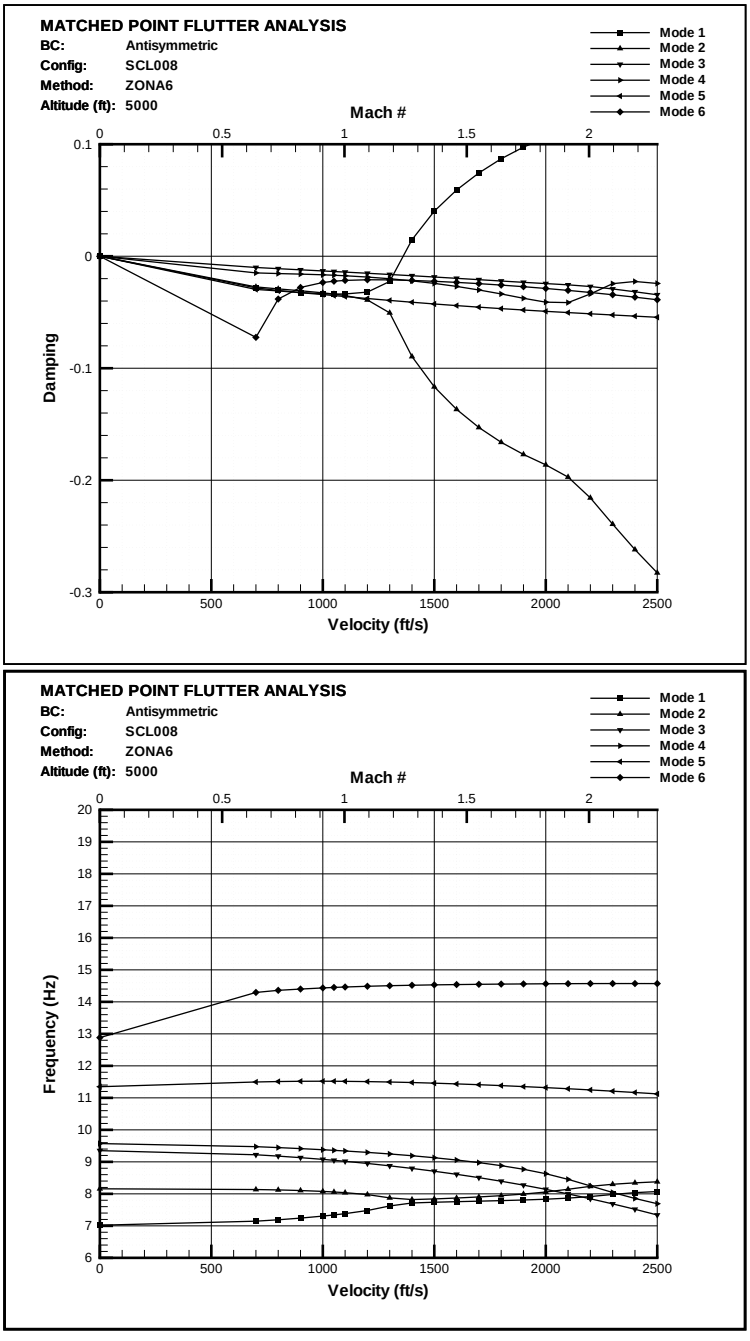

Figure A.14 SCL008 V-g/V-ω Plot (5000 ft, 0% Damping)

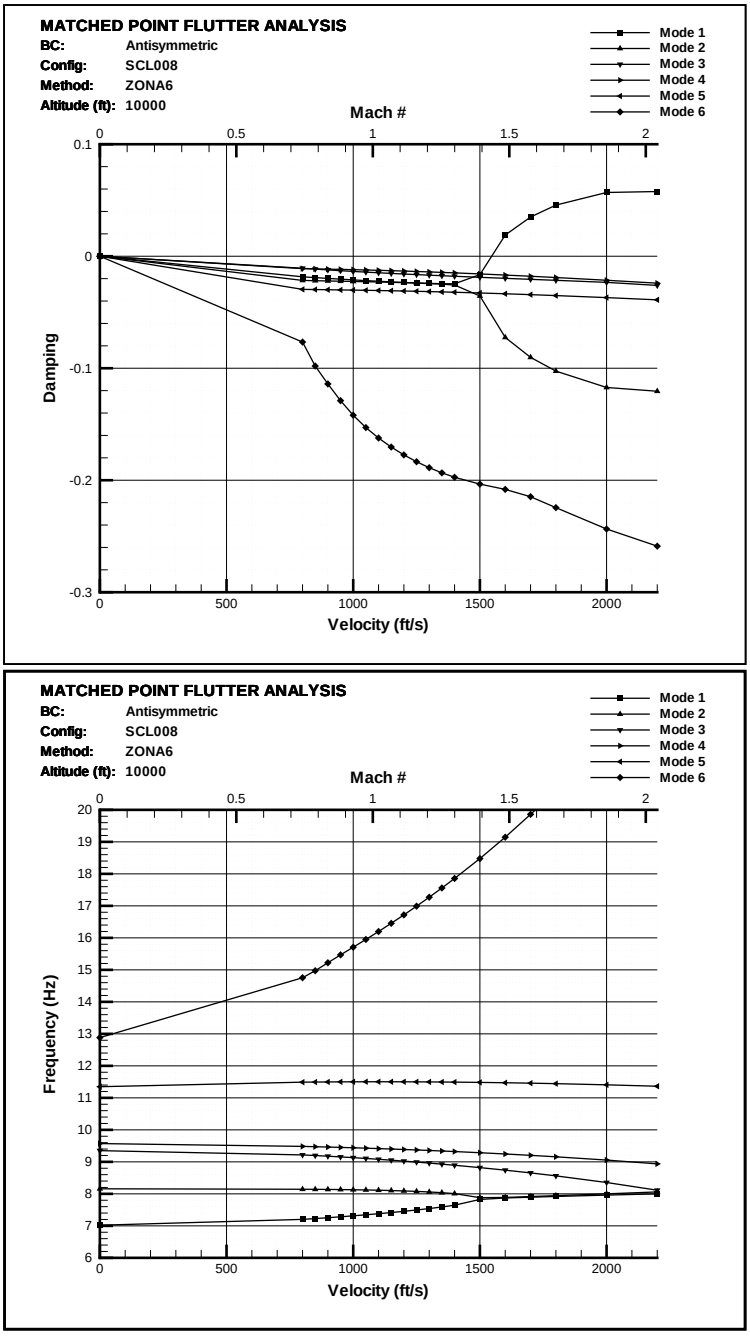

Figure A.15 SCL008 V-g/V-ω Plot (10000 ft, 0% Damping)

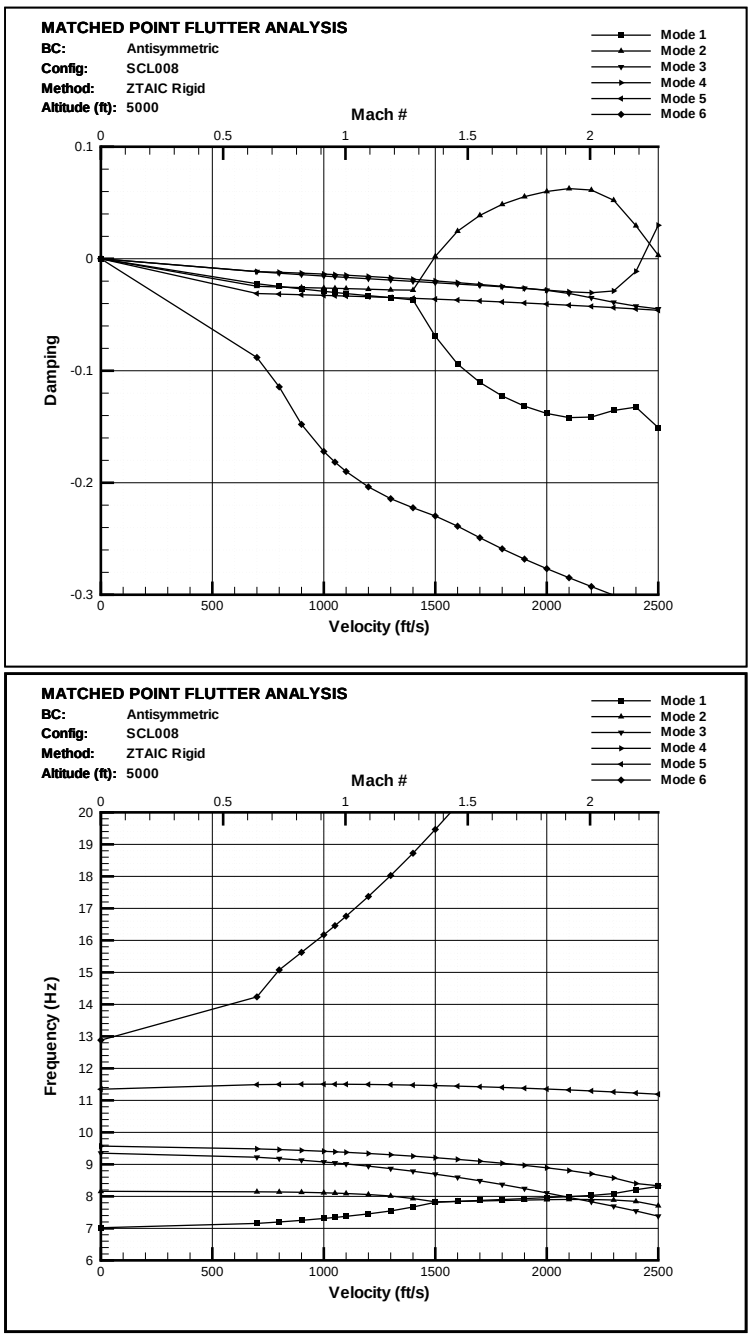

Figure A.16 SCL008 V-g/V-ω Plot Rigid C_p (5000 ft, 0% Damping)

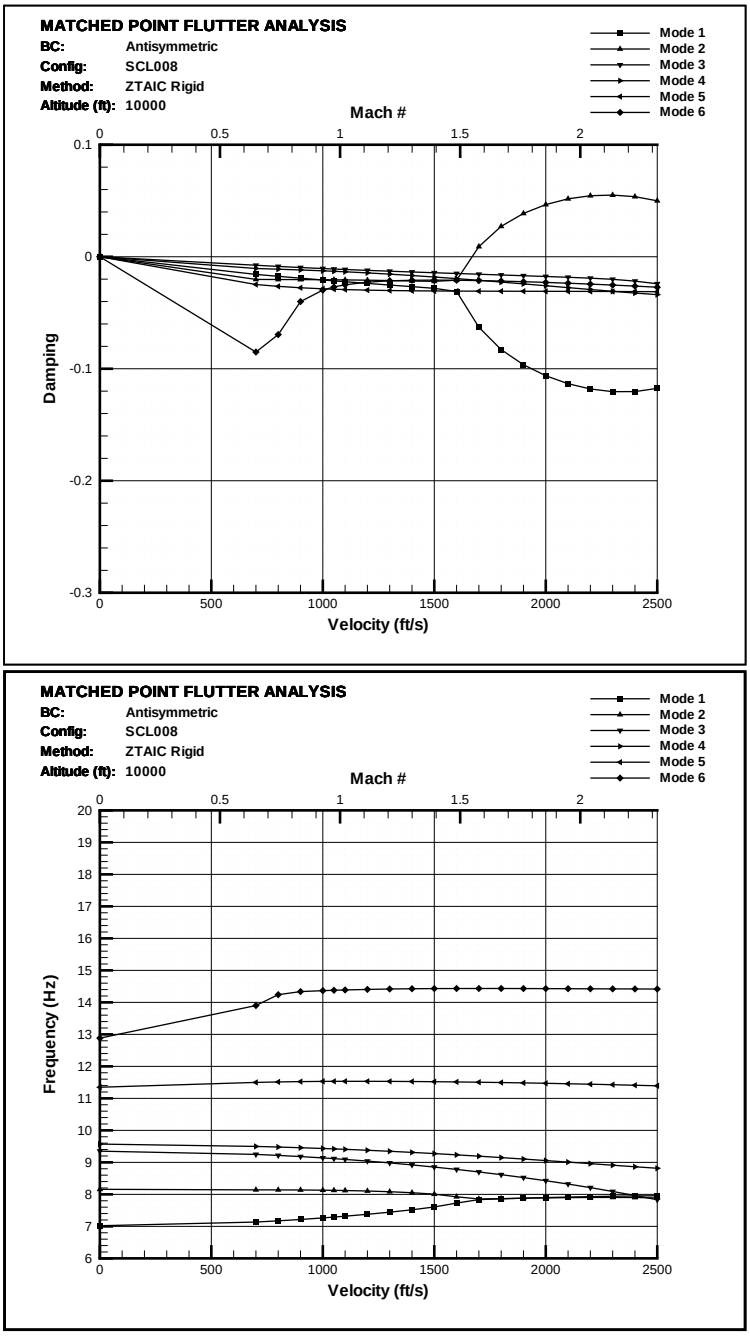

Figure A.17 SCL008 V-g/V-ω Plot Rigid C_p (10000 ft, 0% Damping)

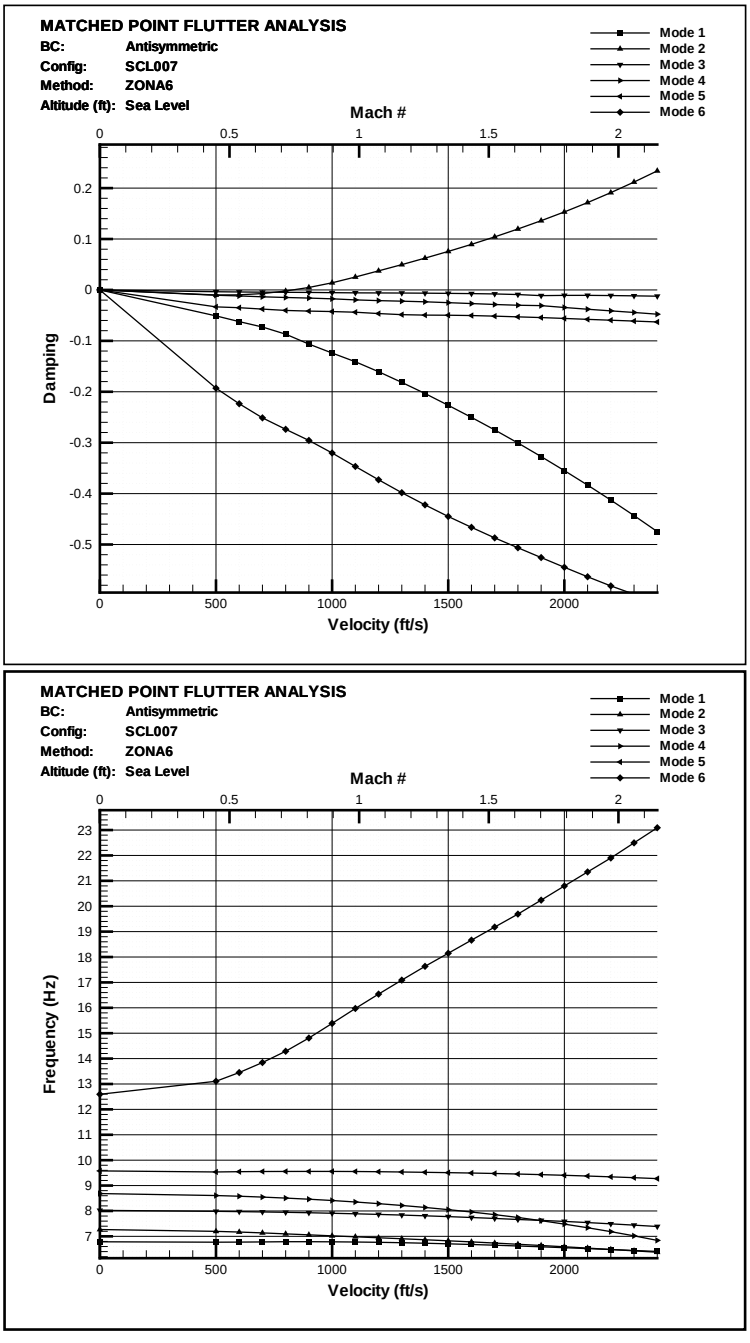

Figure A.18 Tuned SCL007 V-g/V-ω Plot (Sea Level, 0% Damping)

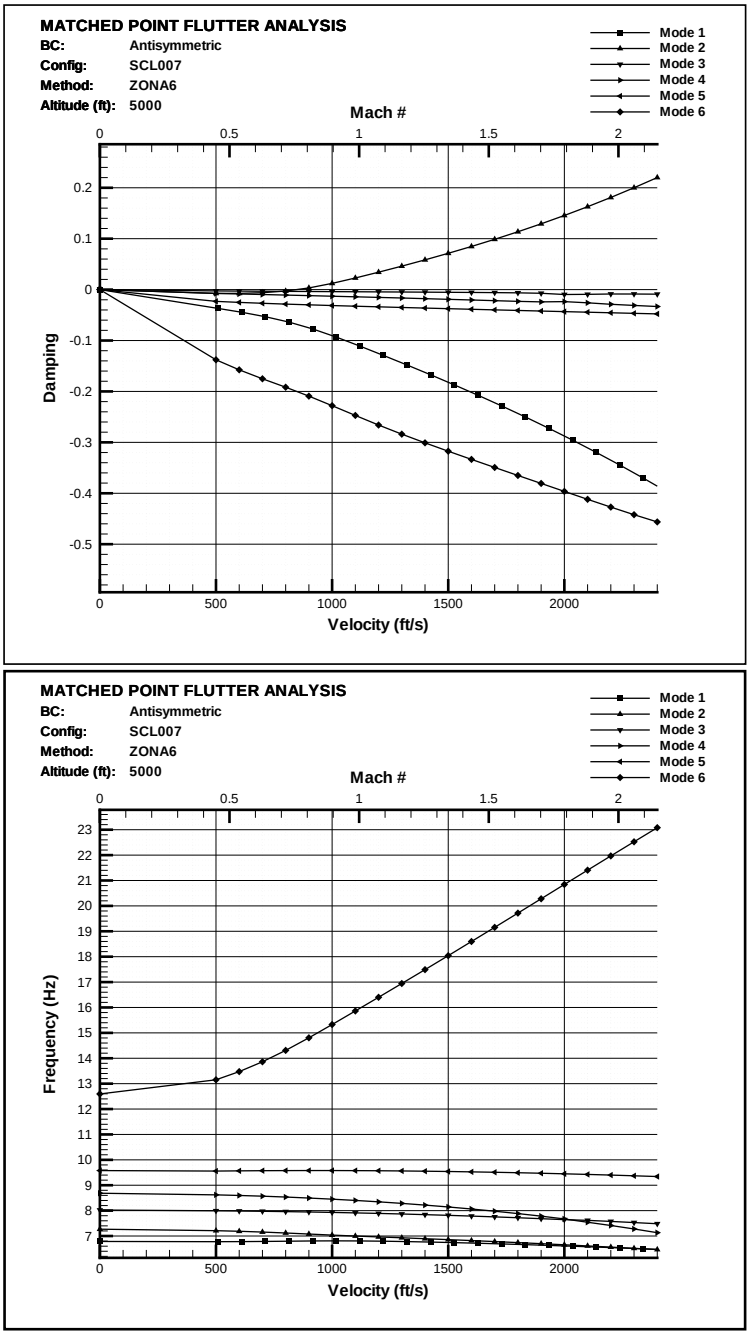

Figure A.19 Tuned SCL007 V-g/V-ω Plot (5000 ft, 0% Damping)

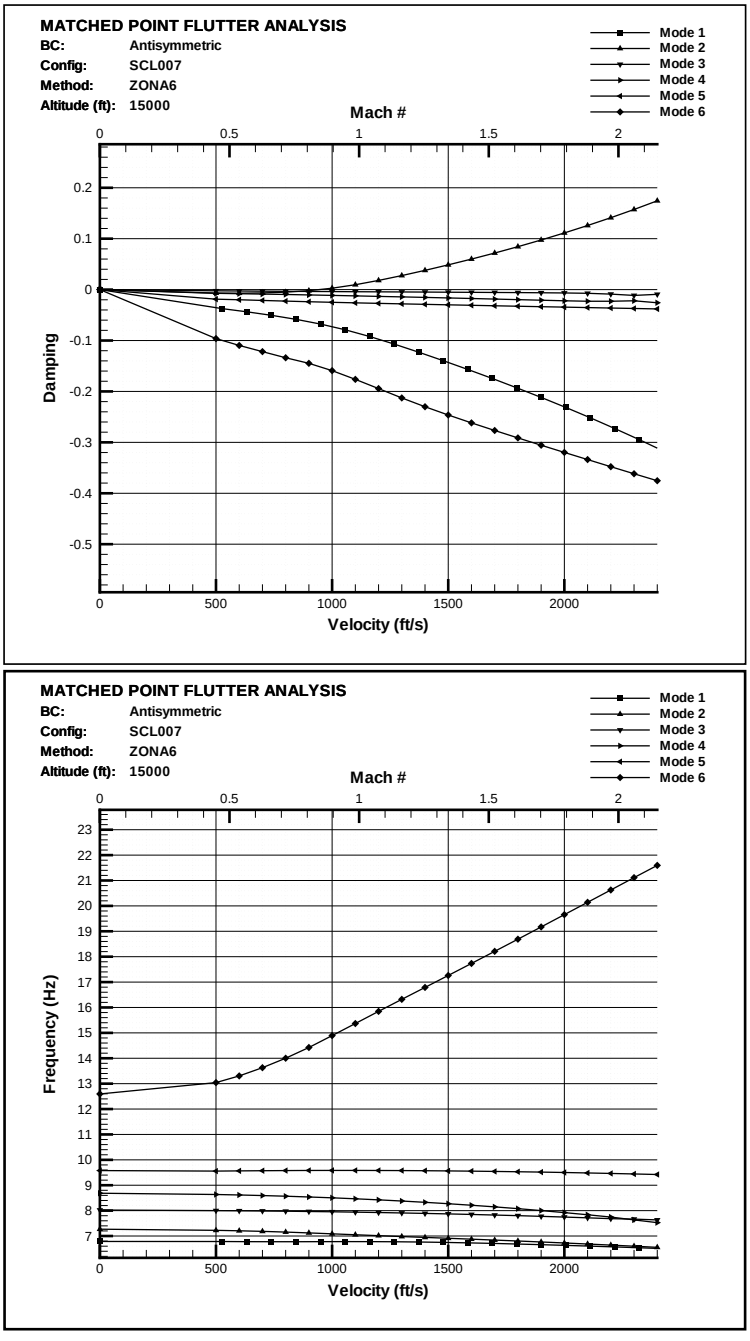

Figure A.20 Tuned SCL007 V-g/V-ω Plot (15000 ft, 0% Damping)

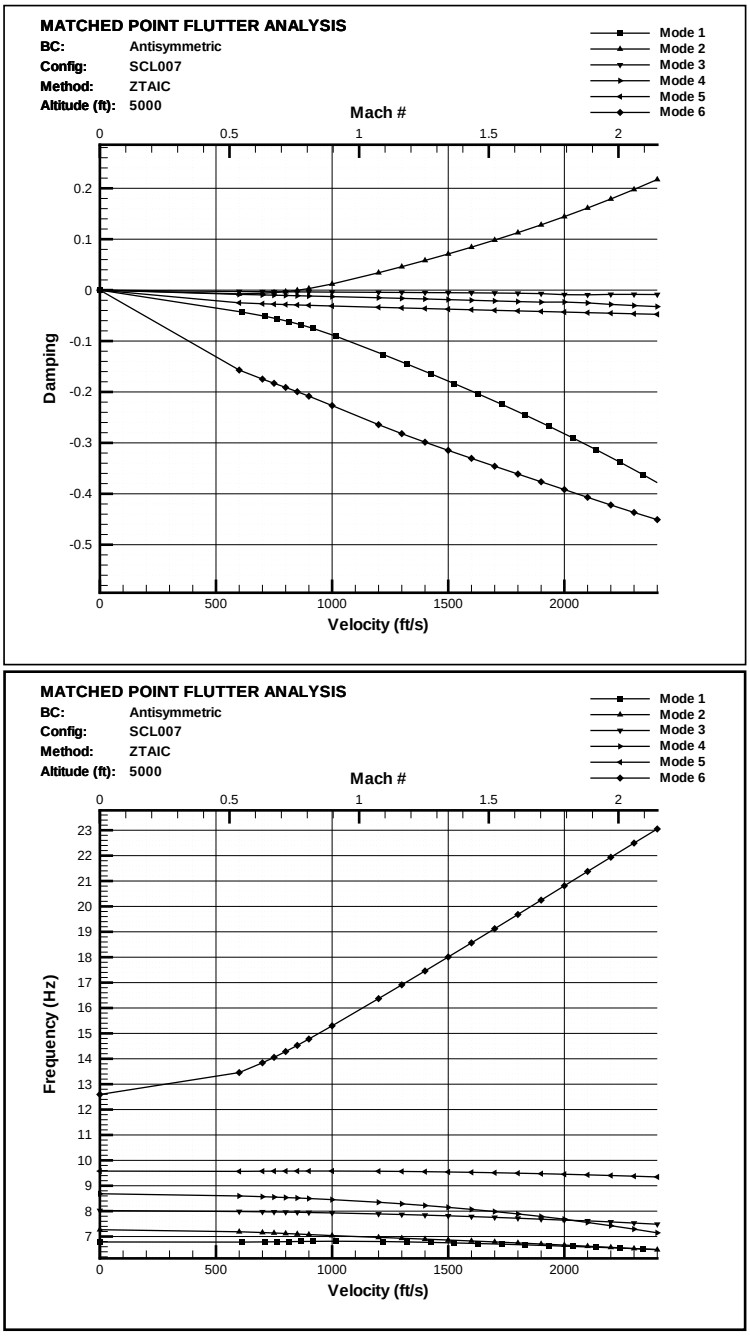

Figure A.21 Tuned SCL007 V-g/V-ω Plot Rigid C_p (5000 ft, 0% Damping)

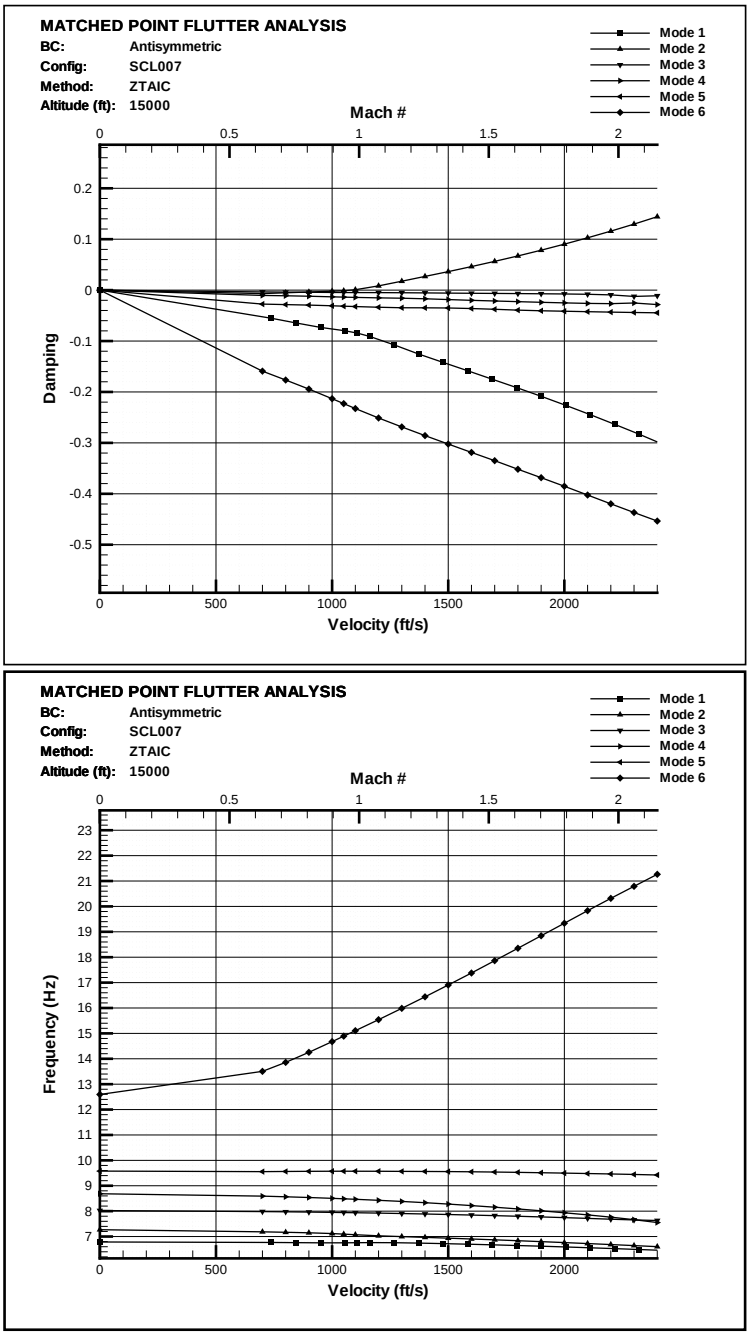

Figure A.22 Tuned SCL007 V-g/V-ω Plot Rigid C_p (15000 ft, 0% Damping)

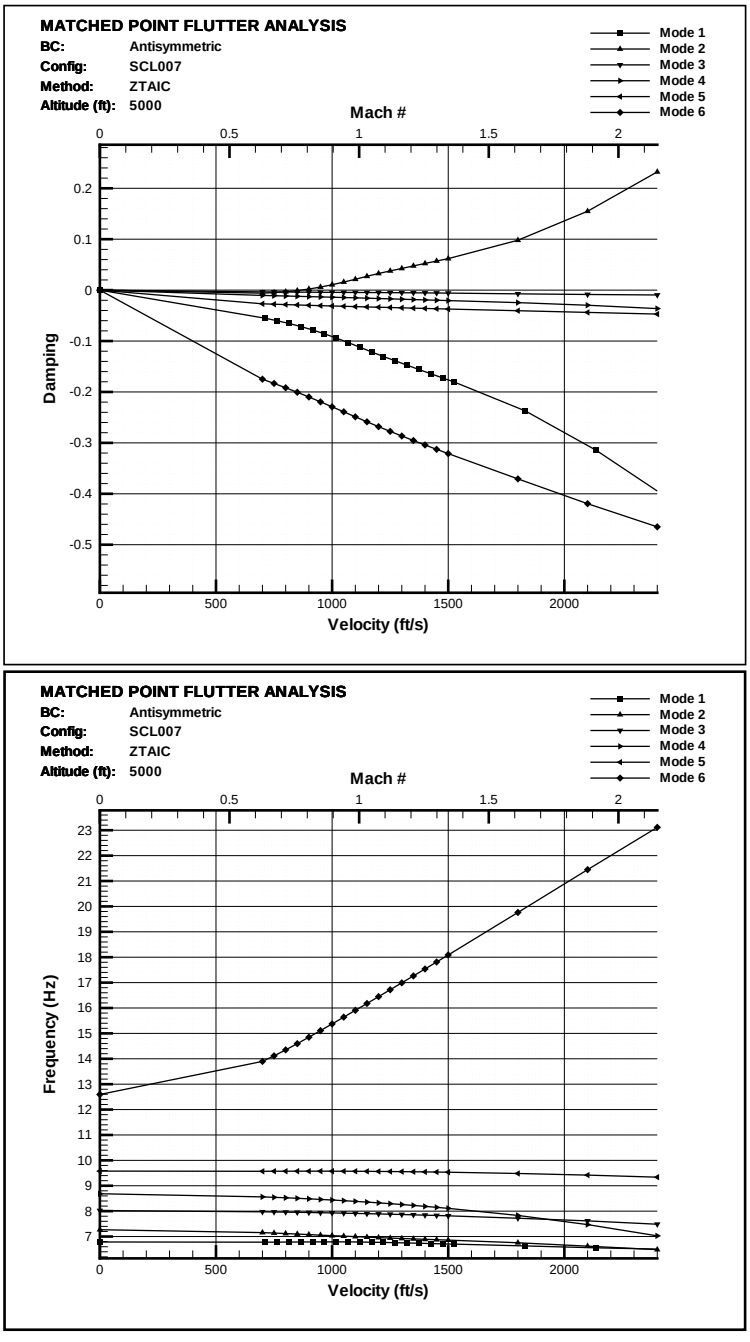

Figure A.23 Tuned SCL007 V-g/V-ω Plot Flexible C_p (5000 ft, 0% Damping)

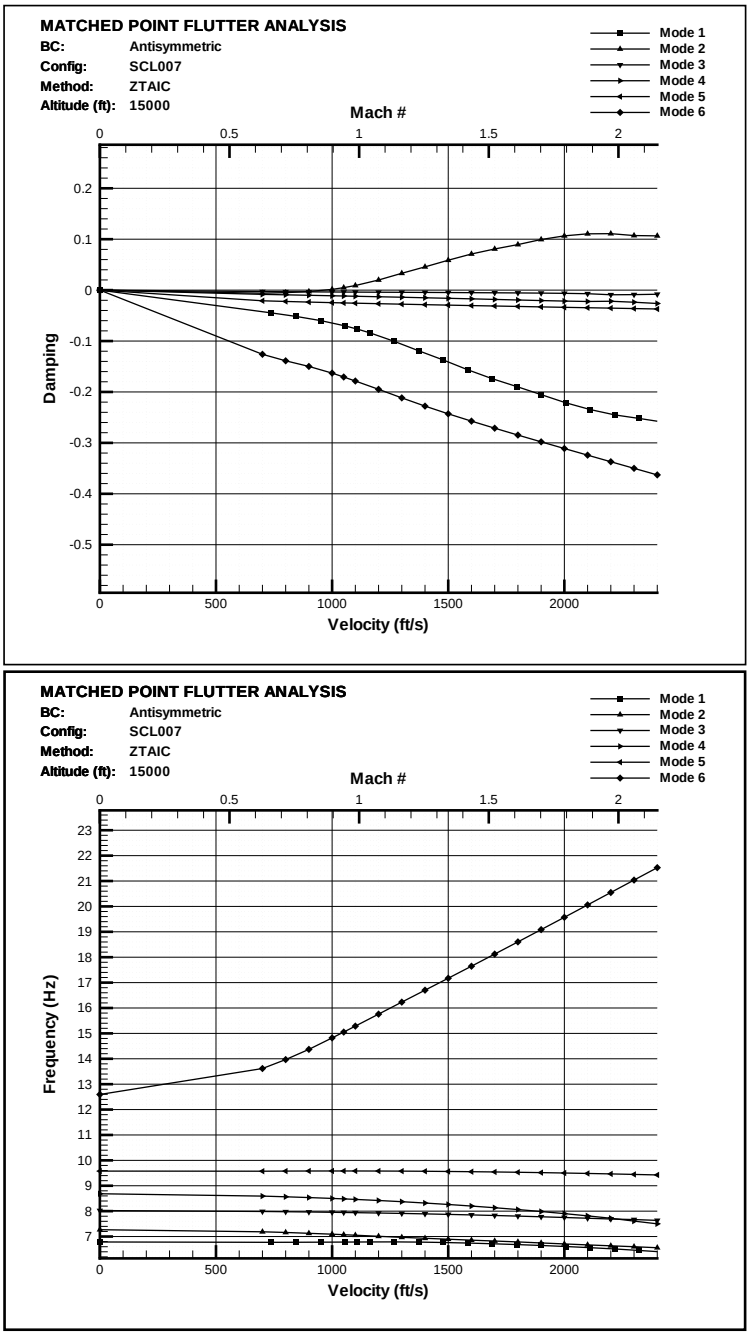

Figure A.24 Tuned SCL007 V-g/V-ω Plot Flexible C_p (15000 ft, 0% Damping)

Appendix B. C_p Data

B.1 CFD and Interpolated Steady C_p Data for SCL007

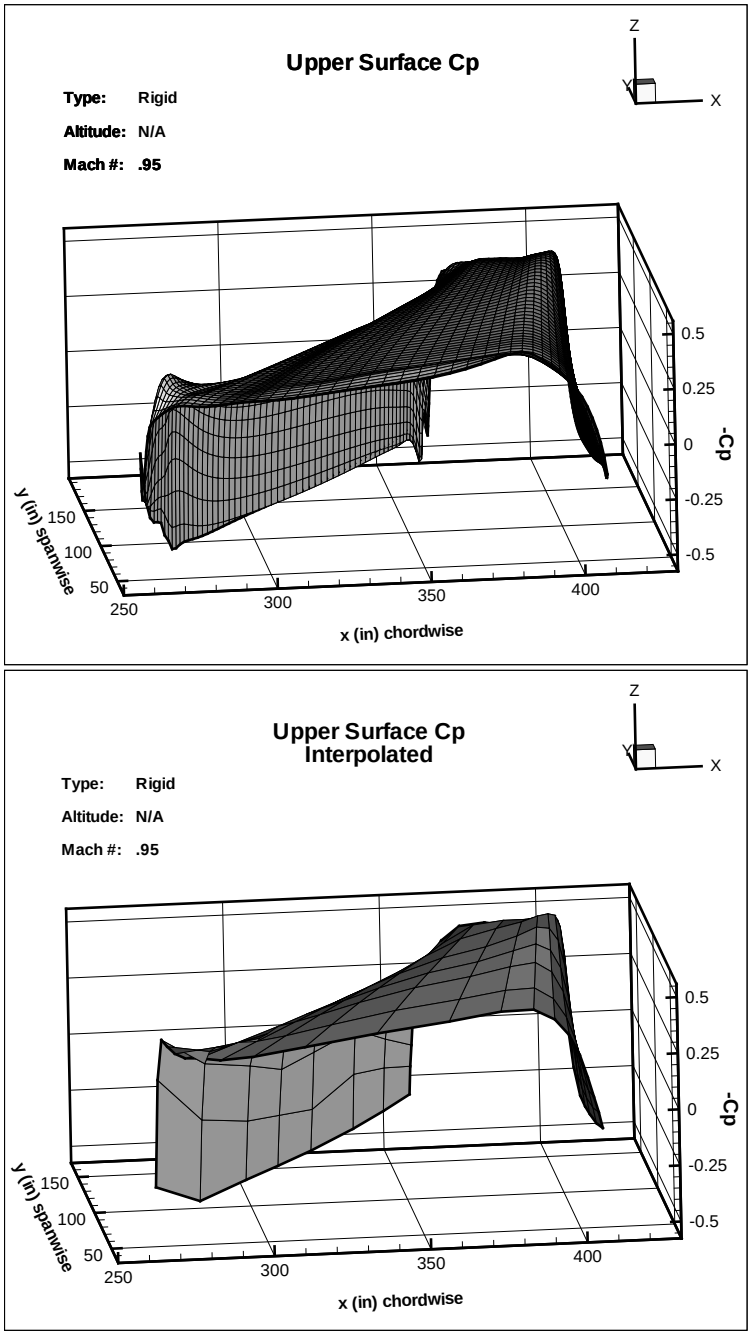

Figure B.1 CFD and Interpolated Upper Surface Steady C_p Data for SCL007

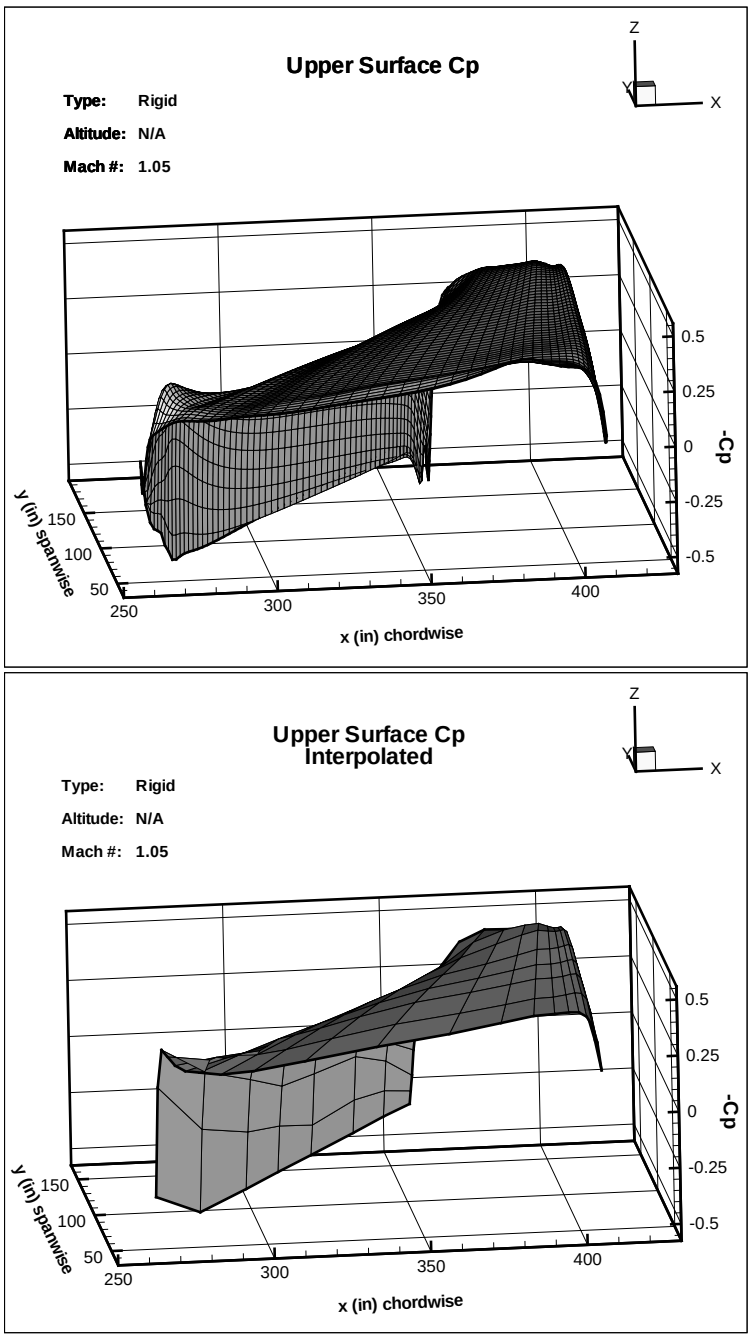

Figure B.2 CFD and Interpolated Upper Surface Steady C_p Data for SCL007

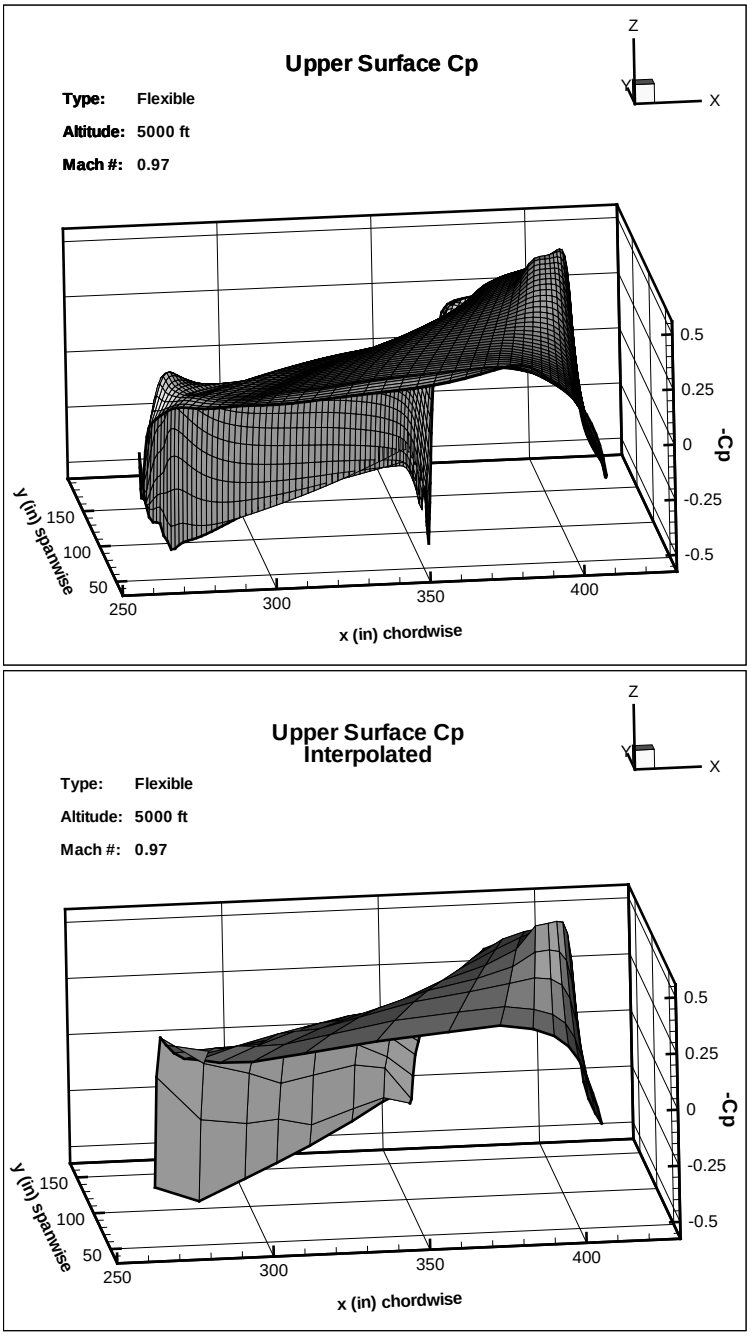

Figure B.3 CFD and Interpolated Upper Surface Steady C_p Data for SCL007

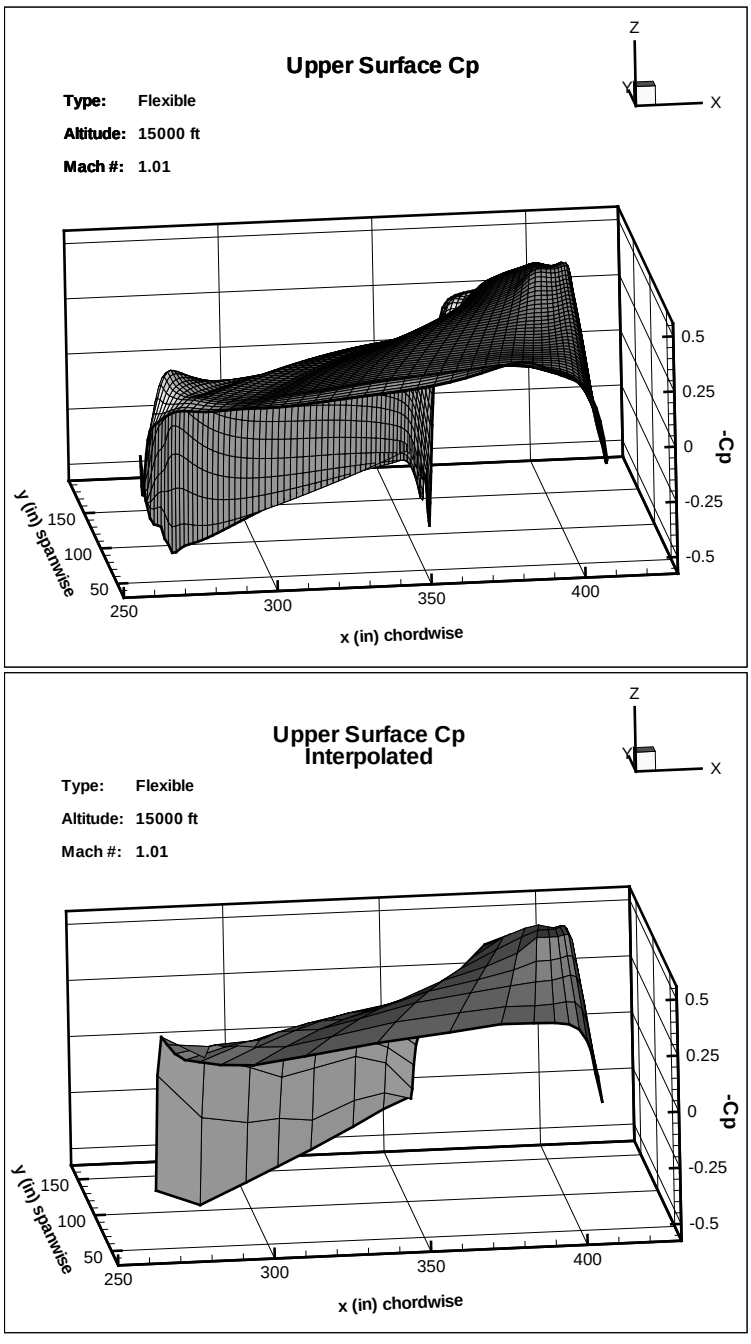

Figure B.4 CFD and Interpolated Upper Surface Steady C_p Data for SCL007

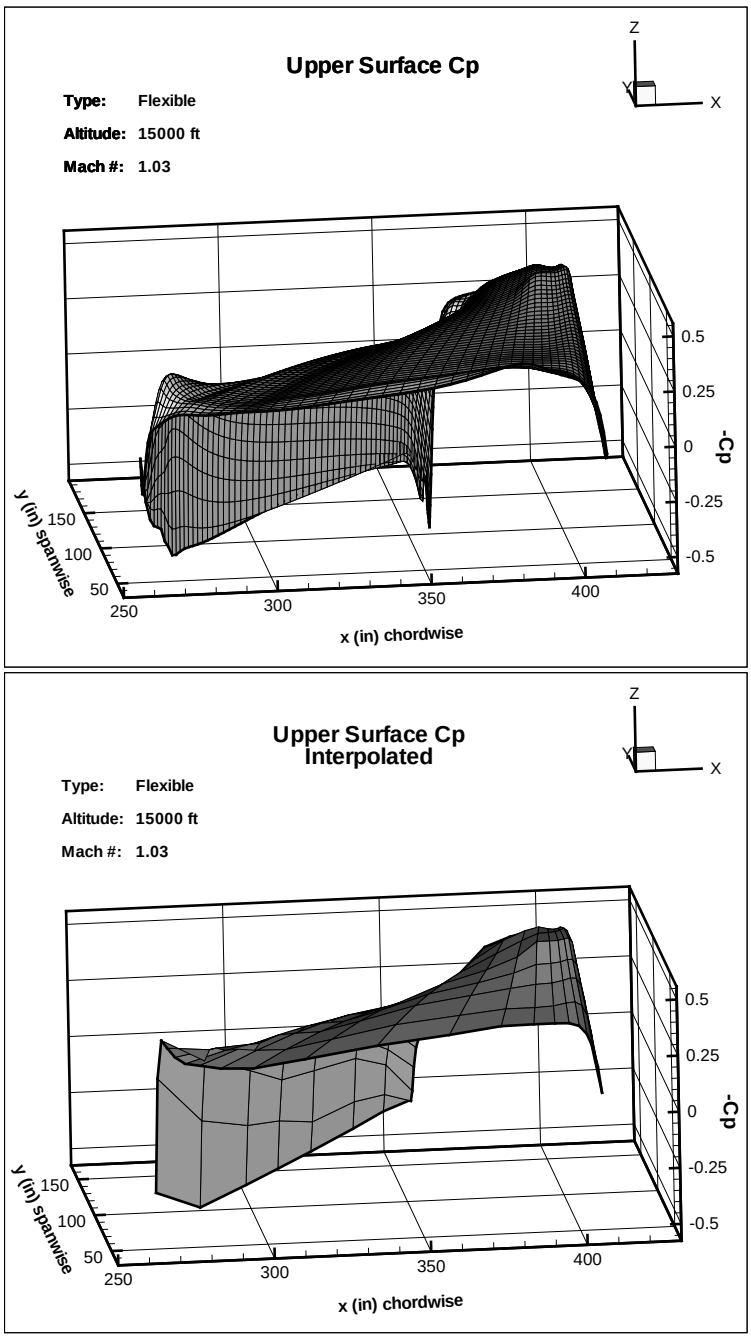

Figure B.5 CFD and Interpolated Upper Surface Steady C_p Data for SCL007

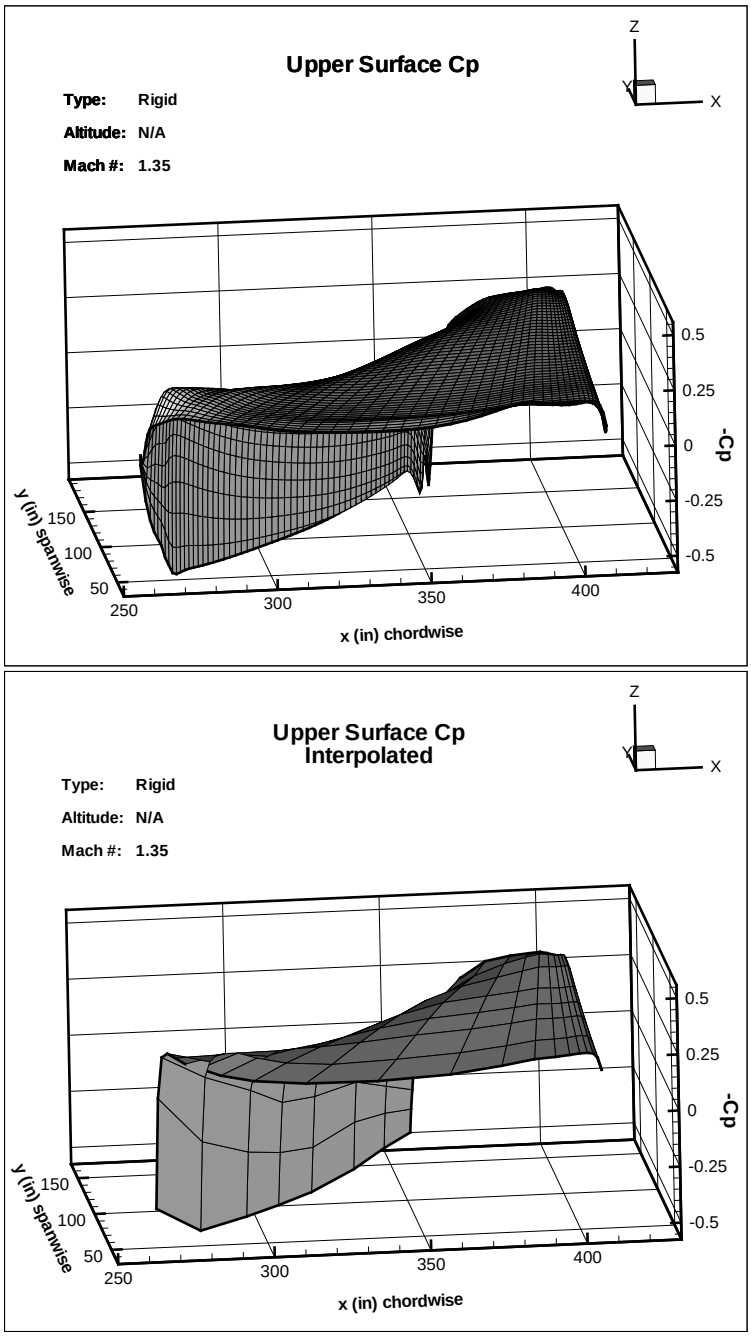

Figure B.6 CFD and Interpolated Upper Surface Steady C_p Data for SCL008

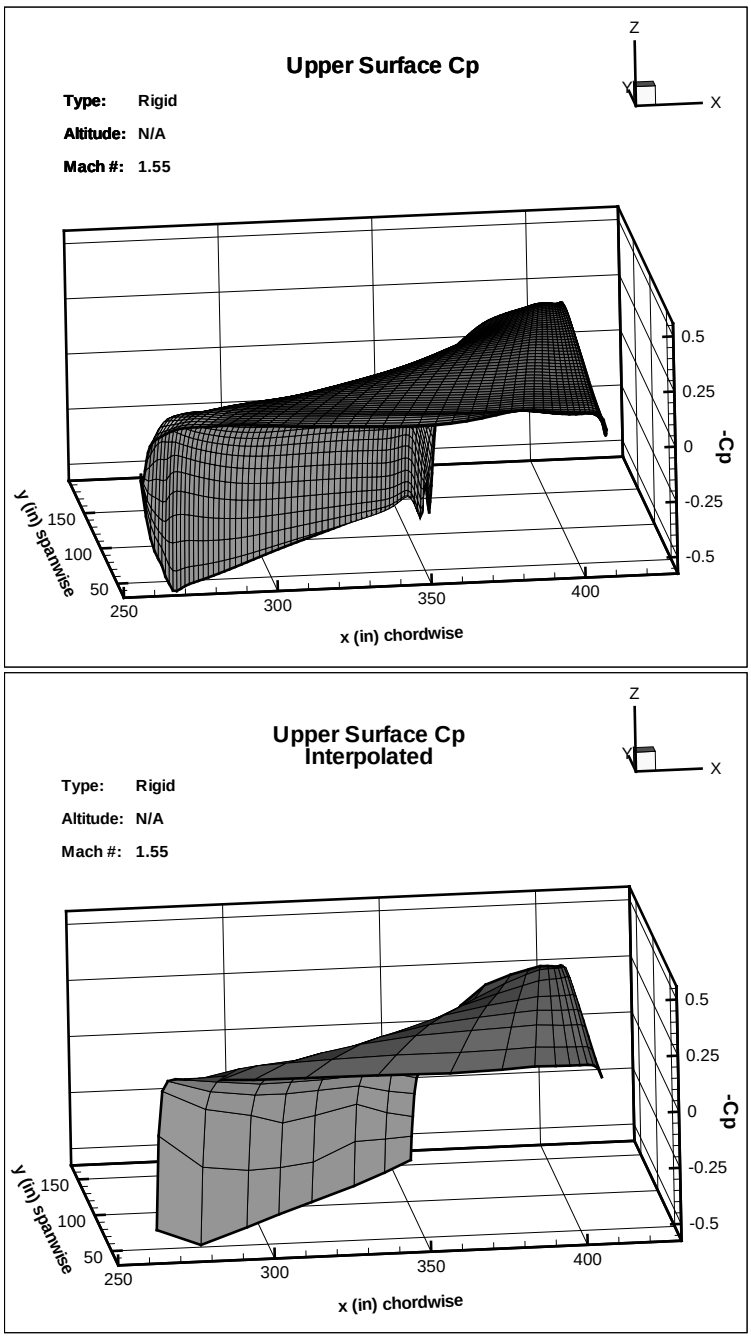

Figure B.7 CFD and Interpolated Upper Surface Steady C_p Data for SCL008

Appendix C. ZAERO Input Files

C.1 SCL007 Bulk Data

```
ASSIGN FEM=C:\BTHESIS\ZAERO\S7M_L.F06, PRINT =0, FORM = MSC, BOUND = ANTI
CEND
$
TITLE =F16 LCO ANALYSIS. CASE SCL007 (LAU129 + AMRAAM + 370 TANK )
ECHO = SORT
$
SUBCASE = 1
        SUBTITLE = ANTI-SYMMETRIC BOUNDARY CONDITION
        LABEL    = MATCH POINT FLUTTER AT SEA LEVEL FROM M=0.75 TO M=0.95
$
        FLUTTER = 10
$
BEGIN BULK
$************************************************************************
$
$      ----   F - 1 6    A E R O D Y N A M I C    M O D E L   ----
$                    (  C A S E    S C L 0 0 7  )
$
$************************************************************************
$
$AEROZ  ACSID   XZSYM   FLIP    FMMUNIT FMLUNIT REFC    REFB    REFS    CONT
AEROZ   77      YES     YES     SLIN    IN      121.5                   +AE1
+AE1    0.0     0.0     0.0
$CORD2R CID     RID     A1      A2      A3      B1      B2      B3      CONT
CORD2R  77              0.      0.      0.      0.      0.      100.    +C2R1
+C2R1   0.      -100.   0.
$
$ FUSELAGE
ACOORD        10     0.0     0.0    -5.0     0.0     0.0     0.0
BODY7       1001FUSELAGE              10       1    1001
SEGMESH     1001      33       5                                       +SEG11
+SEG11         3    8.00                             101     102         +SEG12
+SEG12         3   25.00                             103     104         +SEG13
+SEG13         3   42.00                             105     106         +SEG14
+SEG14         3   59.00                             107     108         +SEG15
+SEG15         3   76.00                             109     110         +SEG16
+SEG16         3   93.00                             111     112         +SEG17
+SEG17         3  110.00                             113     114         +SEG18
+SEG18         3  127.00                             115     116         +SEG19
```

```
+SEG19          3  144.00                                  117     118          +SEG20
+SEG20          3  161.00                                  119     120          +SEG21
+SEG21          3  178.00                                  121     122          +SEG22
+SEG22          3  197.85                                  121     122          +SEG23
+SEG23          3  217.70                                  121     122          +SEG24
+SEG24          3  237.54                                  121     122          +SEG25
+SEG25          3  257.39                                  121     122          +SEG26
+SEG26          3  277.24                                  121     122          +SEG27
+SEG27          3  297.09                                  121     122          +SEG28
+SEG28          3  316.94                                  121     122          +SEG29
+SEG29          3  336.78                                  121     122          +SEG30
+SEG30          3  356.63                                  121     122          +SEG31
+SEG31          3  376.48                                  121     122          +SEG32
+SEG32          3  392.70                                  121     122          +SEG33
+SEG33          3  408.92                                  121     122          +SEG34
+SEG34          3  421.75                                  121     122          +SEG35
+SEG35          3  434.58                                  121     122          +SEG36
+SEG36          3  447.40                                  121     122          +SEG37
+SEG37          3  460.23                                  121     122          +SEG38
+SEG38          3  473.06                                  121     122          +SEG39
+SEG39          3  485.89                                  121     122          +SEG40
+SEG40          3  498.72                                  121     122          +SEG41
+SEG41          3  511.54                                  121     122          +SEG42
+SEG42          3  524.37                                  121     122          +SEG43
+SEG43          3  537.20                                  121     122
AEFACT       101  0.00    0.00   0.00    0.00    0.00
AEFACT       102  0.00    0.00   0.00    0.00    0.00
AEFACT       103  0.00    2.00   3.00    2.00    0.00
AEFACT       104 -2.90   -2.30   0.50    2.50    3.20
AEFACT       105  0.00    4.00   6.00    4.00    0.00
AEFACT       106 -5.80   -4.60   1.00    5.00    6.40
AEFACT       107  0.00    6.00   9.00    6.00    0.00
AEFACT       108 -8.70   -6.90   1.50    7.50    9.60
AEFACT       109  0.00    8.00  12.00    8.00    0.00
AEFACT       110-11.60   -9.20   2.00   10.00   12.80
AEFACT       111  0.00   10.00  15.00   10.00    0.00
AEFACT       112-14.50  -11.50   2.50   12.50   16.00
AEFACT       113  0.00   12.00  18.00   12.00    0.00
AEFACT       114-17.40  -13.80   3.00   15.00   19.20
AEFACT       115  0.00   14.00  21.00   14.00    0.00
AEFACT       116-20.30  -16.10   3.50   17.50   22.40
AEFACT       117  0.00   16.00  24.00   16.00    0.00
AEFACT       118-23.20  -18.40   4.00   20.00   25.60
```

```
AEFACT       119  0.00   18.00  27.00   18.00    0.00
AEFACT       120-26.10  -20.70   4.50   22.50   28.80
AEFACT       121  0.00   20.00  30.00   20.00    0.00
AEFACT       122-29.00  -23.00   5.00   25.00   32.00
$
$ 370 GALLON TANK (FEF - HALF FULL)
$
ACOORD        20  185.78    71.0   -30.5     0.0     0.0     0.0
BODY7       2001 TANK370      11      20       1    2001
PBODY7        11       0                                          0
SEGMESH     2001      15       9                                     +SEG11
+SEG11         1    0.00     0.0     0.0                            +SEG12
+SEG12         1   24.22     0.0     8.0                            +SEG13
+SEG13         1   35.47     0.0    9.31                            +SEG14
+SEG14         1   46.72     0.0   10.63                            +SEG15
+SEG15         1   57.97     0.0   11.94                            +SEG16
+SEG16         1   69.22     0.0   13.25                            +SEG17
+SEG17         1   85.05     0.0   13.25                            +SEG18
+SEG18         1  100.89     0.0   13.25                            +SEG19
+SEG19         1  116.72     0.0   13.25                            +SEG20
+SEG20         1  132.55     0.0   13.25                            +SEG21
+SEG21         1  148.39     0.0   13.25                            +SEG22
+SEG22         1  164.22     0.0   13.25                            +SEG23
+SEG23         1  180.89     0.0   12.17                            +SEG24
+SEG24         1  197.55     0.0   11.08                            +SEG25
+SEG25         1  214.22     0.0   10.00
$
$ 370 GALLON TANK PYLON
$
CAERO7      2501TANK370P      20       3       5     201       0       0   +CA71
+CA71      93.22    0.00   13.25  105.50     202    2001                   +CA72
+CA72     118.72    0.00   30.50   80.00     202
AEFACT       201    0.00   50.00  100.00
AEFACT       202    0.00   25.00   50.00   75.00  100.00
$
$ COORD SYSTEM LOCATING LAU-129 FOR STA 1
$
ACOORD        57  303.59  188.50     0.0     0.0     0.0     0.0
$
$ LAU-129 LAUNCHER FOR STA 1 (EMPTY)
$
CAERO7      4501LAU-STA1      57       2      17     301       0       0   +CA71
+CA71       9.16   -2.50     0.0  102.95     302       0                   +CA72
```

```
+CA72       9.16   -8.50     0.0  102.95     302       0
AEFACT       301    0.00  100.00
AEFACT       302    0.00    6.25   12.50   18.75   25.00   31.25   37.50   +AE1
+AE1       43.75   50.00   56.25   62.50   68.75   75.00   81.25   87.50   +AE2
+AE2       93.75  100.00
$
$ AMRAAM MISSILE
$
ACOORD        40  270.85  157.00  -18.37     0.0     0.0
BODY7       4001AMRAAM        13      40       1    4001
PBODY7        13       0                                              0
SEGMESH     4001      20       9                                          +SEG01
+SEG01         1    -3.2     0.0    0.00                                  +SEG02
+SEG02         1    11.8     0.0    3.50                                  +SEG03
+SEG03         1  20.997     0.0    3.50                                  +SEG04
+SEG04         1  30.194     0.0    3.50                                  +SEG05
+SEG05         1  39.391     0.0    3.50                                  +SEG06
+SEG06         1  48.588     0.0    3.50                                  +SEG07
+SEG07         1  57.785     0.0    3.50                                  +SEG08
+SEG08         1    63.7     0.0    3.50                                  +SEG81
+SEG81         1 67.7675     0.0    3.50                                  +SEG82
+SEG82         1 71.8337     0.0    3.50                                  +SEG09
+SEG09         1    75.9     0.0    3.50                                  +SEG10
+SEG10         1  85.376     0.0    3.50                                  +SEG11
+SEG11         1  94.573     0.0    3.50                                  +SEG12
+SEG12         1  103.77     0.0    3.50                                  +SEG13
+SEG13         1 112.967     0.0    3.50                                  +SEG14
+SEG14         1 122.164     0.0    3.50                                  +SEG15
+SEG15         1  127.07     0.0    3.50                                  +SEG51
+SEG51         1 131.566     0.0    3.50                                  +SEG52
+SEG52         1 136.060     0.0    3.50                                  +SEG16
+SEG16         1 140.555     0.0    3.50
$
$ AMRAAM FINS
$
$ *** FORWARD CANARD #1 ***
CAERO7      3001    CAN1      40       5       4    1002       0       0   +CA71
+CA71       63.7  2.4749  2.4749    12.2    1001    4001                   +CA72
+CA72       75.5  7.4246  7.4246    0.20    1001       0
$ *** FORWARD CANARD #2 ***
CAERO7      3101    CAN2      40       5       4    1002       0       0   +CA71
+CA71       63.7 -2.4749  2.4749    12.2    1001    4001                   +CA72
+CA72       75.5 -7.4246  7.4246    0.20    1001       0
```

```
$ *** FORWARD CANARD #3 ***
CAERO7      3201    CAN3      40       5       4    1002       0       0   +CA71
+CA71       63.7  2.4749 -2.4749    12.2    1001    4001                   +CA72
+CA72       75.5  7.4246 -7.4246    0.20    1001       0
$ *** FORWARD CANARD #4 ***
CAERO7      3301    CAN4      40       5       4    1002       0       0   +CA71
+CA71       63.7 -2.4749 -2.4749    12.2    1001    4001                   +CA72
+CA72       75.5 -7.4246 -7.4246    0.20    1001       0
AEFACT      1001    0.00   33.34   66.67  100.00
AEFACT      1002    0.00 24.7617 49.5233 74.2857  100.00
$ *** REAR FIN #1 ***
CAERO7     16001    FIN1      40       4       4    1001       0       0   +CA71
+CA71     127.07  2.4749  2.4749  13.485    1001    4001                   +CA72
+CA72     133.60  6.1518  6.1518   6.932    1001       0
$ *** REAR FIN #2 ***
CAERO7     16201    FIN2      40       4       4    1001       0       0   +CA71
+CA71     127.07 -2.4749  2.4749  13.485    1001    4001                   +CA72
+CA72     133.60 -6.1518  6.1518   6.932    1001       0
$ *** REAR FIN #3 ***
CAERO7     16401    FIN3      40       4       4    1001       0       0   +CA71
+CA71     127.07  2.4749 -2.4749  13.485    1001    4001                   +CA72
+CA72     133.60  6.1518 -6.1518   6.932    1001       0
$ *** REAR FIN #4 ***
CAERO7     16601    FIN4      40       4       4    1001       0       0   +CA71
+CA71     127.07 -2.4749 -2.4749  13.485    1001    4001                   +CA72
+CA72     133.60 -6.1518 -6.1518   6.932    1001       0
$
$ ADAPTER BL-157
$
CAERO7      8001   BL157      50       3       5     520       0       0   +CA71
+CA71     359.00  157.00   -7.63   28.90     507       0                   +CA72
+CA72     362.30  157.00    0.00   25.60     507       0
AEFACT       520    0.00   50.00  100.00
$
$ BL-15 LAUNCHER LAU-129 STA 2
$
CAERO7      8501   BL15L      50       2       9     510       0       0   +CA71
+CA71     302.70  157.00  -14.87  102.90     511    4001                   +CA72
+CA72     302.70  157.00   -7.63  102.90     511
AEFACT       510    0.00  100.00
AEFACT       511    0.00   12.50   25.00   37.50   50.00   62.50   75.00   +CA71
+CA71      87.50  100.00
$
```

```
$ COORD SYSTEM LOCATING WING
$
ACOORD        50     0.0     0.0     0.0     0.0     0.0     0.0
$
$ MAIN WING
$
CAERO7      5001    WING       50       9      19     501       0       0   +CA71
+CA71     258.74   54.00    0.00   150.2     502       0                   +CA72
+CA72     364.47  180.00    0.00   44.42     502       0
AEFACT       501    0.00   13.49   30.23   45.34   52.38   68.25   81.75   +AE1
+AE1        89.42  100.00
AEFACT       502    0.00    4.77    9.53   14.30   19.06   26.80   34.53   +AE1
+AE1        42.26   49.99   57.72   65.45   73.18   80.91   84.10   87.28   +AE2
+AE2        90.46   93.64   96.82  100.00
$
$ FORWARD STRAKE
$
CAERO7      1501FORSTRAK       10       3      19     150       0       0   +CA71
+CA71     178.00   30.00    5.00  230.92     151    1001                   +CA72
+CA72     258.74   54.00    5.00 150.171     502       0
AEFACT       150    0.00   47.92  100.00
AEFACT       151    0.00    7.16   14.33   21.49   28.65   35.82   42.98   +AE1
+AE1        50.14   57.30   64.46   71.62   78.79   85.95   88.29   90.63   +AE2
+AE2        92.97   95.31   97.66  100.00
$
$ REAR STRAKE
$
CAERO7      1701AFTSTRAK       10       2      13     170       0       0   +CA71
+CA71     408.92   30.00    5.00  128.28     175    1001                   +CA72
+CA72     408.93   41.50    5.00  140.29     175       0
AEFACT       170    0.00  100.00
AEFACT       175    0.00    8.33   16.67   25.00   33.33   41.67   50.00   +AE1
+AE1        58.33   66.67   75.00   83.33   91.67  100.00
$
$ VERTICAL TAIL
$
CAERO7      1801VTAILB         10       3      15     160       0       0   +CA71
+CA71     368.00    0.00   32.00  159.10     180    1001                   +CA72
+CA72     430.28    0.00   49.85   96.82     180       0
AEFACT       160    0.00   50.00  100.00
AEFACT       180    0.00   6.995   13.99  20.988  27.985  34.982  41.978   +AE1
+AE1       48.975  55.971  62.968  69.965  77.474  84.982  92.491  100.00
$
```

```
$ VENTRAL FIN
$
CAERO7      1901 VENTFIN      10       3       9     190       0       0   +CA71
+CA71     388.75   20.00  -23.00   56.25     191    1001                   +CA72
+CA72     402.17   26.02  -45.46   42.83     191       0
AEFACT       190    0.00   50.00  100.00
AEFACT       191    0.00   12.50   25.00   37.50   50.00   62.50   75.00   +AE1
+AE1       87.50  100.00
$
$ VERTICAL TAIL TOP
$
CAERO7      6501   VTAIL      50       7      11     506       0       0   +CA71
+CA71     430.28    0.00   44.85   67.74     505       0                   +CA72
+CA72     519.22    0.00  126.50   32.15     505       0
AEFACT       505    0.00   10.00   20.00   30.00   40.00   50.00   60.00   +AE1
+AE1       70.00   80.00   90.00  100.00
AEFACT       506    0.00   16.67   33.33   50.00   66.67   83.33  100.00
$
$ RUDDER
$
CAERO7      7001  RUDDER      50       7       5     506       0       0   +CA71
+CA71     498.02    0.00   44.85   29.08     507       0                   +CA72
+CA72     551.37    0.00  126.50   15.35     507       0
AEFACT       507    0.00   25.00   50.00   75.00  100.00
$
$ HORIZONTAL TAIL
$
CAERO7      7501   HTAIL      50       5       9     508       0       0   +CA71
+CA71     453.40   41.50    0.00   95.82     509       0                   +CA72
+CA72     511.83  111.13  -12.09   37.39     509       0
AEFACT       508    0.00   17.95   42.37   72.65  100.00
AEFACT       509    0.00   12.50   25.00   37.50   50.00   62.50   75.00   +AE1
+AE1       87.50  100.00
$
$*************************************************************************
$                      SPLINE OF STRUCTURE TO AERO MODEL
$*************************************************************************
$
$ FUSELAGE SPLINE (BEAM SPLINE)
$
SPLINE2 10              10      10
SET1    10      163     153     154     155     156     42      71      +SET1
+SET1   286     410     281
```

```
PANLST2 10      1001    1001    THRU    1128
$
$ FORWARD STRAKE (FRONT PORTION)
$
SPLINE1 20                      20      20
SET1    20      9       11      13      15      17      19      72      +SE1
+SE1    85      20      60      73      86      21      61      74      +SE2
+SE2    87      51      62      75      88      26      52      64      +SE3
+SE3    77      29      44      53      65      78      31      37      +SE4
+SE4    45      54      66      121     274     257
PANLST1 20      1501    1501    1530
$
$ FORWARD STRAKE (AFT LEFT = OLD MID STRAKE)
$
SPLINE1 30                      30      20
PANLST2 30      1501    1513    THRU    1518
$
$ FORWARD STRAKE FLAPERON PORTION
$
SPLINE1 35                      35      110
PANLST2 35      1501    1531    THRU    1536
$
$ AFT STRAKE
$
SPLINE1 40                      40      20
PANLST2 40      1701    1701    THRU    1712
$
$ VERTICAL TAIL- BASE
$
SPLINE1 50                      50      30
SET1    30      407     367     368     369     370     371     373     +SE1
+SE1    359     360     361     362     364     281     409     384     +SE2
+SE2    385     386     387     381     408
PANLST2 50      1801    1801    THRU    1828
$
$ VENTRAL FIN
$
SPLINE1 60                      60      40
SET1    40      286     281     409
PANLST2 60      1901    1901    THRU    1916
$
$ AMRAAM MISSILE (BEAM SPLINE)
$
```

```
SPLINE2 70              70      50
SET1    50      3111    THRU    3115
PANLST2 70      4001    4001    THRU    4152
$
$ FORWARD FIN #1
$
ATTACH  80      FFIN#1  80      3112
PANLST2 80      3001    3001    THRU    3012
$
$ FORWARD FIN #2
$
ATTACH  90      FFIN#2  90      3112
PANLST2 90      3101    3101    THRU    3112
$
$ FORWARD FIN #3
$
ATTACH  100     FFIN#3  100     3112
PANLST2 100     3201    3201    THRU    3212
$
$ FORWARD FIN #4
$
ATTACH  110     FFIN#4  110     3112
PANLST2 110     3301    3301    THRU    3312
$
$ REAR FIN #1
$
ATTACH  120     RFIN#1  120     3115
PANLST2 120     16001   16001   THRU    16009
$
$ REAR FIN #2
$
ATTACH  130     RFIN#2  130     3115
PANLST2 130     16201   16201   THRU    16209
$
$ REAR FIN #3
$
ATTACH  140     RFIN#3  140     3115
PANLST2 140     16401   16401   THRU    16409
$
$ REAR FIN #4
$
ATTACH  150     RFIN#4  150     3115
PANLST2 150     16601   16601   THRU    16609
```

```
$
$ ADAPTER BL-157
$
SPLINE1 270                     270     150
SET1    150     21      61      74      3105    3107    3110
PANLST2 270     8001    8001    THRU    8008
$
$ BL-157 LAUNCHER
$
SPLINE1 280                     280     160
SET1    160     3112    3105    3114    3106    3115    3110
PANLST2 280     8501    8501    THRU    8508
$
$ AIM9-P LAUNCHER (BEAM SPLINE)
$ LOCAL COORDINATE TO SET UP THE SPLINE AXIS
$
CORD2R  70              -182.88 -318.68  0.0     -182.88 -318.68  1.0     +CRD1
+CRD1   -150.00 -318.68  0.0
ATTACH  4501    LAU     4501    3036
PANLST1 4501    4501    4501    4516
$
$ 370 GAL TANK (BEAM SPLINE)
$
SPLINE2 160             160     60
SET1    60      3210    THRU    3213
PANLST2 160     2001    2001    THRU    2112
$
$ 370 GAL TANK PYLON
$
SPLINE1 170                     170     70
SET1    70      3207    29      53
PANLST2 170     2501    2501    THRU    2508
$
$ MAIN WING - SAME SPLINE (I.E. GRIDS) AS STRAKES
$
SPLINE1 200                     200     20
PANLST1 200     5001    5005    5138
$
$ WING OUTBOARD - SAME SPLINE (I.E. GRIDS) AS STRAKES
$
SPLINE1 210                     210     20
PANLST1 210     5001    5103    5144
$
```

```
$ L.E. FLAP
$
SPLINE1 220                     220     100
SET1    100     2       3       4       5       6       9       11      +SE1
+SE1    13      15      17
PANLST1 220     5001    5001    5130
$
$ FLAPERON
$
SPLINE1 230                     230     110
SET1    110     75      77      78      121     134     90      91      +SE1
+SE1    92      93      95      102     103     104     105     106     +SE2
+SE2    107     108     109     110     111     112     113     96
PANLST1 230     5001    5013    5090
$
$ VERTICAL TAIL - TOP PORTION
$
SPLINE1 240                     240     120
SET1    120     407     367     368     369     370     371     373     +SE1
+SE1    359     360     361     362     364     281     409     384     +SE2
+SE2    385     386     387     381     408
PANLST2 240     6501    6501    THRU    6560
$
$ RUDDER
$
SPLINE1 250                     250     130
SET1    130     384     385     386     387     389     390     391     +SE1
+SE1    392     382
PANLST2 250     7001    7001    THRU    7024
$
$ HORIZONTAL TAIL
$
SPLINE1 260                     260     140
SET1    140     280     252     253     254     255     256     274     +SE1
+SE1    257     258     259     260     261     262     263     264     +SE2
+SE2    265     266
PANLST2 260     7501    7501    THRU    7532
$*************************************************************************
$
$ MATCH POINT FLUTTER ANALYSIS AT SEA LEVEL MACH FROM 0.75 TO 0.95
$
$*************************************************************************
$       SETID   SYM     FIX     NMODE   TABDMP  MLIST   CONMLST
```

```
FLUTTER 10      ANTI    20      15
$
$       SETID   ALT     IDATM   FTMUNIT FTLUNIT VREF    FLUTTF  PRINT
FIXHATM  20     0.      0       SLUG    FT      1.68    0       2       +FI1
+FI1     31     32      33
$
MKAEROZ 31      0.75      0      0      SAVE    LA00K075          0     +MK1
+MK1    0.12    0.25    0.28    0.31    0.45    0.58    0.72    0.86
MKAEROZ 32      0.85      0      0      SAVE    LA00K085          0     +MK2
+MK2    0.11    0.22    0.24    0.27    0.39    0.52    0.64    0.76
MKAEROZ 33      0.95      0      0      SAVE    LA00K095        0       +MK3
+MK3    0.10    0.19    0.22    0.24    0.35    0.46    0.57    0.68
$
PLTVG   10      10      6       V               s7v30vg.dat
PLTCP   25      ANTI    10      3       1       TECPLOT s7v30cp1.plt
PLTCP   27      ANTI    10      3       2       TECPLOT s7v30cp2.plt
PLTCP   27      ANTI    10      3       4       TECPLOT s7v30cp4.plt
PLTFLUT 30      10      1       20      0.15    TECPLOT s7v30flt.plt
PLTMODE 40      ANTI    1               0.2     FEMAP   s7v30m1.neu
PLTMODE 50      ANTI    2               0.2     FEMAP   s7v30m2.neu
PLTMODE 60      ANTI    3               0.2     FEMAP   s7v30m3.neu
PLTAERO 105     YES             FEMAP   s7v30.neu
PLTAERO 106     YES             TECPLOT s7v30.plt
ENDDATA
```

C.2 SCL008 Bulk Data

```
ASSIGN FEM=C:\BTHESIS\ZAERO\S8M_L.F06, PRINT =0, FORM = MSC, BOUND = ANTI
CEND
$
TITLE =F16 LCO ANALYSIS. CASE SCL008 (2 X LAU129 + 2 X AMRAAM)
ECHO = SORT
SUBCASE = 1
        SUBTITLE = ANTI-SYMMETRIC BOUNDARY CONDITION
        LABEL    = MATCH POINT FLUTTER ANALYSIS AT SEA LEVEL FROM 1.15 TO 1.25 MACH
FLUTTER = 10
BEGIN BULK
$*************************************************************************
$
$      ----   F - 1 6    A E R O D Y N A M I C    M O D E L   ----
$                    (  C A S E   S C L 0 0 8  )
$
$*************************************************************************
$
$AEROZ  ACSID   XZSYM   FLIP    FMMUNIT FMLUNIT REFC    REFB    REFS    CONT
AEROZ   77      YES     YES     SLIN    IN      121.5                   +AE1
+AE1    0.0     0.0     0.0
$CORD2R CID     RID     A1      A2      A3      B1      B2      B3      CONT
CORD2R  77              0.      0.      0.      0.      0.      100.    +C2R1
+C2R1   0.      -100.   0.
$
$ FUSELAGE
$
ACOORD        10     0.0     0.0    -5.0     0.0     0.0     0.0
BODY7       1001FUSELAGE              10       1    1001
SEGMESH     1001       33       5                                       +SEG11
+SEG11         3    8.00                             101     102         +SEG12
+SEG12         3   25.00                             103     104         +SEG13
+SEG13         3   42.00                             105     106         +SEG14
+SEG14         3   59.00                             107     108         +SEG15
+SEG15         3   76.00                             109     110         +SEG16
+SEG16         3   93.00                             111     112         +SEG17
+SEG17         3  110.00                             113     114         +SEG18
+SEG18         3  127.00                             115     116         +SEG19
+SEG19         3  144.00                             117     118         +SEG20
+SEG20         3  161.00                             119     120         +SEG21
+SEG21         3  178.00                             121     122         +SEG22
+SEG22         3  197.85                             121     122         +SEG23
+SEG23         3  217.70                             121     122         +SEG24
```

```
+SEG24          3  237.54                                  121     122          +SEG25
+SEG25          3  257.39                                  121     122          +SEG26
+SEG26          3  277.24                                  121     122          +SEG27
+SEG27          3  297.09                                  121     122          +SEG28
+SEG28          3  316.94                                  121     122          +SEG29
+SEG29          3  336.78                                  121     122          +SEG30
+SEG30          3  356.63                                  121     122          +SEG31
+SEG31          3  376.48                                  121     122          +SEG32
+SEG32          3  392.70                                  121     122          +SEG33
+SEG33          3  408.92                                  121     122          +SEG34
+SEG34          3  421.75                                  121     122          +SEG35
+SEG35          3  434.58                                  121     122          +SEG36
+SEG36          3  447.40                                  121     122          +SEG37
+SEG37          3  460.23                                  121     122          +SEG38
+SEG38          3  473.06                                  121     122          +SEG39
+SEG39          3  485.89                                  121     122          +SEG40
+SEG40          3  498.72                                  121     122          +SEG41
+SEG41          3  511.54                                  121     122          +SEG42
+SEG42          3  524.37                                  121     122          +SEG43
+SEG43          3  537.20                                  121     122
AEFACT       101  0.00    0.00   0.00    0.00    0.00
AEFACT       102  0.00    0.00   0.00    0.00    0.00
AEFACT       103  0.00    2.00   3.00    2.00    0.00
AEFACT       104 -2.90   -2.30   0.50    2.50    3.20
AEFACT       105  0.00    4.00   6.00    4.00    0.00
AEFACT       106 -5.80   -4.60   1.00    5.00    6.40
AEFACT       107  0.00    6.00   9.00    6.00    0.00
AEFACT       108 -8.70   -6.90   1.50    7.50    9.60
AEFACT       109  0.00    8.00  12.00    8.00    0.00
AEFACT       110-11.60   -9.20   2.00   10.00   12.80
AEFACT       111  0.00   10.00  15.00   10.00    0.00
AEFACT       112-14.50  -11.50   2.50   12.50   16.00
AEFACT       113  0.00   12.00  18.00   12.00    0.00
AEFACT       114-17.40  -13.80   3.00   15.00   19.20
AEFACT       115  0.00   14.00  21.00   14.00    0.00
AEFACT       116-20.30  -16.10   3.50   17.50   22.40
AEFACT       117  0.00   16.00  24.00   16.00    0.00
AEFACT       118-23.20  -18.40   4.00   20.00   25.60
AEFACT       119  0.00   18.00  27.00   18.00    0.00
AEFACT       120-26.10  -20.70   4.50   22.50   28.80
AEFACT       121  0.00   20.00  30.00   20.00    0.00
AEFACT       122-29.00  -23.00   5.00   25.00   32.00
$
```

```
$ COORD SYSTEM LOCATING LAU-129 FOR STA 1
$
ACOORD        57  303.59  188.50     0.0     0.0     0.0     0.0
$
$ LAU-129 LAUNCHER FOR STA 1 (EMPTY)
$
CAERO7      4501LAU-STA1      57       2      17     301       0       0   +CA71
+CA71       9.16   -2.50     0.0  102.95     302       0                   +CA72
+CA72       9.16   -8.50     0.0  102.95     302       0
AEFACT       301    0.00  100.00
AEFACT       302    0.00    6.25   12.50   18.75   25.00   31.25   37.50   +AE1
+AE1       43.75   50.00   56.25   62.50   68.75   75.00   81.25   87.50   +AE2
+AE2       93.75  100.00
$*********************************************************************************
$ AMRAAM MISSILE STA 2
$*********************************************************************************
ACOORD        40  270.85  157.00  -18.37     0.0     0.0
BODY7       4001AMRAAM2       13      40       1    4001
PBODY7        13       0                                                 0
SEGMESH     4001      20       9                                          +SEG01
+SEG01         1    -3.2     0.0    0.00                                  +SEG02
+SEG02         1    11.8     0.0    3.50                                  +SEG03
+SEG03         1  20.997     0.0    3.50                                  +SEG04
+SEG04         1  30.194     0.0    3.50                                  +SEG05
+SEG05         1  39.391     0.0    3.50                                  +SEG06
+SEG06         1  48.588     0.0    3.50                                  +SEG07
+SEG07         1  57.785     0.0    3.50                                  +SEG08
+SEG08         1    63.7     0.0    3.50                                  +SEG81
+SEG81         1 67.7675     0.0    3.50                                  +SEG82
+SEG82         1 71.8337     0.0    3.50                                  +SEG09
+SEG09         1    75.9     0.0    3.50                                  +SEG10
+SEG10         1  85.376     0.0    3.50                                  +SEG11
+SEG11         1  94.573     0.0    3.50                                  +SEG12
+SEG12         1  103.77     0.0    3.50                                  +SEG13
+SEG13         1 112.967     0.0    3.50                                  +SEG14
+SEG14         1 122.164     0.0    3.50                                  +SEG15
+SEG15         1  127.07     0.0    3.50                                  +SEG51
+SEG51         1 131.566     0.0    3.50                                  +SEG52
+SEG52         1 136.060     0.0    3.50                                  +SEG16
+SEG16         1 140.555     0.0    3.50
$
$ AMRAAM FINS
$
```

```
$ *** FORWARD CANARD #1 ***
CAERO7      3001    CAN1      40       5       4    1002       0       0   +CA71
+CA71       63.7  2.4749  2.4749    12.2    1001    4001                   +CA72
+CA72       75.5  7.4246  7.4246    0.20    1001       0
$ *** FORWARD CANARD #2 ***
CAERO7      3101    CAN2      40       5       4    1002       0       0   +CA71
+CA71       63.7 -2.4749  2.4749    12.2    1001    4001                   +CA72
+CA72       75.5 -7.4246  7.4246    0.20    1001       0
$ *** FORWARD CANARD #3 ***
CAERO7      3201    CAN3      40       5       4    1002       0       0   +CA71
+CA71       63.7  2.4749 -2.4749    12.2    1001    4001                   +CA72
+CA72       75.5  7.4246 -7.4246    0.20    1001       0
$ *** FORWARD CANARD #4 ***
CAERO7      3301    CAN4      40       5       4    1002       0       0   +CA71
+CA71       63.7 -2.4749 -2.4749    12.2    1001    4001                   +CA72
+CA72       75.5 -7.4246 -7.4246    0.20    1001       0
AEFACT      1001    0.00   33.34   66.67  100.00
AEFACT      1002    0.00 24.7617 49.5233 74.2857  100.00
$ *** REAR FIN #1 ***
CAERO7     16001    FIN1      40       4       4    1001       0       0   +CA71
+CA71     127.07  2.4749  2.4749  13.485    1001    4001                   +CA72
+CA72     133.60  6.1518  6.1518   6.932    1001       0
$ *** REAR FIN #2 ***
CAERO7     16201    FIN2      40       4       4    1001       0       0   +CA71
+CA71     127.07 -2.4749  2.4749  13.485    1001    4001                   +CA72
+CA72     133.60 -6.1518  6.1518   6.932    1001       0
$ *** REAR FIN #3 ***
CAERO7     16401    FIN3      40       4       4    1001       0       0   +CA71
+CA71     127.07  2.4749 -2.4749  13.485    1001    4001                   +CA72
+CA72     133.60  6.1518 -6.1518   6.932    1001       0
$ *** REAR FIN #4 ***
CAERO7     16601    FIN4      40       4       4    1001       0       0   +CA71
+CA71     127.07 -2.4749 -2.4749  13.485    1001    4001                   +CA72
+CA72     133.60 -6.1518 -6.1518   6.932    1001       0
$ ADAPTER BL-157
CAERO7      8001   BL157      50       3       5     520       0       0   +CA71
+CA71     359.00  157.00   -7.63   28.90     507       0                   +CA72
+CA72     362.30  157.00    0.00   25.60     507       0
AEFACT       520    0.00   50.00  100.00
$ BL-15 LAUNCHER LAU-129 STA 2
CAERO7      8501   BL15L      50       2       9     510       0       0   +CA71
+CA71     302.70  157.00  -14.87  102.90     511    4001                   +CA72
+CA72     302.70  157.00   -7.63  102.90     511       0
```

```
AEFACT       510    0.00  100.00
AEFACT       511    0.00   12.50   25.00   37.50   50.00   62.50   75.00   +CA71
+CA71      87.50  100.00
$*************************************************************************
$ AMRAAM MISSILE STA 3
$*************************************************************************
ACOORD        45  238.40  120.00  -18.37     0.0     0.0
BODY7       6001AMRAAM3       13      45       1    6001
PBODY7        13       0                                          0
SEGMESH     6001      20       9                                     +SEG01
+SEG01         1    -3.2     0.0    0.00                             +SEG02
+SEG02         1    11.8     0.0    3.50                             +SEG03
+SEG03         1  20.997     0.0    3.50                             +SEG04
+SEG04         1  30.194     0.0    3.50                             +SEG05
+SEG05         1  39.391     0.0    3.50                             +SEG06
+SEG06         1  48.588     0.0    3.50                             +SEG07
+SEG07         1  57.785     0.0    3.50                             +SEG08
+SEG08         1    63.7     0.0    3.50                             +SEG81
+SEG81         1 67.7675     0.0    3.50                             +SEG82
+SEG82         1 71.8337     0.0    3.50                             +SEG09
+SEG09         1    75.9     0.0    3.50                             +SEG10
+SEG10         1  85.376     0.0    3.50                             +SEG11
+SEG11         1  94.573     0.0    3.50                             +SEG12
+SEG12         1  103.77     0.0    3.50                             +SEG13
+SEG13         1 112.967     0.0    3.50                             +SEG14
+SEG14         1 122.164     0.0    3.50                             +SEG15
+SEG15         1  127.07     0.0    3.50                             +SEG51
+SEG51         1 131.566     0.0    3.50                             +SEG52
+SEG52         1 136.060     0.0    3.50                             +SEG16
+SEG16         1 140.555     0.0    3.50
$
$ AMRAAM FINS
$
$ *** FORWARD CANARD #1 ***
CAERO7      9001    CAN5      45       5       4    1002       0       0   +CA71
+CA71       63.7  2.4749  2.4749    12.2    1001    6001                   +CA72
+CA72       75.5  7.4246  7.4246    0.20    1001       0
$ *** FORWARD CANARD #2 ***
CAERO7      9101    CAN6      45       5       4    1002       0       0   +CA71
+CA71       63.7 -2.4749  2.4749    12.2    1001    6001                   +CA72
+CA72       75.5 -7.4246  7.4246    0.20    1001       0
$ *** FORWARD CANARD #3 ***
CAERO7      9201    CAN7      45       5       4    1002       0       0   +CA71
```

```
+CA71       63.7  2.4749 -2.4749    12.2    1001    6001                  +CA72
+CA72       75.5  7.4246 -7.4246    0.20    1001       0
$ *** FORWARD CANARD #4 ***
CAERO7      9301    CAN8      45       5       4    1002       0       0   +CA71
+CA71       63.7 -2.4749 -2.4749    12.2    1001    6001                  +CA72
+CA72       75.5 -7.4246 -7.4246    0.20    1001       0
$ *** REAR FIN #1 ***
CAERO7     17001    FIN5      45       4       4    1001       0       0   +CA71
+CA71     127.07  2.4749  2.4749  13.485    1001    6001                  +CA72
+CA72     133.60  6.1518  6.1518   6.932    1001       0
$ *** REAR FIN #2 ***
CAERO7     17201    FIN6      45       4       4    1001       0       0   +CA71
+CA71     127.07 -2.4749  2.4749  13.485    1001    6001                  +CA72
+CA72     133.60 -6.1518  6.1518   6.932    1001       0
$ *** REAR FIN #3 ***
CAERO7     17401    FIN7      45       4       4    1001       0       0   +CA71
+CA71     127.07  2.4749 -2.4749  13.485    1001    6001                  +CA72
+CA72     133.60  6.1518 -6.1518   6.932    1001       0
$ *** REAR FIN #4 ***
CAERO7     17601    FIN8      45       4       4    1001       0       0   +CA71
+CA71     127.07 -2.4749 -2.4749  13.485    1001    6001                  +CA72
+CA72     133.60 -6.1518 -6.1518   6.932    1001       0
$ ADAPTER BL-157
CAERO7      8101 BL157-3      45       3       5     520       0       0   +CA71
+CA71      88.15    0.00   10.74   28.90     507       0                  +CA72
+CA72      91.45    0.00   18.37   25.60     507       0
$ BL-15 LAUNCHER LAU-129 STA 3
CAERO7      8601 BL15L-3      45       2       9     510       0       0   +CA71
+CA71      31.85    0.00    3.50  102.90     511    6001                  +CA72
+CA72      31.85    0.00   10.74  102.90     511       0
$*************************************************************************
$ WING
$*************************************************************************
ACOORD        50     0.0     0.0     0.0     0.0     0.0     0.0
$ MAIN WING
CAERO7      5001    WING      50       9      19     501       0       0   +CA71
+CA71     258.74   54.00    0.00 150.171     502       0                  +CA72
+CA72     364.47  180.00    0.00   44.46     502       0
AEFACT       501    0.00   13.49   30.23   45.34   52.38   68.25   81.75   +AE1
+AE1        89.42  100.00
AEFACT       502    0.00    4.77    9.53   14.30   19.06   26.80   34.53   +AE1
+AE1        42.26   49.99   57.72   65.45   73.18   80.91   84.10   87.28   +AE2
+AE2        90.46   93.64   96.82  100.00
```

```
$
$ FORWARD STRAKE
$
CAERO7      1501FORSTRAK       10        3       19      150        0        0   +CA71
+CA71     178.00    30.00     5.00   230.92      151     1001                     +CA72
+CA72     258.74    54.00     5.00  150.171      502        0
AEFACT       150     0.00    47.92   100.00
AEFACT       151     0.00     7.16    14.33    21.49    28.65    35.82    42.98   +AE1
+AE1       50.14    57.30    64.46    71.62    78.79    85.95    88.29    90.63   +AE2
+AE2       92.97    95.31    97.66   100.00
$
$ REAR STRAKE
$
CAERO7      1701AFTSTRAK       10        2       13      170        0        0   +CA71
+CA71     408.92    30.00     5.00   128.28      175     1001                     +CA72
+CA72     408.93    41.50     5.00   140.29      175        0
AEFACT       170     0.00   100.00
AEFACT       175     0.00     8.33    16.67    25.00    33.33    41.67    50.00   +AE1
+AE1       58.33    66.67    75.00    83.33    91.67   100.00
$
$ VERTICAL TAIL
$
CAERO7      1801VTAILB         10        3       15      160        0        0   +CA71
+CA71     368.00     0.00    32.00   159.10      180     1001                     +CA72
+CA72     430.28     0.00    49.85    96.82      180        0
AEFACT       160     0.00    50.00   100.00
AEFACT       180     0.00     6.995   13.99   20.988   27.985   34.982   41.978   +AE1
+AE1      48.975   55.971   62.968   69.965   77.474   84.982   92.491   100.00
$
$ VENTRAL FIN
$
CAERO7      1901 VENTFIN       10        3        9      190        0        0   +CA71
+CA71     388.75    20.00   -23.00    56.25      191     1001                     +CA72
+CA72     402.17    26.02   -45.46    42.83      191        0
AEFACT       190     0.00    50.00   100.00
AEFACT       191     0.00    12.50    25.00    37.50    50.00    62.50    75.00   +AE1
+AE1       87.50   100.00
$
$ VERTICAL TAIL TOP
$
CAERO7      6501   VTAIL       50        7       11      506        0        0   +CA71
+CA71     430.28     0.00    44.85    67.74      505        0                     +CA72
+CA72     519.22     0.00   126.50    32.15      505        0
```

```
AEFACT       505    0.00   10.00   20.00   30.00   40.00   50.00   60.00   +AE1
+AE1        70.00   80.00   90.00  100.00
AEFACT       506    0.00   16.67   33.33   50.00   66.67   83.33  100.00
$
$ RUDDER
$
CAERO7      7001  RUDDER      50       7       5     506       0       0   +CA71
+CA71     498.02    0.00   44.85   29.08     507       0                   +CA72
+CA72     551.37    0.00  126.50   15.35     507       0
AEFACT       507    0.00   25.00   50.00   75.00  100.00
$
$ HORIZONTAL TAIL
$
CAERO7      7501   HTAIL      50       5       9     508       0       0   +CA71
+CA71     453.40   41.50    0.00   95.82     509       0                   +CA72
+CA72     511.83  111.13  -12.09   37.39     509       0
AEFACT       508    0.00   17.95   42.37   72.65  100.00
AEFACT       509    0.00   12.50   25.00   37.50   50.00   62.50   75.00   +AE1
+AE1        87.50  100.00
$
$*************************************************************************
$                      SPLINE OF STRUCTURE TO AERO MODEL
$*************************************************************************
$
$ FUSELAGE SPLINE (BEAM SPLINE)
$
SPLINE2 10              10      10
SET1    10      163     153     154     155     156     42      71      +SET1
+SET1   286     410     281
PANLST2 10      1001    1001    THRU    1128
$
$ FORWARD STRAKE (FRONT PORTION)
$
SPLINE1 20                      20      20
SET1    20      9       11      13      15      17      19      72      +SE1
+SE1    85      20      60      73      86      21      61      74      +SE2
+SE2    87      51      62      75      88      26      52      64      +SE3
+SE3    77      29      44      53      65      78      31      37      +SE4
+SE4    45      54      66      121     274     257
PANLST1 20      1501    1501    1530
$
$ FORWARD STRAKE (AFT LEFT = OLD MID STRAKE)
$
```

```
SPLINE1 30                      30      20
PANLST2 30      1501    1513    THRU    1518
$
$ FORWARD STRAKE FLAPERON PORTION
$
SPLINE1 35                      35      110
PANLST2 35      1501    1531    THRU    1536
$
$ AFT STRAKE
$
SPLINE1 40                      40      20
PANLST2 40      1701    1701    THRU    1712
$
$ VERTICAL TAIL- BASE
$
SPLINE1 50                      50      30
SET1    30      407     367     368     369     370     371     373     +SE1
+SE1    359     360     361     362     364     281     409     384     +SE2
+SE2    385     386     387     381     408
PANLST2 50      1801    1801    THRU    1828
$
$ VENTRAL FIN
$
SPLINE1 60                      60      40
SET1    40      286     281     409
PANLST2 60      1901    1901    THRU    1916
$
$*************************************************************************
$ AMRAAM MISSILE (BEAM SPLINE) STA 2
$*************************************************************************
SPLINE2 70              70      50
SET1    50      3111    THRU    3115
PANLST2 70      4001    4001    THRU    4152
$
$ FORWARD FIN #1
ATTACH  80      FFIN#1  80      3105
PANLST2 80      3001    3001    THRU    3012
$
$ FORWARD FIN #2
ATTACH  90      FFIN#2  90      3105
PANLST2 90      3101    3101    THRU    3112
$
$ FORWARD FIN #3
```

```
ATTACH  100     FFIN#3  100     3105
PANLST2 100     3201    3201    THRU    3212
$
$ FORWARD FIN #4
ATTACH  110     FFIN#4  110     3105
PANLST2 110     3301    3301    THRU    3312
$
$ REAR FIN #1
ATTACH  120     RFIN#1  120     3115
PANLST2 120     16001   16001   THRU    16009
$
$ REAR FIN #2
ATTACH  130     RFIN#2  130     3115
PANLST2 130     16201   16201   THRU    16209
$
$ REAR FIN #3
ATTACH  140     RFIN#3  140     3115
PANLST2 140     16401   16401   THRU    16409
$
$ REAR FIN #4
ATTACH  150     RFIN#4  150     3115
PANLST2 150     16601   16601   THRU    16609
$
$*************************************************************************
$ AMRAAM MISSILE (BEAM SPLINE) STA 3
$*************************************************************************
SPLINE2 75              75      55
SET1    55      4111    THRU    4115
PANLST2 75      6001    6001    THRU    6152
$
$ FORWARD FIN #1
ATTACH  85      FFIN#1  85      4105
PANLST2 85      9001    9001    THRU    9012
$
$ FORWARD FIN #2
ATTACH  95      FFIN#2  95      4105
PANLST2 95      9101    9101    THRU    9112
$
$ FORWARD FIN #3
ATTACH  105     FFIN#3  105     4105
PANLST2 105     9201    9201    THRU    9212
$
$ FORWARD FIN #4
```

```
ATTACH  115     FFIN#4  115     4105
PANLST2 115     9301    9301    THRU    9312
$
$ REAR FIN #1
ATTACH  125     RFIN#1  125     4115
PANLST2 125     17001   17001   THRU    17009
$
$ REAR FIN #2
ATTACH  135     RFIN#2  135     4115
PANLST2 135     17201   17201   THRU    17209
$
$ REAR FIN #3
ATTACH  145     RFIN#3  145     4115
PANLST2 145     17401   17401   THRU    17409
$
$ REAR FIN #4
ATTACH  155     RFIN#4  155     4115
PANLST2 155     17601   17601   THRU    17609
$
$ MAIN WING - SAME SPLINE (I.E. GRIDS) AS STRAKES
$
SPLINE1 200                     200     20
PANLST1 200     5001    5005    5138
$
$ WING OUTBOARD - SAME SPLINE (I.E. GRIDS) AS STRAKES
$
SPLINE1 210                     210     20
PANLST1 210     5001    5103    5144
$
$ L.E. FLAP
$
SPLINE1 220                     220     100
SET1    100     2       3       4       5       6       9       11      +SE1
+SE1    13      15      17
PANLST1 220     5001    5001    5130
$
$ FLAPERON
$
SPLINE1 230                     230     110
SET1    110     75      77      78      121     134     90      91      +SE1
+SE1    92      93      95      102     103     104     105     106     +SE2
+SE2    107     108     109     110     111     112     113     96
PANLST1 230     5001    5013    5090
```

```
$
$ VERTICAL TAIL - TOP PORTION
$
SPLINE1 240                     240     120
SET1    120     407     367     368     369     370     371     373     +SE1
+SE1    359     360     361     362     364     281     409     384     +SE2
+SE2    385     386     387     381     408
PANLST2 240     6501    6501    THRU    6560
$
$ RUDDER
$
SPLINE1 250                     250     130
SET1    130     384     385     386     387     389     390     391     +SE1
+SE1    392     382
PANLST2 250     7001    7001    THRU    7024
$
$ HORIZONTAL TAIL
$
SPLINE1 260                     260     140
SET1    140     280     252     253     254     255     256     274     +SE1
+SE1    257     258     259     260     261     262     263     264     +SE2
+SE2    265     266
PANLST2 260     7501    7501    THRU    7532
$
$ ADAPTER BL-157 STA 2
$
SPLINE1 270                     270     150
SET1    150     21      61      74      3105    3107    3110
PANLST2 270     8001    8001    THRU    8008
$
$ BL-157 LAUNCHER STA 2
$
SPLINE1 280                     280     160
SET1    160     3112    3105    3114    3106    3115    3110
PANLST2 280     8501    8501    THRU    8508
$
$ ADAPTER BL-157 STA 3
$
SPLINE1 275                     275     155
SET1    155     26      3147    64      4105    4107    4110
PANLST2 275     8101    8101    THRU    8108
$
$ BL-157 LAUNCHER STA 3
```

```
$
SPLINE1 285                     285     165
SET1    165     4112    4105    4114    4106    4115    4110
PANLST2 285     8601    8601    THRU    8608
$
$ AIM9-P LAUNCHER (BEAM SPLINE)
$ LOCAL COORDINATE TO SET UP THE SPLINE AXIS
$                                $
CORD2R  70              -182.88 -318.68  0.0     -182.88 -318.68  1.0     +CRD1
+CRD1   -150.00 -318.68  0.0
SPLINE2 4501            4501    170                     70
SET1    170     3032    THRU    3037
PANLST1 4501    4501    4501    4516
$*************************************************************************
$
$ MATCH POINT FLUTTER ANALYSIS AT SEA LEVEL FROM 1.15 TO 1.25 MACH
$
$*************************************************************************
$       SETID   SYM     FIX     NMODE   TABDMP  MLIST   CONMLST
FLUTTER 10      ANTI    20      15
$
$       SETID   ALT     IDATM   FTMUNIT FTLUNIT VREF    FLUTTF  PRINT
FIXHATM  20     0.      0       SLUG    FT      1.68    0       2       +FI1
+FI1     31     32
MKAEROZ 31      1.15      0      0      ACQUIRE LA00K115.AIC    0       +MK1
+MK1    0.09    0.18    0.20    0.22    0.32    0.42    0.52    0.62
MKAEROZ 32      1.25      0      0      ACQUIRE LA00K125.AIC    0       +MK2
+MK2    0.07    0.15    0.17    0.18    0.27    0.35    0.43    0.52
$
PLTVG   10      10      6       V               s8v30vg.dat
PLTCP   25      ANTI    10      3       1       TECPLOT s8v30cp1.plt
PLTCP   27      ANTI    10      3       2       TECPLOT s8v30cp2.plt
PLTFLUT 30      10      1       20      0.15    TECPLOT s8v30flt.plt
PLTFLUT 31      10      1       20      0.15    FEMAP   s8v30flt.neu
PLTMODE 40      ANTI    1               0.2     FEMAP   s8v30m1.neu
PLTMODE 50      ANTI    2               0.2     FEMAP   s8v30m2.neu
PLTAERO 105     YES             FEMAP   s8v30.NEU
PLTAERO 106     YES             TECPLOT s8v30.plt
ENDDATA
```

```
$************************************************************************
$
$ MATCH POINT FLUTTER ANALYSIS AT 15K' FROM .95M TO 1.05M RIGID Cp
$
$************************************************************************
$
$ ZTAIC TRANSONIC DATA INPUT
$
$       ID      NFLAP   MACHCP1 MACHCP2 MACHCP3 MACHCP4 MACHCP5 MACHCP6
ZTAIC   01      2       85      90                                      +ZT1
$       LABEL1  HINGE1  INBDY1  OUTBDY1 LABEL2  HINGE2  INBDY2  OUTBDY2
+ZT1    LE      5       1       9       TE      13      1       6
$
$
MACHCP  85      0.85    3       1       1       851     2       852     +MA1
+MA1    3       853     4       854     5       855     6       856     +MA2
+MA2    7       857     8       858
$
$ Cp DATA
$
CHORDCP 851     0.0058  0.3381  0.3616  0.8301  -0.2293 0.2434          +CH1
+CH1            1.8482  -0.3929 0.0099  3.1354  -0.3929 0.0099          +CH2
+CH2            4.8097  -0.2859 -0.0452 7.0649  -0.2859 -0.0452         +CH3
+CH3            10.2366 -0.2400 -0.0951 14.9319 -0.2400 -0.0951         +CH4
+CH4            22.2512 -0.1865 -0.1232 33.8317 -0.1865 -0.1232         +CH5
+CH5            50.0000 -0.2556 -0.0730 66.1683 -0.2556 -0.0730         +CH6
+CH6            77.7488 -0.2313 0.0235  85.0681 -0.2313 0.0235          +CH7
+CH7            89.7634 -0.1038 0.0528  92.9351 -0.1038 0.0528          +CH8
+CH8            95.1903 -0.0052 0.0645  96.8646 -0.0052 0.0645          +CH9
+CH9            98.1518 0.0637  0.0837  99.1699 0.0637  0.0837          +CH10
+CH10           99.9942 0.1315  0.1077
$
CHORDCP 852     0.0058  0.4795  0.4831  0.8301  0.0262  0.2041          +CH1
+CH1            1.8482  -0.2739 0.0070  3.1354  -0.2739 0.0070          +CH2
+CH2            4.8097  -0.2717 -0.0367 7.0649  -0.2717 -0.0367         +CH3
+CH3            10.2366 -0.2471 -0.0684 14.9319 -0.2471 -0.0684         +CH4
+CH4            22.2512 -0.2021 -0.1134 33.8317 -0.2021 -0.1134         +CH5
+CH5            50.0000 -0.2866 -0.0721 66.1683 -0.2866 -0.0721         +CH6
+CH6            77.7488 -0.2310 0.0392  85.0681 -0.2310 0.0392          +CH7
+CH7            89.7634 -0.0904 0.0647  92.9351 -0.0904 0.0647          +CH8
+CH8            95.1903 0.0068  0.0735  96.8646 0.0068  0.0735          +CH9
+CH9            98.1518 0.0741  0.0936  99.1699 0.0741  0.0936          +CH10
```

```
+CH10           99.9942 0.1400  0.1209
$
CHORDCP 853     0.0058  0.4687  0.4705  0.8301  0.1142  0.2288          +CH1
+CH1            1.8482  -0.2256 0.0146  3.1354  -0.2256 0.0146          +CH2
+CH2            4.8097  -0.2619 -0.0370 7.0649  -0.2619 -0.0370         +CH3
+CH3            10.2366 -0.2533 -0.0649 14.9319 -0.2533 -0.0649         +CH4
+CH4            22.2512 -0.2189 -0.1125 33.8317 -0.2189 -0.1125         +CH5
+CH5            50.0000 -0.3090 -0.0691 66.1683 -0.3090 -0.0691         +CH6
+CH6            77.7488 -0.2455 0.0563  85.0681 -0.2455 0.0563          +CH7
+CH7            89.7634 -0.0937 0.0828  92.9351 -0.0937 0.0828          +CH8
+CH8            95.1903 0.0152  0.0823  96.8646 0.0152  0.0823          +CH9
+CH9            98.1518 0.0824  0.1008  99.1699 0.0824  0.1008          +CH10
+CH10           99.9942 0.1475  0.1277
$
CHORDCP 854     0.0058  0.4561  0.4574  0.8301  0.1522  0.2421          +CH1
+CH1            1.8482  -0.1601 0.0225  3.1354  -0.1601 0.0225          +CH2
+CH2            4.8097  -0.2587 -0.0442 7.0649  -0.2587 -0.0442         +CH3
+CH3            10.2366 -0.2562 -0.0687 14.9319 -0.2562 -0.0687         +CH4
+CH4            22.2512 -0.2264 -0.1148 33.8317 -0.2264 -0.1148         +CH5
+CH5            50.0000 -0.3210 -0.0672 66.1683 -0.3210 -0.0672         +CH6
+CH6            77.7488 -0.2616 0.0705  85.0681 -0.2616 0.0705          +CH7
+CH7            89.7634 -0.1015 0.0956  92.9351 -0.1015 0.0956          +CH8
+CH8            95.1903 0.0225  0.0841  96.8646 0.0225  0.0841          +CH9
+CH9            98.1518 0.0890  0.1017  99.1699 0.0890  0.1017          +CH10
+CH10           99.9942 0.1530  0.1282
$
CHORDCP 855     0.0058  0.4369  0.4376  0.8301  0.1158  0.2396          +CH1
+CH1            1.8482  -0.1777 -0.0279 3.1354  -0.1777 -0.0279         +CH2
+CH2            4.8097  -0.2474 -0.0582 7.0649  -0.2474 -0.0582         +CH3
+CH3            10.2366 -0.2530 -0.0770 14.9319 -0.2530 -0.0770         +CH4
+CH4            22.2512 -0.2318 -0.1180 33.8317 -0.2318 -0.1180         +CH5
+CH5            50.0000 -0.3302 -0.0663 66.1683 -0.3302 -0.0663         +CH6
+CH6            77.7488 -0.2788 0.0838  85.0681 -0.2788 0.0838          +CH7
+CH7            89.7634 -0.1192 0.1116  92.9351 -0.1192 0.1116          +CH8
+CH8            95.1903 0.0165  0.0921  96.8646 0.0165  0.0921          +CH9
+CH9            98.1518 0.0857  0.1073  99.1699 0.0857  0.1073          +CH10
+CH10           99.9942 0.1560  0.1289
$
CHORDCP 856     0.0058  0.4029  0.4028  0.8301  0.0106  0.0224          +CH1
+CH1            1.8482  -0.1716 -0.1225 3.1354  -0.1716 -0.1225         +CH2
+CH2            4.8097  -0.2247 -0.0879 7.0649  -0.2247 -0.0879         +CH3
+CH3            10.2366 -0.2428 -0.0948 14.9319 -0.2428 -0.0948         +CH4
+CH4            22.2512 -0.2361 -0.1211 33.8317 -0.2361 -0.1211         +CH5
```

```
+CH5            50.0000 -0.3352 -0.0687 66.1683 -0.3352 -0.0687         +CH6
+CH6            77.7488 -0.2650 0.0732  85.0681 -0.2650 0.0732          +CH7
+CH7            89.7634 -0.0979 0.0831  92.9351 -0.0979 0.0831          +CH8
+CH8            95.1903 0.0054  0.0813  96.8646 0.0054  0.0813          +CH9
+CH9            98.1518 0.0668  0.1044  99.1699 0.0668  0.1044          +CH10
+CH10           99.9942 0.1270  0.1418
$
CHORDCP 857     0.0058  0.3715  0.3715  0.8301  0.0939  0.0204          +CH1
+CH1            1.8482  -0.0146 -0.0440 3.1354  -0.0146 -0.0440         +CH2
+CH2            4.8097  -0.1863 -0.1274 7.0649  -0.1863 -0.1274         +CH3
+CH3            10.2366 -0.2196 -0.1150 14.9319 -0.2196 -0.1150         +CH4
+CH4            22.2512 -0.2313 -0.1342 33.8317 -0.2313 -0.1342         +CH5
+CH5            50.0000 -0.3278 -0.0716 66.1683 -0.3278 -0.0716         +CH6
+CH6            77.7488 -0.2488 0.0651  85.0681 -0.2488 0.0651          +CH7
+CH7            89.7634 -0.1028 0.0729  92.9351 -0.1028 0.0729          +CH8
+CH8            95.1903 -0.0095 0.0741  96.8646 -0.0095 0.0741          +CH9
+CH9            98.1518 0.0520  0.0959  99.1699 0.0520  0.0959          +CH10
+CH10           99.9942 0.1124  0.1349
$
CHORDCP 858     0.0058  0.3369  0.3369  0.8301  0.1648  -0.0524         +CH1
+CH1            1.8482  0.0678  -0.2124 3.1354  0.0678  -0.2124         +CH2
+CH2            4.8097  -0.1248 -0.2008 7.0649  -0.1248 -0.2008         +CH3
+CH3            10.2366 -0.2046 -0.1678 14.9319 -0.2046 -0.1678         +CH4
+CH4            22.2512 -0.2641 -0.1614 33.8317 -0.2641 -0.1614         +CH5
+CH5            50.0000 -0.2858 -0.0660 66.1683 -0.2858 -0.0660         +CH6
+CH6            77.7488 -0.2256 0.0559  85.0681 -0.2256 0.0559          +CH7
+CH7            89.7634 -0.1155 0.0623  92.9351 -0.1155 0.0623          +CH8
+CH8            95.1903 -0.0321 0.0595  96.8646 -0.0321 0.0595          +CH9
+CH9            98.1518 0.0272  0.0834  99.1699 0.0272  0.0834          +CH10
+CH10           99.9942 0.0895  0.1366
$
MACHCP  90      0.90    3       1       1       901     2       902     +MA1
+MA1    3       903     4       904     5       905     6       906     +MA2
+MA2    7       907     8       908
$
$ Cp DATA
$
CHORDCP 901     0.0058  0.3433  0.3652  0.8301  -0.2075 0.2398          +CH1
+CH1            1.8482  -0.3813 -0.0013 3.1354  -0.3813 -0.0013         +CH2
+CH2            4.8097  -0.2865 -0.0732 7.0649  -0.2865 -0.0732         +CH3
+CH3            10.2366 -0.2403 -0.1316 14.9319 -0.2403 -0.1316         +CH4
+CH4            22.2512 -0.1885 -0.1506 33.8317 -0.1885 -0.1506         +CH5
+CH5            50.0000 -0.2648 -0.0796 66.1683 -0.2648 -0.0796         +CH6
```

```
+CH6            77.7488 -0.2658 0.0200  85.0681 -0.2658 0.0200          +CH7
+CH7            89.7634 -0.1365 0.0560  92.9351 -0.1365 0.0560          +CH8
+CH8            95.1903 -0.0133 0.0739  96.8646 -0.0133 0.0739          +CH9
+CH9            98.1518 0.0745  0.0962  99.1699 0.0745  0.0962          +CH10
+CH10           99.9942 0.1470  0.1239
$
CHORDCP 902     0.0058  0.4808  0.4833  0.8301  0.0439  0.1835          +CH1
+CH1            1.8482  -0.2490 -0.0287 3.1354  -0.2490 -0.0287         +CH2
+CH2            4.8097  -0.2665 -0.0695 7.0649  -0.2665 -0.0695         +CH3
+CH3            10.2366 -0.2432 -0.0972 14.9319 -0.2432 -0.0972         +CH4
+CH4            22.2512 -0.2012 -0.1345 33.8317 -0.2012 -0.1345         +CH5
+CH5            50.0000 -0.2980 -0.0833 66.1683 -0.2980 -0.0833         +CH6
+CH6            77.7488 -0.2750 0.0366  85.0681 -0.2750 0.0366          +CH7
+CH7            89.7634 -0.1248 0.0721  92.9351 -0.1248 0.0721          +CH8
+CH8            95.1903 0.0054  0.0865  96.8646 0.0054  0.0865          +CH9
+CH9            98.1518 0.0925  0.1095  99.1699 0.0925  0.1095          +CH10
+CH10           99.9942 0.1608  0.1410
$
CHORDCP 903     0.0058  0.4715  0.4721  0.8301  0.1371  0.2075          +CH1
+CH1            1.8482  -0.1798 -0.0295 3.1354  -0.1798 -0.0295         +CH2
+CH2            4.8097  -0.2445 -0.0686 7.0649  -0.2445 -0.0686         +CH3
+CH3            10.2366 -0.2443 -0.0890 14.9319 -0.2443 -0.0890         +CH4
+CH4            22.2512 -0.2155 -0.1336 33.8317 -0.2155 -0.1336         +CH5
+CH5            50.0000 -0.3226 -0.0846 66.1683 -0.3226 -0.0846         +CH6
+CH6            77.7488 -0.3025 0.0573  85.0681 -0.3025 0.0573          +CH7
+CH7            89.7634 -0.1350 0.0965  92.9351 -0.1350 0.0965          +CH8
+CH8            95.1903 0.0204  0.0987  96.8646 0.0204  0.0987          +CH9
+CH9            98.1518 0.1089  0.1188  99.1699 0.1089  0.1188          +CH10
+CH10           99.9942 0.1729  0.1497
$
CHORDCP 904     0.0058  0.4602  0.4603  0.8301  0.1754  0.2233          +CH1
+CH1            1.8482  -0.1050 -0.0244 3.1354  -0.1050 -0.0244         +CH2
+CH2            4.8097  -0.2359 -0.0761 7.0649  -0.2359 -0.0761         +CH3
+CH3            10.2366 -0.2443 -0.0932 14.9319 -0.2443 -0.0932         +CH4
+CH4            22.2512 -0.2210 -0.1385 33.8317 -0.2210 -0.1385         +CH5
+CH5            50.0000 -0.3355 -0.0851 66.1683 -0.3355 -0.0851         +CH6
+CH6            77.7488 -0.3310 0.0754  85.0681 -0.3310 0.0754          +CH7
+CH7            89.7634 -0.1502 0.1138  92.9351 -0.1502 0.1138          +CH8
+CH8            95.1903 0.0344  0.1013  96.8646 0.0344  0.1013          +CH9
+CH9            98.1518 0.1228  0.1196  99.1699 0.1228  0.1196          +CH10
+CH10           99.9942 0.1818  0.1504
$
CHORDCP 905     0.0058  0.4420  0.4416  0.8301  0.1683  0.2055          +CH1
```

```
+CH1            1.8482  -0.1162 -0.0819 3.1354  -0.1162 -0.0819         +CH2
+CH2            4.8097  -0.2207 -0.0939 7.0649  -0.2207 -0.0939         +CH3
+CH3            10.2366 -0.2384 -0.1046 14.9319 -0.2384 -0.1046         +CH4
+CH4            22.2512 -0.2235 -0.1461 33.8317 -0.2235 -0.1461         +CH5
+CH5            50.0000 -0.3453 -0.0862 66.1683 -0.3453 -0.0862         +CH6
+CH6            77.7488 -0.3621 0.0930  85.0681 -0.3621 0.0930          +CH7
+CH7            89.7634 -0.1762 0.1346  92.9351 -0.1762 0.1346          +CH8
+CH8            95.1903 0.0324  0.1112  96.8646 0.0324  0.1112          +CH9
+CH9            98.1518 0.1227  0.1264  99.1699 0.1227  0.1264          +CH10
+CH10           99.9942 0.1857  0.1517
$
CHORDCP 906     0.0058  0.4042  0.4042  0.8301  0.0872  -0.0462         +CH1
+CH1            1.8482  -0.1088 -0.1969 3.1354  -0.1088 -0.1969         +CH2
+CH2            4.8097  -0.1927 -0.1330 7.0649  -0.1927 -0.1330         +CH3
+CH3            10.2366 -0.2230 -0.1292 14.9319 -0.2230 -0.1292         +CH4
+CH4            22.2512 -0.2225 -0.1559 33.8317 -0.2225 -0.1559         +CH5
+CH5            50.0000 -0.3531 -0.0897 66.1683 -0.3531 -0.0897         +CH6
+CH6            77.7488 -0.3558 0.0823  85.0681 -0.3558 0.0823          +CH7
+CH7            89.7634 -0.1440 0.0982  92.9351 -0.1440 0.0982          +CH8
+CH8            95.1903 0.0214  0.0955  96.8646 0.0214  0.0955          +CH9
+CH9            98.1518 0.0962  0.1212  99.1699 0.0962  0.1212          +CH10
+CH10           99.9942 0.1489  0.1648
$
CHORDCP 907     0.0058  0.3663  0.3663  0.8301  0.1512  -0.0466         +CH1
+CH1            1.8482  0.0278  -0.1168 3.1354  0.0278  -0.1168         +CH2
+CH2            4.8097  -0.1446 -0.1895 7.0649  -0.1446 -0.1895         +CH3
+CH3            10.2366 -0.1924 -0.1575 14.9319 -0.1924 -0.1575         +CH4
+CH4            22.2512 -0.2129 -0.1752 33.8317 -0.2129 -0.1752         +CH5
+CH5            50.0000 -0.3522 -0.0903 66.1683 -0.3522 -0.0903         +CH6
+CH6            77.7488 -0.3317 0.0731  85.0681 -0.3317 0.0731          +CH7
+CH7            89.7634 -0.1464 0.0848  92.9351 -0.1464 0.0848          +CH8
+CH8            95.1903 -0.0036 0.0861  96.8646 -0.0036 0.0861          +CH9
+CH9            98.1518 0.0710  0.1107  99.1699 0.0710  0.1107          +CH10
+CH10           99.9942 0.1278  0.1546
$
CHORDCP 908     0.0058  0.3426  0.3426  0.8301  0.2208  -0.1372         +CH1
+CH1            1.8482  0.1390  -0.3417 3.1354  0.1390  -0.3417         +CH2
+CH2            4.8097  -0.0641 -0.3025 7.0649  -0.0641 -0.3025         +CH3
+CH3            10.2366 -0.1626 -0.2256 14.9319 -0.1626 -0.2256         +CH4
+CH4            22.2512 -0.2530 -0.2050 33.8317 -0.2530 -0.2050         +CH5
+CH5            50.0000 -0.3146 -0.0781 66.1683 -0.3146 -0.0781         +CH6
+CH6            77.7488 -0.2876 0.0611  85.0681 -0.2876 0.0611          +CH7
+CH7            89.7634 -0.1703 0.0716  92.9351 -0.1703 0.0716          +CH8
```

```
+CH8            95.1903 -0.0598 0.0680  96.8646 -0.0598 0.0680          +CH9
+CH9            98.1518 0.0171  0.0921  99.1699 0.0171  0.0921          +CH10
+CH10           99.9942 0.0873  0.1486
$
$
$       SETID   SYM     FIX     NMODE   TABDMP  MLIST   CONMLST
FLUTTER 10      ANTI    20      11
$
$       SETID   ALT     IDATM   FTMUNIT FTLUNIT VREF    FLUTTF  PRINT
FIXHATM 20      15000.  0       SLUG    FT      1.68    0       2       +FI1
+FI1    31      32
$+FI1    31      32      33
$
MKAEROZ 31      0.85      1     10      SAVE    NAVAK085.AIC    0       +MK1
+MK1    0.11    0.22    0.24    0.27    0.39    0.52    0.64    0.76
MKAEROZ 32      0.90      1     10      SAVE    NAVAK090.AIC    0       +MK2
+MK2    0.10    0.21    0.23    0.26    0.37    0.49    0.60    0.72
$MKAEROZ 33      0.95      1      0      ACQUIRE NAVAK095.AIC    0       +MK3
$+MK3    0.09    0.18    0.20    0.22    0.32    0.42    0.52    0.62
$*************************************************************************
$       IDFLT   TITLA   ALPHA
TRIMFLT 10              1.5
$*************************************************************************
ENDDATA
```

Appendix D. MATLAB Scripts

D.1 CFD Mesh Interpolation

```
% This script is used to interpolate Cp data from Dr. Reid Melville's Euler CFD grid to the
% ZAERO grid.  This enables ZAERO to used the CFD data.

clear

% Get data from CFD output.  Ensure data is in the current MATLAB directory and that the
% file extension is included.
name=input('Input filename where Cp data is located enclosed in single quotes  ');
upper=dlmread(name,' ','a4..d3358');
lower=dlmread(name,' ','a3362..d6716');
xu=upper(:,1);
yu=upper(:,2);
cpu=upper(:,4);
xl=lower(:,1);
yl=lower(:,2);
cpl=lower(:,4);

% ZAERO wing strip locations
xa=[265.871256 281.8518246 298.6886104 310.3979101 322.5090547 338.0349151 349.2259869 358.8735349;
408.936626 408.9290652 408.9210993 408.9155593 408.9098292 408.9024835 408.8971887 408.8926242];
ya=[62.4987 81.5436 101.6089 115.5635 129.997 148.5 161.837 173.3345];

% Build chordwise cut locations
x=[];
nchord=0:.05:1;

% Create the chordwise distribution.  This distributes the chordwise cuts so that more information is
% available at the leading and trailing edges of the wing.
cd=((atan(3*pi*(nchord-.5)))/2.7237)+.5;
c=[];
m=size(xa,2);
for n=1:m
    c(n)=xa(2,n)-xa(1,n);
    for j=1:size(nchord,2)
        x(j,n)=c(n)*cd(j)+xa(1,n);
    end
end

% Fill y array to same size as x
```

```
y=zeros(size(x,1),size(x,2));
h=1;
for i=1:size(x,1)
    y(i,:)=ya(1,:);
end

% Interpolate from midplane data to ZAERO locations
ucp=griddata(xu,yu,cpu,x,y);
lcp=griddata(xl,yl,cpl,x,y);
delcp=ucp-lcp;

% This figure is just a check to make sure the interpolation looks good.
figure
plot3(x(:,1),y(:,1),-delcp(:,1));
hold
for i=2:8
    plot3(x(:,i),y(:,i),-delcp(:,i));
end
hold

% x location in percentage of chord length
pc=cd*100;
pc=pc';

% Create the output file that is readable by TECPLOT.
file=input('Input filename for CHORDCP card data in single quotes   ');
r=input('Input base number for CHORDCP id   ');
m=input('Input mach number for MACHCP card   ');
fid = fopen(file,'w');
fprintf(fid,'MACHCP  %-8.0f%-8.2f3       1       1       %-8.0f2       %-8.0f+MA1\n',[m*100 m r+1 r+2]');
fprintf(fid,'+MA1    %-8.0f%-8.0f%-8.0f%-8.0f%-8.0f%-8.0f%-8.0f%-8.0f+MA2\n',[3 r+3 4 r+4 5 r+5 6 r+6]');
fprintf(fid,'+MA2    %-8.0f%-8.0f%-8.0f%-8.0f\n',[7 r+7 8 r+8]');
fprintf(fid,'$\n');
fprintf(fid,'$ Cp DATA\n');
fprintf(fid,'$\n');
for e=1:8
    q=r+e;
    fprintf(fid,'CHORDCP %-8.0f%-8.4f%-8.4f%-8.4f%-8.4f%-8.4f%-8.4f        ...
     +CH1\n',[q pc(1,1) ucp(1,e) lcp(1,e) pc(2,1) ucp(2,e) lcp(2,e)]');
    b=3;d=4;
    for k=1:9
        a=k+1;
        fprintf(fid,'+CH%-2.0f           %-8.4f%-8.4f%-8.4f%-8.4f%-8.4f%-8.4f        ...
```

```
          +CH%-2.0f\n',[k pc(b,1) ucp(b,e) lcp(b,e) pc(d,1) ucp(b,e) lcp(b,e) a]');
         b=d+1;d=d+2;
    end
    fprintf(fid,'+CH%-2.0f           %-8.4f%-8.4f%-8.4f\n',[a pc(21,1) ucp(21,e) lcp(21,e)]');
    fprintf(fid,'$\n');
end
fclose(fid);
```

D.2 Wind Tunnel Mesh Interpolation

```
% This script is used to interpolate windtunnel Cp data to the
% ZAERO grid.  This enables ZAERO to used the wind tunnel data.

clear

% Change directory to where the wind tunnel data is stored
cd('c:\bthesis\plots\cp');

% Read in wind tunnel pressure port locations
x1=dlmread('pressport.dat',' ','a4..a93');
x1=x1*12;
y1=dlmread('pressport.dat',' ','b4..b93');
y1=y1*12;

% Read in wind tunnel Cp data.  Set "name" to the desired mach number
% to get the appropriate data.
name=('cp95.dat');
cpu=dlmread(name,' ','b6..b95');
cpl=dlmread(name,' ','b96..b185');

% ZAERO wing strip locations
xa=[265.871256 281.8518246 298.6886104 310.3979101 322.5090547 338.0349151 349.2259869 358.8735349
    406.0 406.0 406.0 406.0 406.0 406.0 406.0 406.0];
ya=[62.4987 81.5436 101.6089 115.5635 129.997 148.5 161.837 172.0];

% Build chordwise cut locations
x=[];
nchord=0:.05:1;

% Create the chordwise distribution.  This distributes the chordwise cuts so that more information is
% available at the leading and trailing edges of the wing.
cd=((atan(3*pi*(nchord-.5)))/2.7237)+.5;
c=[];
m=size(xa,2);
for n=1:m
    c(n)=xa(2,n)-xa(1,n);
    for j=1:size(nchord,2)
        x(j,n)=c(n)*cd(j)+xa(1,n);
    end
end

% Fill y array to same size as x
```

```
y=zeros(size(x,1),size(x,2));
h=1;
for i=1:size(x,1)
    y(i,:)=ya(1,:);
end

% Interpolate from midplane data to ZAERO locations
ucp=griddata(x1,y1,cpu,x,y);
lcp=griddata(x1,y1,cpl,x,y);
delcp=ucp-lcp;

k=0;
for i=1:6
    for j=1:15
        k=k+1;
        x2(j,i)=x1(k,1);
        y2(j,i)=y1(k,1);
        cpup(j,i)=cpu(k,1);
        cplo(j,i)=cpl(k,1);
    end
 end

% Create the output file that is readable by TECPLOT.
fid = fopen('cpwt95.plt','w');
fprintf(fid,'TITLE = "Cp Upper Surface"\n');
fprintf(fid,'VARIABLES = "X", "Y", "-Cp"\n');
fprintf(fid,'ZONE I=21, J=8, F=POINT\n');
for i=1:6
    fprintf(fid,'%-8.3f%-8.3f%-8.3f\n',[x2(:,i) y2(:,i) -cpup(:,i)]');
end
fclose(fid);

% This figure is just a check to make sure the interpolation looks good.
set(0,'DefaultLineLineWidth',2)
plot3(x2(:,1),y2(:,1),-cpup(:,1));
hold
for i=2:6
    figure(1);
    plot3(x2(:,i),y2(:,i),-cpup(:,i));
end
xlabel('x (in)','FontWeight','Bold');
ylabel('y (in)','FontWeight','Bold');
zlabel('-C_{p}','FontWeight','Bold');
```

```
view([1,62]);
title('Upper Suface Wind Tunnel C_{p} @ .95M','FontWeight','Bold');
hold
```

D.3 Conversion Script from ZAERO to TECPLOT for V-g/V-ω Plots

```
% This script is used to read ZAERO V-g/V-w information generated from the PLTVG card.  ZAERO outputs
% the data into a simple text file in column format.  This then reads that data and converts it into
% a formatted layout file for TECPLOT.

clear

% Set MATLAB directory to where the V-g information is stored.  The script is looking for a file with
% a ".dat" file extension, so no extension needs to be specified when inputting the filename.  You must,
% however, specify the number of velocities used in the PLTVG card from ZAERO.
cd('c:\bthesis\plots\vg');
file=input('Input filename containing V-g/V-w information inside single quotes (without extension)  ');
n=input('How many velocities did you use?   ');
p=n+2;
name=([file,'.dat']);
vgplt=([file(1,1:5),'vg.plt']);
vwplt=([file(1,1:5),'vw.plt']);

r1=(['a3..g', num2str(p)]);
r2=(['i3..n', num2str(p)]);
vg=dlmread(name,' ',r1);
w=dlmread(name,' ',r2);
V=vg(:,1);
g=vg(:,2:7);
% a is the speed of sound in feet per second at sea level, 5K, 10K, and 15K feet, standard day.
a=[1116.45 1097.1 1077.4 1057.36];
for i=1:4
    M(:,i)=V/a(i);
end

% Create TECPLOT layout file.
s1='Config:';
s2='Method:';
s3='Altitude (ft):';
t1=strvcat(s1,s2,s3);
l1=input('Enter configuration.    1 = Clean Wing 2 = SCL007 3 = SCL008   ');
if l1==1
    con='Clean Wing';
elseif l1==2
    con='SCL007    ';
elseif l1==3
    con='SCL008    ';
end
```

```
l2=input('Enter solution method.  1 = ZONA6      2 = ZTAIC   ');
if l2==1
    meth='ZONA6    ';
elseif l2==2
    meth='ZTAIC    ';
end
l3=input('Enter altitude of run.  1 = Sea Level  2 = 5 kft  3 = 10 kft  4 = 15 kft   ');
if l3==1
    alt='Sea Level ';
elseif l3==2
    alt='5000      ';
elseif l3==3
    alt='10000     ';
elseif l3==4
    alt='15000     ';
end

t2=strvcat(con,meth,alt);

fid=fopen(vgplt,'w');
fprintf(fid,'TITLE = "%11s"\n',vgplt);
fprintf(fid,'VARIABLES = "Velocity (ft/s)"\n "Mach #"\n');
fprintf(fid,'"Damping"\n');
fprintf(fid,'TEXT\n CS=FRAME\n C=BLACK\n S=LOCAL\n X=5,Y=96\n');
fprintf(fid,'HU=POINT\n LS=1 AN=LEFT\n BXM=20 LT=0.1 BXO=BLACK BXF=WHITE\n F=HELV-BOLD\n');
fprintf(fid,'H=14 A=0\n MFC=""\n');
fprintf(fid,'T="MATCHED POINT FLUTTER ANALYSIS"\n');
fprintf(fid,'TEXT\n CS=FRAME\n C=BLACK\n S=LOCAL\n X=5,Y=93\n');
fprintf(fid,'HU=POINT\n LS=1 AN=LEFT\n BXM=20 LT=0.1 BXO=BLACK BXF=WHITE\n F=HELV-BOLD\n');
fprintf(fid,'H=12 A=0\n MFC=""\n');
fprintf(fid,'T="BC:"\n');
fprintf(fid,'TEXT\n CS=FRAME\n C=BLACK\n S=LOCAL\n X=16.5,Y=93\n');
fprintf(fid,'HU=POINT\n LS=1 AN=LEFT\n BXM=20 LT=0.1 BXO=BLACK BXF=WHITE\n F=HELV-BOLD\n');
fprintf(fid,'H=12 A=0\n MFC=""\n');
fprintf(fid,'T="Antisymmetric"\n');

for i=1:3
    y=93-(3*i);
    fprintf(fid,'TEXT\n CS=FRAME\n C=BLACK\n S=LOCAL\n X=5,Y=%3.1f\n',y);
    fprintf(fid,'HU=POINT\n LS=1 AN=LEFT\n BXM=20 LT=0.1 BXO=BLACK BXF=WHITE\n F=HELV-BOLD\n');
    fprintf(fid,'H=12 A=0\n MFC=""\n');
    fprintf(fid,'T="%14s%1c',[t1(i,:) '"']');
    fprintf(fid,'\n');
```

```
    fprintf(fid,'TEXT\n CS=FRAME\n C=BLACK\n S=LOCAL\n X=15,Y=%3.1f\n',y);
    fprintf(fid,'HU=POINT\n LS=1 AN=LEFT\n BXM=20 LT=0.1 BXO=BLACK BXF=WHITE\n F=HELV-BOLD\n');
    fprintf(fid,'H=12 A=0\n MFC=""\n');
    fprintf(fid,'T="%14s%1c',[t2(i,:) '"']');
    fprintf(fid,'\n');
end

for i=1:6
    fprintf(fid,'ZONE T="Mode %1.0f"\n',i);
    fprintf(fid,'I=%-2.0f, J=1, K=1, F=POINT\n',n);
    fprintf(fid,'DT= (SINGLE SINGLE SINGLE)\n');
    fprintf(fid,'%8.4E %8.4E %8.4E\n',[V M(:,l3) g(:,i)]');
end
fclose(fid)

fid=fopen(vwplt,'w');
fprintf(fid,'TITLE = "%11s"\n',vwplt);
fprintf(fid,'VARIABLES = "Velocity (ft/s)"\n "Mach #"\n');
fprintf(fid,'"Frequency (Hz)"\n');
fprintf(fid,'TEXT\n CS=FRAME\n C=BLACK\n S=LOCAL\n X=5,Y=96\n');
fprintf(fid,'HU=POINT\n LS=1 AN=LEFT\n BXM=20 LT=0.1 BXO=BLACK BXF=WHITE\n F=HELV-BOLD\n');
fprintf(fid,'H=14 A=0\n MFC=""\n');
fprintf(fid,'T="MATCHED POINT FLUTTER ANALYSIS"\n');
fprintf(fid,'TEXT\n CS=FRAME\n C=BLACK\n S=LOCAL\n X=5,Y=93\n');
fprintf(fid,'HU=POINT\n LS=1 AN=LEFT\n BXM=20 LT=0.1 BXO=BLACK BXF=WHITE\n F=HELV-BOLD\n');
fprintf(fid,'H=12 A=0\n MFC=""\n');
fprintf(fid,'T="BC:"\n');
fprintf(fid,'TEXT\n CS=FRAME\n C=BLACK\n S=LOCAL\n X=16.5,Y=93\n');
fprintf(fid,'HU=POINT\n LS=1 AN=LEFT\n BXM=20 LT=0.1 BXO=BLACK BXF=WHITE\n F=HELV-BOLD\n');
fprintf(fid,'H=12 A=0\n MFC=""\n');
fprintf(fid,'T="Antisymmetric"\n');

for i=1:3
    y=93-(3*i);
    fprintf(fid,'TEXT\n CS=FRAME\n C=BLACK\n S=LOCAL\n X=5,Y=%3.1f\n',y);
    fprintf(fid,'HU=POINT\n LS=1 AN=LEFT\n BXM=20 LT=0.1 BXO=BLACK BXF=WHITE\n F=HELV-BOLD\n');
    fprintf(fid,'H=12 A=0\n MFC=""\n');
    fprintf(fid,'T="%14s%1c',[t1(i,:) '"']');
    fprintf(fid,'\n');
    fprintf(fid,'TEXT\n CS=FRAME\n C=BLACK\n S=LOCAL\n X=15,Y=%3.1f\n',y);
    fprintf(fid,'HU=POINT\n LS=1 AN=LEFT\n BXM=20 LT=0.1 BXO=BLACK BXF=WHITE\n F=HELV-BOLD\n');
    fprintf(fid,'H=12 A=0\n MFC=""\n');
    fprintf(fid,'T="%14s%1c',[t2(i,:) '"']');
```

```
    fprintf(fid,'\n');
end

for i=1:6
    fprintf(fid,'ZONE T="Mode %1.0f"\n',i);
    fprintf(fid,'I=%-2.0f, J=1, K=1, F=POINT\n',n);
    fprintf(fid,'DT= (SINGLE SINGLE SINGLE)\n');
    fprintf(fid,'%8.4E %8.4E %8.4E\n',[V M(:,13) w(:,i)]');
end
fclose(fid)
```

Bibliography

1. Albano, E. and W. P. Rodden. "A Doublet-Lattice Method for Calculating Lift Distribution on Oscillating Surfaces in Subsonic Flows," *AIAA Journal*, *7*(2):279–285 (February 1969).
2. Bennett, R. M., et al. "Wing-Flutter Calculations with the CAP-TSD Unsteady Transonic Small Disturbance Program," *Journal of Aircraft*, *26*(9):876–882 (Sep 1989).
3. Brink-Spalink, J. and J. M. Bruns. "Correction of Unsteady Aerodynamic Influence Coefficients Using Experimental or CFD Data." *41st AIAA/ASME/ASCE/AHS/ASC Structures, Structural Dynamics, and Materials Conference and Exhibit*. AIAA, 2000.
4. Bunton, Robert W. and Charles M. Denegri. "Limit Cycle Oscillation Characteristics of Fighter Aircraft," *Journal of Aircraft*, *37*:916–918 (September-October 2000).
5. Champion, Laura S. *F-16C/D Block 40 with Advanced Medium-Range Air-to-Air Missile (AMRAAM) Flutter Flight Test Evaluation*. AFFTC Technical Report AFFTC-TR-92-19, Air Force Flight Test Center, December 1992.
6. Chen, P. C. Vice-President, ZONA Technologies, Scottsdale AZ. Telephone interview. 3 October 2001.
7. Chen, P. C. "A Damping Perturbation Method for Flutter Solution: The g-Method," *AIAA Journal*, *38*:1519–1524 (September 2000).
8. Chen, P. C., et al. "Limit-Cycle-Oscillation Studies of a Fighter with External Stores." *39th AIAA/ASME/ASCE/AHS/ASC Structures, Structural Dynamics, and Materials Conference and Exhibit*. AIAA, 1998.
9. Chen, P. C., et al. "Transonic-Aerodynamic-Influence-Coefficient Approach for Aeroelastic and MDO Applications," *Journal of Aircraft*, *37*(1):85–94 (January-February 2000).
10. Chen, P. C., et al. "A Comprehensive Rapid-Assessment-of-Flutter/Ejection-Loads (RAFEL) Software System for Aircraft/Store Compatibility." *Aerospace Flutter and Dynamics Council*. October 2001.
11. Dawson, Kenneth S. and J. Chris Sussingham. "F-16 Limit Cycle Oscillation Testing with Asymmetric Stores." *17th AIAA Applied Aerodynamics Conference*. AIAA, 1999.
12. Denegri, Jr., Charles M. *F-16 Block 40 Theoretical Flutter Analysis Model Verification and Validation*. AFDTC Technical Report ADB202611, AFSEO/SKP, Eglin AFB, FL: Air Force Development Test Center, June 1995.

13. Denegri, Jr., Charles M. "Limit Cycle Oscillation Flight Test Results of a Fighter with External Stores," *Journal of Aircraft*, *37*:761–769 (September-October 2000).

14. Fung, K. Y. and A. Chung. "Computations of Unsteady Transonic Aerodynamics Using Prescribed Steady Pressures," *Journal of Aircraft*, *20*(12):1058–1061 (December 1983).

15. Gordnier, R. E. and R. B. Melville. "Physical Mechanisms for Limit-Cycle-Oscillations of a Cropped Delta Wing." *30th AIAA Fluid Dynamics Conference*. AIAA, 1999.

16. Gordnier, R. E. and R. B. Melville. "Transonic Flutter Simulations Using an Implicit Aeroelastic Solver," *Journal of Aircraft*, *37*:872–879 (September-October 2000).

17. Greco, Jr., P. C., et al. "Frequency Domain Unsteady Transonic Aerodynamics for Flutter and Limit Cycle Oscillation Prediction." *35th Aerospace Sciences Meeting and Exhibit*. AIAA, 1997.

18. Hassig, H. J. "An Approximate True Damping Solution of the Flutter Equation by Determinant Iteration," *Jounal of Aircraft*, *8*(11):885–889 (November 1971).

19. Hodges, Dewey H. and G. Alvin Pierce. *Introduction to Structural Dynamics and Aeroelasticity* (1st Edition). Cambridge, England: Cambridge University Press, 2002.

20. Jadic, Ioan, et al. "Improving the Aerodynamic Approximation in Linear Aeroelasticity." *41st AIAA/ASME/ASCE/AHS/ASC Structures, Structural Dynamics, and Materials Conference and Exhibit*. AIAA, 2000.

21. Johnson, Gregg E. *Supersonic Flutter Analysis for F-16 Stores Configuration Clearance*. MS Thesis, School of Engineering, Air Force Institute of Technology (AU), Wright-Patterson AFB OH, March 1997.

22. Kolonay, R., et al. "A Methodology of Large Scale Computational Aeroelasticity for the MDA/MDO Environment." *8th AIAA/NASA/USAF/ISSMO Symposium on MDO*. AIAA, 2000.

23. Liu, D. D., et al. "An Efficient Method for Computing Unsteady Transonic Aerodynamics of Swept Wings with Control Surfaces," *Journal of Aircraft*, *25*(1):25–31 (January 1988).

24. Meijer, J. J. *Determination of Transonic Unsteady Aerodynamic Loads to Predict the Aeroelastic Stability of Fighter Aircraft*. Technical Report NLR TP 97304, Amsterdam: National Aerospace Laboratory NLR, June 1997.

25. Meijer, J. J. and A. M. Cunningham. *Development of a Method to Predict Transonic Limit Cycle Oscillation Characteristics of Fighter Aircraft*. Techni-

cal Report NLR TP 91359, Amsterdam: National Aerospace Laboratory NLR, October 1991.

26. Meirovitch, Leonard. *Elements of Vibration Analysis* (2nd Edition). Boston, Massachusetts: McGraw-Hill, 1986.

27. Melville, Reid. "Dynamic Aeroelastic Simulation of Complex Configurations Using Overset Grid Systems." *Fluids 2000*. AIAA, 2000.

28. Melville, Reid. "Nonlinear Simulation of F-16 Aeroelastic Instability." *39th AIAA Aerospace Sciences Meeting and Exhibit*. AIAA, 2001.

29. Mignolet, M. P., et al. "On the Nonlinear Structural Damping Mechanism of the Wing/Store Limit Cycle Oscillation." *40th AIAA/ASME/ASCE/AHS/ASC Structures, Structural Dynamics, and Materials Conference and Exhibit*. AIAA, 1999.

30. Oyibo, Gabriel. "Formulation of Three-Dimensional Hodograph Method and Separable Solutions for Nonlinear Transonic Flows," *AIAA Journal*, *28*(10):1745–1750 (October 1990).

31. Pipeno, Serge, et al. "Energy Based Design and Analysis of Staggered Solvers for Nonlinear Transient Aeroelastic Problems." *4st AIAA/ASME/ASCE/AHS/ASC Structures, Structural Dynamics, and Materials Conference and Exhibit*. AIAA, 2000.

32. Rodden, W. P., et al. *Aeroelastic Addition to NASTRAN*. Technical Report NASA CR 3094, NASA, 1979.

33. Sheta, Essam F., et al. "Computational and Experimental Investigation of Limit Cycle Oscillations in Nonlinear Aeroelastic Systems." *41st AIAA/ASME/ASCE/AHS/ASC Structures, Structural Dynamics, and Materials Conference and Exhibit*. AIAA, 2000.

34. Tang, Deman and Earl H. Dowell. "Effects of Angle of Attack on Nonlinear Flutter of a Delta Wing," *AIAA Journal*, *39*:15–21 (January 2001).

35. Turner, C. D. "Effect of Store Aerodynamics on Wing/Store Flutter," *Journal of Aircraft*, *19*:574–580 (July 1982).

36. ZONA Technology, Scottsdale. *ZAERO Version 5.2 Theoretical Manual*, June 2001.

37. ZONA Technology, Scottsdale. *ZAERO Version 5.2 User's Manual*, June 2001.

Vita

Major Raymond G. Toth was born and raised in Philadelphia, Pennsylvania. He graduated from George Washington High School in 1984. He went on to the Pennsylvania State University where he earned a Bachelor of Science degree in Aerospace Engineering with a concentration in Aircraft Propulsion Systems.

After graduation he attended Undergraduate Navigator Training at Mather AFB, CA where he earned the ATC Commader's Trophy as the top graduate of his class. Following F-15E RTU at Luke AFB, AZ, Major Toth was assigned to the 336th Fighter Squadron at Seymour-Johnson AFB, NC where he was responsible for planning deployments, maintaining mission support systems, and ensuring crews met all standardization and evaluation requirements. In 1994, he was selected to attend Undergraduate Pilot Training at Laughlin AFB, TX. After earning the AETC Commander's Trophy as the top graduate of his class and graduating as a Distinguished Graduate from F-16 RTU at Luke AFB, AZ, he was assigned to the 23d Fighter Squadron at Spangdahlem AB, Germany. While at Spangdahlem AB, he was responsible for pilot training programs, standardization and evaluation, mobility and plans, and finished his tour as a Flight Commander, Mission Commander and four-ship flight lead. After leaving Germany, Major Toth was assigned to the 435th Fighter Squadron at Randolph AFB, TX as an AT-38 Instructor Pilot for the Introduction to Fighter Fundamentals program.

Shortly after arriving at Randolph, he was selected for the Air Force Institute of Technology (AFIT)/Test Pilot School program. He entered the Air Force Institute of Technology master's degree program in August of 2000. This thesis provides the final document required for him to earn his Master of Sciences Degree in Aeronautical Engineering.

REPORT DOCUMENTATION PAGE	Form Approved OMB No. 0704-0188

PLEASE DO NOT RETURN YOUR FORM TO THE ABOVE ADDRESS.

1. REPORT DATE *(DD-MM-YYYY)*	2. REPORT TYPE	3. DATES COVERED *(From - To)*
03-2003	Master's Thesis	04/2001 - 01/2003

4. TITLE AND SUBTITLE

NONLINEAR, TRANSONIC FLUTTER PREDICTION FOR F-16 STORES CONFIGURATION CLEARANCE

5a. CONTRACT NUMBER

5b. GRANT NUMBER

5c. PROGRAM ELEMENT NUMBER

6. AUTHOR(S)

Toth, Raymond G. Maj, USAF

5d. PROJECT NUMBER

5e. TASK NUMBER

5f. WORK UNIT NUMBER

7. PERFORMING ORGANIZATION NAME(S) AND ADDRESS(ES)

Air Force Institute of Technology
Graduate School of Engineering and Management (AFIT/EN)
2950 P Street, Building 640
WPAFB OH 45433-7765

8. PERFORMING ORGANIZATION REPORT NUMBER

AFIT/GAE/ENY/03-8

9. SPONSORING/MONITORING AGENCY NAME(S) AND ADDRESS(ES)

Charles M. Denegri, GS-13
46 SK/SKE
205 West D Ave Suite 348 Building 350
Eglin AFB FL 32542
DSN 872-0396

10. SPONSOR/MONITOR'S ACRONYM(S)

11. SPONSOR/MONITOR'S REPORT NUMBER(S)

12. DISTRIBUTION/AVAILABILITY STATEMENT

APPROVED FOR PUBLIC RELEASE; DISTRIBUTION UNLIMITED.

13. SUPPLEMENTARY NOTES

14. ABSTRACT

Limit cycle oscillation (LCO) has been an issue for the F-16 since its operational deployment. Configuration validation requires large investments in time and resources due to the very specific and stringent guidelines used during flight test to ensure the aircraft does not encounter classical flutter or excessive LCO. A new approach, incorporating inherent nonlinearities that drive LCO is investigated using the Transonic Equivalent Strip method to account for wing thickness effects and shock structure. The g-method flutter solution is used to include first-order aerodynamic damping effects. Two F-16 store configurations are examined to correlate predicted flutter onset speeds, frequencies, and character with those found in flight test, as well as the aerodynamic effect of modeling underwing stores on the flutter solution. Results show small changes in the tuning of the structural model resulted in large changes in the flutter boundary. The aerodynamic influence of underwing stores proved significant, particularly for the two most outboard wing stations. Most importantly, the character of the instability was predicted by the new method.

15. SUBJECT TERMS

Limit Cycle Oscillation, Aeroelastic, Flutter, Nonlinear

16. SECURITY CLASSIFICATION OF:			17. LIMITATION OF ABSTRACT	18. NUMBER OF PAGES	19a. NAME OF RESPONSIBLE PERSON
a. REPORT	b. ABSTRACT	c. THIS PAGE			Robert Canfield, LtCol, ENY
U	U	U	UU	180	19b. TELEPHONE NUMBER *(Include area code)* (937) 255-3636 x4641